POLITECHNIKA POZNAŃSKA
WYDZIAŁ BUDOWY MASZYN I ZARZĄDZANIA

mgr inż. Mateusz SOPATA

Rozprawa doktorska

„*Wytwarzanie i właściwości nanokrystalicznych stopów i kompozytów na bazie tantalu*"

Promotor: dr hab. inż. Jarosław JAKUBOWICZ, prof. PP
Promotor pomocniczy: dr inż. Grzegorz ADAMEK

Poznań, maj 2019

STRESZCZENIE

Rozprawa doktorska stanowi zbiór siedmiu, jednotematycznych publikacji dotyczących wytwarzania i analizy nanokrystalicznych stopów i kompozytów na bazie tantalu. Cztery z publikacji znajdują się na liście A czasopism Ministerstwa Nauki i Szkolnictwa Wyższego (MNiSW) i posiadają sumaryczny wskaźnik cytowań (*impact factor*) wynoszący 7,889. Pozostałe trzy czasopisma znajdują się na liście B lub są indeksowane w Web of Science.

Stopy i kompozyty na bazie tantalu wytworzono stosując mechaniczna syntezę oraz prasowanie na gorąco. Dodatkami stopowymi były niob, molibden i wolfram, a fazą ceramiczną tlenek cyrkonu (IV), tlenek itru (III) oraz węglik tantalu. Proszki mieszano w stosunkach wagowych 5, 10, 20, 40%. Technologie mechanicznej syntezy i prasowania na gorąco pozwoliły na otrzymanie materiałów o strukturze nanokrystalicznej. Dla proszków średnia wielkość ziarna wynosiła od 31 nm do 87 nm, a dla prasowanych na gorąco materiałów od 43 do 195 nm. Materiały poddano badaniom: struktury, mikrostruktury i morfologii powierzchni, właściwości mechanicznych, odporności korozyjnej oraz stabilności temperaturowej. Otrzymane wyniki porównano z próbką kontrolną, którą był mikrokrystaliczny tantal.

Badania struktury wykazały, że podczas mechanicznej syntezy stopów powstają roztwory stałe, a w przypadku kompozytów materiały wielofazowe. Równocześnie dochodzi do rozdrobnienia mikrostruktury oraz częściowej amorfizacji proszków. Właściwości mechaniczne takie jak, twardość oraz moduł Younga, zbadano wykorzystując nanoindentację. Wszystkie materiały charakteryzowały się większą twardością w porównaniu z mikrokrystalicznym tantalem. Taka sama zależność występowała w przypadku modułu Younga. Największą twardość uzyskano dla stopu Ta-10Mo (1481 HV) oraz kompozytu Ta-10TaC (1398 HV). Jest to wzrost o ponad 1000 HV w porównaniu do próbki kontrolnej.

Zastosowanie dodatków stopowych oraz ceramicznych skutkuje polepszeniem odporności na korozję. Wartości gęstości prądu korozyjnego, pomimo znacznego rozdrobnienia mikrostruktury, są takie same lub mniejsze niż w przypadku mikrokrystalicznego tantalu.

Termograwimetria wykazała, że nanokrystaliczne stopy oraz kompozyty posiadają lepszą stabilność temperaturową niż mikrokrystaliczny Ta. Wygrzewanie w atmosferze powietrza powoduje wytworzenie warstwy tlenkowej, która jest słabo związana z podłożem i ulega złuszczaniu. Wykorzystanie atmosfery azotu w procesach wysokotemperaturowych skutkuje wytworzeniem ochronnej dyfuzyjnej warstwy azotków silnie związanej z podłożem.

ABSTRACT

The doctoral dissertation is composed from seven monothematic publications on the formation and analysis of tantalum-based nanocrystalline alloys and composites. Four of the publications are on the "A" list of MNiSW (Ministry of Science and Higher Education) journals and they have a citation ratio (impact factor) of summarized value 7.889. The other three publications are on the "B" list of MNiSW or are indexed in the Web of Science.

Tantalum-based alloys and composites were produced using mechanical alloying and hot pressing processes. The alloy additives were niobium, molybdenum, and tungsten, and the ceramic phase was zirconium (IV) oxide, yttrium (III) oxide, and tantalum carbide. The powders were mixed in a weight ratio of 5, 10, 20, 40%. The technologies of mechanical alloying and hot pressing allowed to obtain materials with a nanocrystalline structure. For powders, the average grain size was from 31 nm to 87 nm, and for hot-pressed materials from 43 nm to 195 nm. The materials structure, microstructure and surface morphology, mechanical properties, corrosion resistance and temperature stability were studied. The results were compared to a control sample, which was microcrystalline tantalum.

The structure investigation has shown that during the mechanical alloying of alloys, solid solutions are formed whereas composite materials have multiphase structure. At the same time, the microstructure refinement and partial amorphization of powders occur. Mechanical properties such as hardness and Young's modulus have been studied using nanoindentation. All materials had higher hardness compared to microcrystalline tantalum. The same relationship was found for Young's modulus. The highest hardness was measured for the Ta-10Mo alloy (1481 HV) and for the Ta-10TaC composite 1398 HV. This was an increase of over 1000 HV comparing to the control sample.

The use of alloy and ceramic additives results in improved corrosion resistance. Corrosion current density values, despite significant microstructure refinement, are the same or smaller in comparison to microcrystalline tantalum.

Thermogravimetry has shown that nanocrystalline alloys and composites have better temperature stability than microcrystalline Ta. Annealing in the ambient atmosphere leads to a formation of an oxide layer that is brittle and weakly bound to the surface. The use of nitrogen in high-temperature processes results in the formation of a protective diffusion layer of nitrides that are strongly bound to the surface.

1. Wstęp

Odpowiedzią na stawiane obecnie wymagania w wielu gałęziach przemysłu są materiały trudnotopliwe (*refractory materials*), które charakteryzują się bardzo dużą odpornością na działanie wysokiej temperatury oraz sił tarcia. Do grupy tych materiałów należą takie metale jak: tantal (Ta), molibden (Mo), niob (Nb), wolfram (W) i ren (Re). Wszystkie te pierwiastki posiadają temperaturę topnienia przekraczającą 2000°C, dużą gęstość oraz dużą wartość modułu Younga (Tabela 1). Zjawisko pasywacji sprawia, że na ich powierzchni tworzy się ochronna warstwa tlenków dzięki czemu są chemicznie odporne na agresywne działanie stężonych kwasów i zasad. Te cechy sprawiły, że znalazły one zastosowanie głównie w przemyśle elektronicznym, chemicznym, nuklearnym, kosmonautyce, lotnictwie, a nawet medycynie [1-4].

Tantal (Ta) posiada temperaturę topnienia około 3017°C. Klasyfikuje go to dokładnie pośrodku pozostałych pierwiastków trudnotopliwych. Jego gęstość wynosi 16,65 g/cm^3, moduł Younga 186 GPa, a twardość Vickersa dla mikrokrystalicznego Ta około 180 HV. W temperaturze pokojowej charakteryzuje się bardzo dobrą ciągliwością. Odkształcenie plastyczne osiąga ponad 20% [5]. Posiada dwie odmiany alotropowe α-Ta (struktura regularna przestrzenie centrowana) i β-Ta (struktura tetragonalna). W skorupie Ziemskiej występuje w postaci tantalitu i szacuje się, że jest go około 2 ppm (*parts per milion*). Tak mała ilość i jednocześnie trudność w otrzymywaniu materiału o wysokiej czystości sprawia, że jest bardzo drogi. Obecnie około 900 ton Ta jest produkowane każdego roku z czego ponad 60% stosuje się w wytwarzaniu elementów elektronicznych, głównie kondensatorów [4,6,7].

Tabela 1. Porównanie podstawowych właściwości metali trudnotopliwych [8]

WŁAŚCIWOŚCI	Tantal	Wolfram	Molibden	Niob	Ren
Temperatura topnienia [°C]	3017	3410	2623	2477	3186
Gęstość [g/cm^3]	16,7	19,3	10,3	8,6	21,0
Moduł Younga [GPa]	186	411	329	105	463
Twardość Vickersa [HV]	180	349	156	134	249

Tantal między innymi ze względu na zdolność do tworzenia różnowęzłowych i międzywęzłowych roztworów stałych jest bardzo dobrym materiałem, aby na jego bazie

wytwarzać nowe stopy oraz kompozyty. Szacuje się, że około 6% całego wydobycia jest zużywane do produkcji nadstopów. Wprowadzając do tantalu dodatki stopowe lub kompozytowe możemy zmieniać jego właściwości fizyczne oraz chemiczne. Najczęściej do modyfikacji używane są takie pierwiastki jak Mo, W, Ti, Nb, a jako dodatki kompozytowe wzmacniające osnowę tantalową stosuje się TaC, ZrO_2, TaN, SiO_2. Ilość wprowadzonych do układu dodatków zależy od wymaganych właściwości końcowych [9-11].

Metale i stopy trudnotopliwe są bardzo trudne w obróbce. Konwencjonalne metody obróbki metalurgicznej są w wielu przypadkach nieefektywne. Związane jest to między innymi z wysoką temperaturą topnienia materiałów jak i różnicą w temperaturze topnienia składników stopu. Metalurgia proszków (*powder metallurgy*) jest jedną z głównych metod, która pozwala na przezwyciężenie tych problemów [12-17]. Wykorzystuje się w niej wysokiej czystości proszki do wytworzenia elementów litych bez konieczności ich topienia. Do otrzymywania stopów i kompozytów trudnotopliwych można zastosować mechaniczną syntezę (*mechanical alloying – MA*). Jest to proces, który polega na mechanicznym otrzymywaniu stopów metali w procesie mielenia w wysokoenergetycznych młynkach. Synteza zachodzi w reaktorach z kulami (mielnikami) do których wsypuje się proszki składników wejściowych. Podczas mielenia dochodzi do wymieszania składników i rozdrobnienia mikrostruktury w wyniku dużego stopnia odkształcenia plastycznego. Przebiega ona w stanie stałym, gdzie podczas trwania syntezy dochodzi do mechanicznie wyzwalanych reakcji pomiędzy składnikami [12,13,18-20].

Modyfikacji właściwości fizyko-chemicznych w procesie MA można również dokonać poprzez zmianę struktury. Podczas procesu MA dochodzi do umocnienia materiału. Za wzrost właściwości mechanicznych w układach wieloskładnikowych podczas procesu MA odpowiada kilka mechanizmów umocnienia: roztworowego, odkształceniowego, granicami ziaren oraz cząstkami [21-24]. W pierwszym przypadku atomy dodatków stopowych lokują się różnowęzłowo i międzywęzłowo rozpuszczając się w sieci krystalicznej metalu rodzimego. W efekcie dochodzi do jej deformacji spowodowanej różnicą w wielkości atomów. W przypadku umocnienia poprzez odkształcenie dochodzi do zgniotu wynikającego z odkształcenia plastycznego. Zależność Halla-Petcha opisuje umocnienie granicami ziaren i wyrażona jest równaniem [5,23,25,26]:

$$\sigma = k \cdot d^{-\frac{1}{2}},$$

gdzie:

k – stała materiałowa zależna od temperatury i prędkości odkształcenia,

d – średnia średnica ziarna.

Im mniejsze ziarno tym większy jest udział granic ziaren w strukturze. Dodatkowo umocnienie następuje poprzez blokowanie dyslokacji. Ta reguła jest szczególnie przydatna przy wytwarzaniu materiałów nanokrystalicznych (posiadających ziarno o umownej wartości poniżej 100 nm) oraz ultradrobnoziarnistych (0,1–2 μm).

Tantal posiada doskonałą odporność na korozje [9,10,27-30]. Niestety tylko 4% całego światowego wydobycia jest wykorzystywane w przemyśle chemicznym. Jest to bezpośrednio związane z jego wysoką ceną, ponieważ obecnie stosowane elementy wykonane są z 5-10 razy tańszej stali nierdzewnej lub tytanu. Warstwa tlenków która powstaje na powierzchni jest bardzo stabilna i silnie związana z podłożem. Dodatkowo odpowiednio przygotowaną powierzchnię można modyfikować elektrochemiczne, na przykład przez zastosowanie anodowania. Takie badania pozwoliłyby na wytworzenie warstwy powierzchniowej o w pełni kontrolowanych właściwościach i grubości [31-33].

Aktualnie brakuje dokładnej analizy i szerokiego spektrum badań porównujących właściwości fizyczne i chemiczne materiałów na bazie tantalu, w szczególności stopów z nanostrukturą. Podczas ostatniej dekady zauważono trend zwłaszcza w użyciu materiałów kompozytowych. Warunki w których pracują elementy wykonane z tych materiałów nie należą do łatwych. W związku z tym zaawansowane stopy oraz kompozyty metalowo-ceramiczne stają się potencjalnymi materiałami do wykonywania elementów maszyn do pracy w podwyższonej temperaturze, agresywnym środowisku korozyjnym oraz w miejscach gdzie występują zwiększone siły tarcia. W dalszym ciągu istnieje potrzeba prowadzenia szerokich badań podstawowych nad takimi materiałami.

2. Cel i zakres badań

Celem przeprowadzonych badań było opracowanie nowych stopów i kompozytów na bazie tantalu o strukturze nanokrystalicznej lub ultradrobnoziarnistej o lepszych właściwościach w stosunku do mikrokrystalicznego tantalu.

Zakres badań, przedstawiony jako zbiór jednotematycznych publikacji [1,9,10,24, 34-36] przedstawia proces wytwarzania oraz badania właściwości dwuskładnikowych

nanokrystalicznych/ultradrobnoziarnistych stopów oraz kompozytów na bazie tantalu. W ramach pracy doktorskiej wytworzono stopy Ta-xNb, Ta-xMo oraz Ta-xW, gdzie „x" przyjmuje wartości 5%, 10%, 20%, 40% wagowych dodatku stopowego. Kompozyty wytworzono stosując analogicznie proporcje dodatków TaC, ZrO_2 i Y_2O_3 jako fazę zbrojącą. Materiały te w postaci proszkowej wytworzono metodą mechanicznej syntezy, które poddano prasowaniu na gorąco przy użyciu prasy wyposażonej w moduł nagrzewania impulsowo-plazmowego (*pulse plasma sintering – PPS*). Wszystkie procedury związane z mechaniczną syntezą, nasypywaniem proszków, opróżnianiem reaktorów, wypełnianiem matryc do spiekania były wykonywane w atmosferze ochronnej argonu. Było to niezbędne, aby ograniczyć proces utleniania. W celu dokładnej charakteryzacji otrzymanych materiałów przeprowadzono następujące badania:

- strukturalne, wykorzystując dyfraktometrię rentgenowską XRD,
- mikrostruktury z użyciem elektronowej mikroskopii transmisyjnej TEM i skaningowej SEM mikroskopii optycznej, oraz sił atomowych AFM, a także technikę dynamicznego rozpraszania światła DLS,
- morfologii z użyciem skaningowej mikroskopii elektronowej SEM,
- właściwości mechanicznych z użyciem metody nanoindentacji,
- odporności na korozję elektrochemiczną z zastosowaniem metody pomiaru krzywych polaryzacji oraz zmian masy i stanu powierzchni w korozji gazowej,
- stabilności temperaturowej z wykorzystaniem termograwimetrii TGA.

Przeprowadzone badania i ich analiza pozwoliły na sformułowanie tezy, że: **proces mechanicznej syntezy umożliwia wytworzenie nanokrystalicznych/ ultradrobnoziarnistych stopów i kompozytów na bazie tantalu. Wprowadzenie dodatków stopowych oraz kompozytowych do tantalu w połączeniu z rozdrobnieniem mikrostruktury prowadzi do polepszenia właściwości fizyko-chemicznych w porównaniu z mikrokrystalicznym tantalem.**

3. Dobór materiałów

Właściwości materiałów na bazie tantalu mogą być modyfikowane poprzez odpowiedni dobór dodatków stopowych oraz fazy ceramicznej [24]. W omawianym cyklu publikacji stanowiących trzon pracy doktorskiej przedstawiono stopy Ta z niobem, wolframem i molibdenem [9,10]. Wszystkie trzy pierwiastki należą do rodziny trudnotopliwych. Podobnie jak tantal charakteryzują się taką samą budową komórki

elementarnej, regularną przestrzennie centrowaną (*body-centered cubic BCC*). Natomiast w przeciwieństwie do tantalu posiadają mniejsze wartości promienia atomowego (Tabela 2). Ta właściwość ma znaczący wpływ na postać i naprężania wprowadzane do sieci krystalicznej w przypadku, gdy atom tantalu zostanie zastąpiony atomem W, Mo, lub Nb. Na postać sieci krystalicznej ma również wpływ stała sieci. Wprowadzenie niobu (3,3066 Å) do tantalu (3,3058 Å) powoduje zwiększenie wartości stałej sieci krystalicznej, a wolfram (3,1649 Å) i molibden (3,1470 Å) powodują jej zmniejszenie. Z taką samą zależnością zmieniają się wartości objętości komórki elementarnej.

Tabela 2. Wybrane właściwości fizyczne i chemiczne wykorzystanych metali [8].

WŁAŚCIWOŚCI	Tantal	Wolfram	Molibden	Niob
Struktura sieci krystalicznej	Regularna przestrzennie centrowana (RPC, A2)	Regularna przestrzennie centrowana (RPC, A2)	Regularna przestrzennie centrowana (RPC, A2)	Regularna przestrzennie centrowana (RPC, A2)
Promień atomowy [pm]	200	193	190	198
Stała sieci krystalicznej [Å]	3,3060	3,1648	3,1470	3,3066
Masa atomowa [u]	180,95	183,84	95,95	92,91

Materiały ceramiczne mają sporo zalet ale również kilka wad. Z jednej strony wysoka odporność na działanie sił tarcia i czynników chemicznych oraz wysoką temperaturę sprawiają, że w niektórych gałęziach przemysłu są niezastąpione. Z drugiej strony są bardzo kruche i nieodporne na kruche pękanie. Ceramika pomimo, iż jest odporna na działanie wysokiej temperatury, to w wielu przypadkach wykazuje brak odporności na gwałtowne zmiany temperatury (szok termiczny). W krytycznych sytuacjach bardzo łatwo dochodzi do pękania. W związku z tym postanowiono połączyć powyższe właściwości wraz z właściwościami tantalu i wytworzyć metaliczne materiały kompozytowe (*metal matrix composites – MMC*).

Węglik tantalu (TaC) został zaproponowany jako jeden z materiałów ceramicznych (Tabela 3). Jego główną zaletą jest bardzo wysoka temperatura topnienia i twardość. TaC jest powszechnie stosowany w przemyśle do wyrobu materiałów skrawających, głównie ze względu na swoją dużą twardość. Ze względu na dużą gęstość TaC oraz korzystne cechy ceramiki tlenkowej postanowiono dodatkowo wytworzyć kompozyty z materiałami

tlenkowymi: ZrO_2 i Y_2O_3 o mniejszej gęstości i porównać ich wpływ na właściwości otrzymanych materiałów.

Tabela 3. Charakterystyka użytych materiałów ceramicznych [8].

WŁAŚCIWOŚCI	Węglik tantalu (IV)	Tlenek cyrkony (IV)	Tlenek itru (III)
Temperatura topnienia [°C]	3880	2680	2425
Gęstość [g/cm^3]	13,9	5,7	5,01
Masa molowa [g/mol]	192,96	123,22	225,81
Twardość [HV]	1530	1122	620

4. Proces wytwarzania materiałów

Stopy i kompozyty na bazie tantalu w postaci proszków wytworzono stosując proces mechanicznej syntezy [34-36].

Mechaniczna synteza przebiega w stanie stałym. Składniki w postaci proszków metali umieszczane są w reaktorze młynka, w atmosferze ochronnej. Podczas procesu w wysokoenergetycznych młynkach dochodzi do zderzeń kula-proszek-kula lub kula-proszek-ścianka reaktora, wskutek czego pojawiają się duże odkształcenia plastyczne. Następnie dochodzi do umocnienia materiału i powstania struktury warstwowej. Równolegle dochodzi do stapiania w stanie stałym i kruszenia składników syntezy. Następnie ziarna pękają i cykl się powtarza. W miarę upływu czasu i liczby defektów dochodzi do znacznego rozdrobnienia struktury ziaren proszków. Podczas gdy synteza prowadzona jest z wykorzystaniem proszków plastycznych i kruchych, jak w przypadku cermetali, uzyskuje się jednorodny rozkład cząstek ceramicznych w plastycznej osnowie metalu. Kinetyka procesu jest uzależniona od wielu czynników. Mają one wpływ na szybkość procesu, stopień rozdrobnienia i amorfizację. Mechaniczna synteza zależy od trzech głównych parametrów: temperatury procesu, energii mielenia i czasu. Zmiana jednego z nich może skutkować otrzymaniem innych efektów niż zaplanowane.

Wszystkie opisane materiały zostały wykonane w jednakowy sposób. Używano młynka typu *shaker* Spex 8000 o prędkości obrotowej 875 obr./min. Jest to istotny parametr, który jest bezpośrednio związany z energią procesu. W reaktorze umieszczono pięć mielników. Stosunek ich masy do masy proszku wynosił 3:1. Celowo wartość ta jest stosunkowo mała żeby ograniczyć wzrost temperatury w reaktorze oraz zanieczyszczenia w postaci żelaza pochodzącego ze stalowych mielników i reaktora. Mogłoby to

doprowadzić do rekrystalizacji proszków i wzrostu krystalitów. Z przeprowadzonych pomiarów wynikało, że wartość temperatury wzrastała najwyżej do 40°C, co nie miało wpływu na produkty końcowe. Ponieważ masa mielników była mniejsza to proces mechanicznej syntezy został wydłużony do 48 godzin [18,19,24].

Tak otrzymane proszki poddano prasowaniu na gorąco. Wykorzystano do tego prasę jednoosiową. Ciśnienie prasowania wynosiło 50 MPa. Otrzymano w ten sposób lite próbki o cylindrycznym kształcie i średnicy około 8 mm. W komorze prasy panowały warunki obniżonego ciśnienia 10^{-2} Pa. Temperatura prasowania została wyznaczona eksperymentalnie i była zależna od składu chemicznego, uzyskanej struktury i porowatości. Próbka odniesienia, czyli mikrokrystaliczny tantal wymagał stosunkowo wysokiej temperatury spiekania 1500°C. Rozdrobnienie struktury w procesie MA skutkuje obniżeniem wymaganej temperatury konsolidacji, która dla nanokrystalicznego tantalu wynosiła 1000°C. Przy wytwarzaniu stopów i kompozytów temperaturę zwiększono do 1300°C. Czas spiekania w zadanej temperaturze wynosił 5s, a szybkość nagrzewania 650 °C/min. Takie parametry pozwalały na uzyskanie litych materiałów o bardzo małej porowatości wynoszącej około 1,5-3% przy zachowaniu struktury nanokrystalicznej lub ultradrobnoziarnistej [18,19,24].

5. Struktura i mikrostruktura

Na każdym etapie badań przeprowadzono analizę struktury metodą dyfraktometrii rentgenowskiej XRD. Identyfikację charakterystycznych refleksów wykonano przy użyciu bazy krystalograficznej ICDD-JCPDS programu Highscore. Kluczowym i równocześnie pierwszym etapem badań było wyznaczenie zmiany struktury czystego mikrokrystalicznego Ta podczas trwania MA w czasie od 0 do 48 godzin [18]. Jak zaobserwowano, w pierwszych godzinach procesu następuje gwałtowny spadek intensywności refleksów. W dalszych etapach postępuje zwiększenie szerokości połówkowej. Powodem tego jest zmniejszenie wielkości krystalitów i wprowadzenie do sieci naprężeń wewnętrznych. Dodatkowo dochodzi do częściowej amorfizacji struktury. Średnia wielkość ziarna dla badanych materiałów proszkowych wynosiła od 31 nm do 87 nm [1]. Widmo na Rys. 1b przedstawia proszek po MA dla stopu Ta-5Mo [10]. Po procesie MA nastąpiło wyraźne zwiększenie wartości szerokości połówkowej i zmniejszenie intensywności refleksów. Nie zaobserwowano dodatkowych refleksów,

które świadczyłyby o powstawaniu dodatkowych faz. Molibden całkowicie rozpuszcza się w tantalu tworząc roztwór stały. Po procesie spiekania (Rys. 1c,d,e) stopy Ta-5Nb, Ta-5Mo i Ta-5W mają strukturę roztworu stałego. Pojawienie się dodatkowej fazy węglikowej wynika z zastosowania matryc grafitowych w procesie prasowania na gorąco [10].
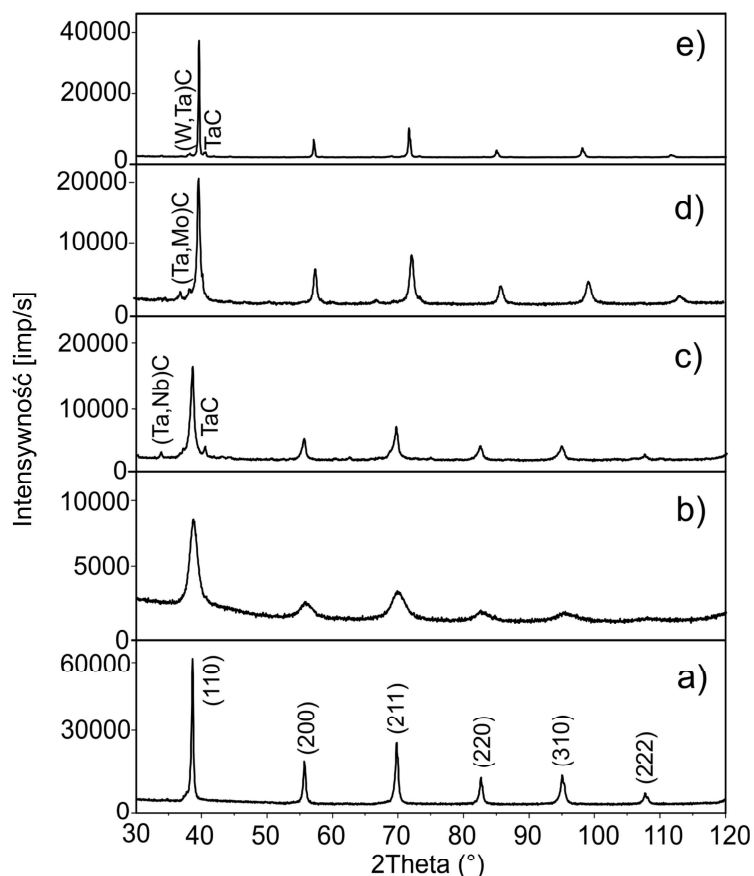
Rysunek 1. Przykładowe widma XRD dla mikrokrystalicznego proszku Ta (a), nanokrystalicznego proszku stopu Ta-5Mo po procesie MA (b) oraz spieków stopów Ta-5Nb (c), Ta-5Mo (d) i Ta-5W (e) [10]

Na Rys. 2 przedstawiono widma dla nanokrystalicznych kompozytów Ta-5ZrO$_2$ i Ta-40ZrO$_2$ [24]. W obu przypadkach dla proszków po procesie MA (Rys. 2c,d) dochodzi do znacznego zwiększenia wartości szerokości połówkowej i zmniejszenia intensywności refleksów. Dla większych stosunków wagowych dodatków ceramicznych zaobserwowano dodatkowe refleksy pochodzące od fazy tlenkowej w przypadku ZrO$_2$ i Y$_2$O$_3$ oraz węglikowej w przypadku TaC. Proces prasowania na gorąco prowadzi do otrzymania nanokompozytów o strukturze dwufazowej. Tak samo jak w przypadku stopów zaobserwowano charakterystyczne refleksy wynikające z obecności węglików powstałych na skutek stosowania matryc grafitowych.
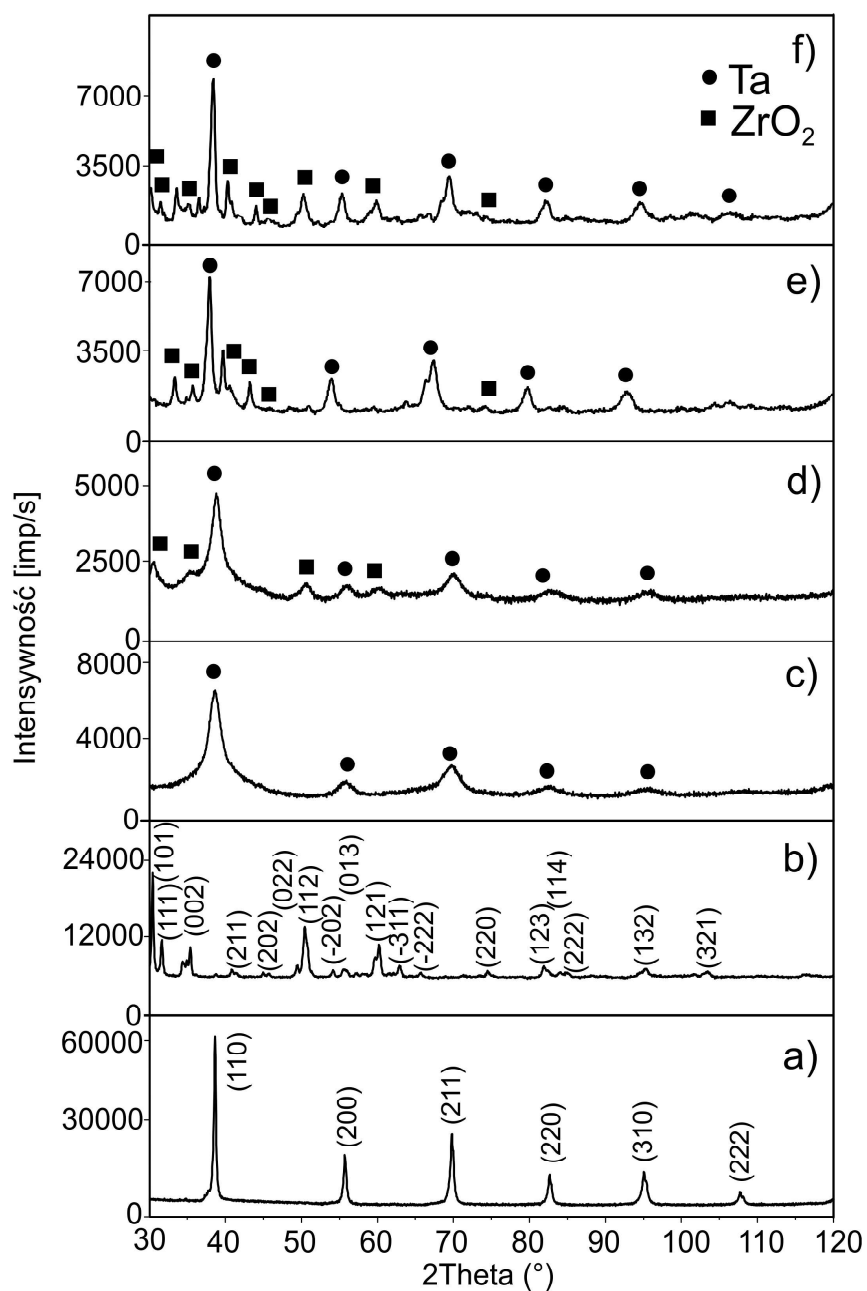
Rysunek 2. Przykładowe widma XRD dla mikrokrystalicznego proszku Ta (a), proszku ZrO₂ (b), proszków po procesie MA nanokrystalicznego kompozytu Ta-5ZrO₂ (c) i Ta-40ZrO₂ (d) oraz nanokrystalicznego spieku kompozytu Ta-5ZrO₂ (e) i Ta-40ZrO₂ (f) [24]

Stosując mikroskop SEM zobrazowano morfologię cząstek proszków oraz mikrostruktury litych spieków. Na Rys. 3a,b bardzo dobrze widoczne są agregaty i aglomeraty, powstałe w procesie MA [18,19,36]. Przykładowe obrazy powierzchni (Rys. 3c,d) zgładów metalograficznych materiałów z dodatkiem 5% niobu i 5% wolframu

potwierdziły ich jednorodność i małą porowatość. Strukturę nanokrystaliczną potwierdzono wykonując obserwację mikroskopem TEM oraz AFM (Rys. 4) [9].
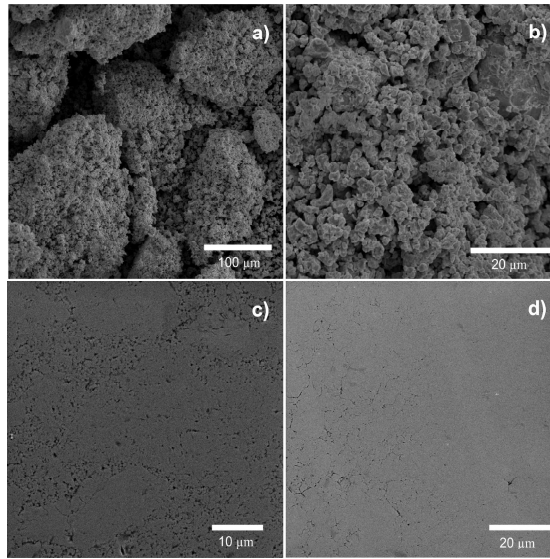
Rysunek 3. Obrazy SEM dla proszku nanokrystalicznego tantalu po wysokoenergetycznym rozdrabnianiu (a) i (b) oraz litych spieków Ta-5Nb (c) i Ta-5W (d) [18,19,36]
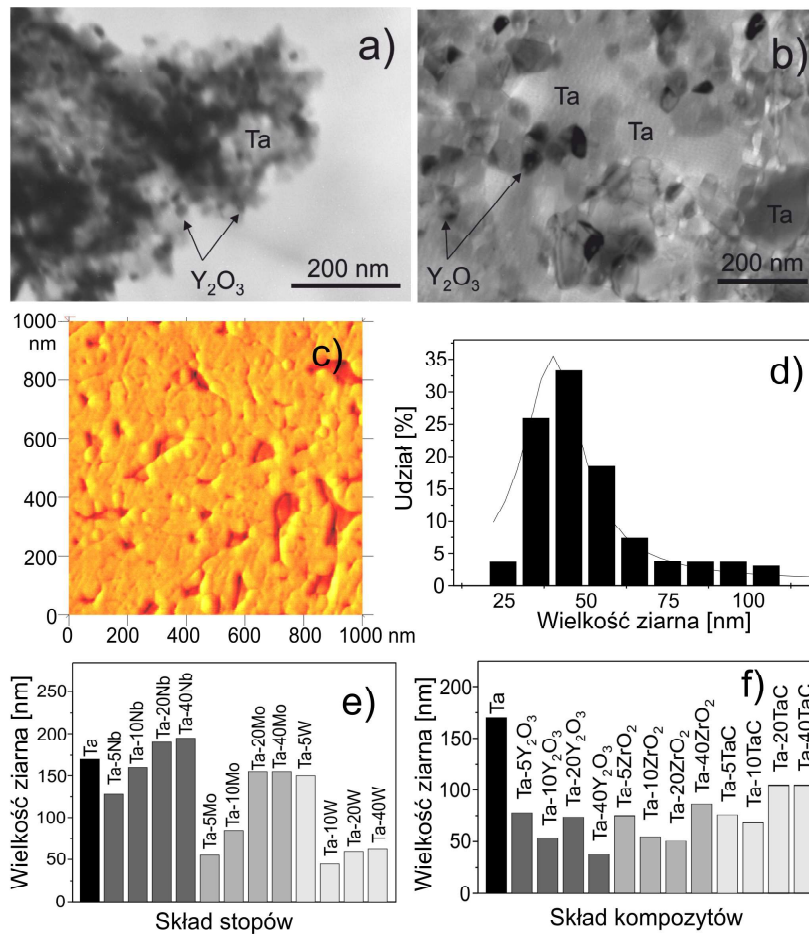
Rysunek 4. Obraz TEM otrzymanego nanokrystalicznego proszku Ta-20Y₂O₃ (a), nanokrystalicznego spieku Ta-20Y₂O₃ (b), obraz AFM nanokrystalicznego spieku Ta-40Y₂O₃ (c), przykładowy rozkład wielkości ziaren spieku Ta-40Y₂O₃ określony na podstawie analizy wyników AFM (d) i wartości średnie wielkości ziaren na podstawie AFM dla nanokrystalicznych spieków (e) oraz kompozytów (f) [9,10]

6. Właściwości mechaniczne

Właściwości mechaniczne zostały określone na podstawie pomiarów krzywych obciążenie-odkształcenie zarejestrowanych w procesie nanoindentacji. Tak zwany nanotwardościomierz umożliwia przeprowadzenie dokładnej analizy zjawisk jakie zachodzą w materiale po przyłożeniu siły deformującej przy małym obciążeniu. Wynikiem badań są krzywe obciążenie-odkształcenie na podstawie których można wyznaczyć między innymi twardość i moduł sprężystości oraz określić jednorodność materiału [24,37].

Wartość przyłożonego obciążenia podczas badań wynosiła 300 mN w czasie 20 sekund. Wykonano pięć pomiarów dla każdej próbki. Z otrzymanych krzywych wynika, że większość wytworzonych materiałów charakteryzują się dużą jednorodnością. Świadczy o tym powtarzalność pomiarów, pokrywanie się otrzymanych krzywych oraz brak odchyleń od liniowości (Rys 5).
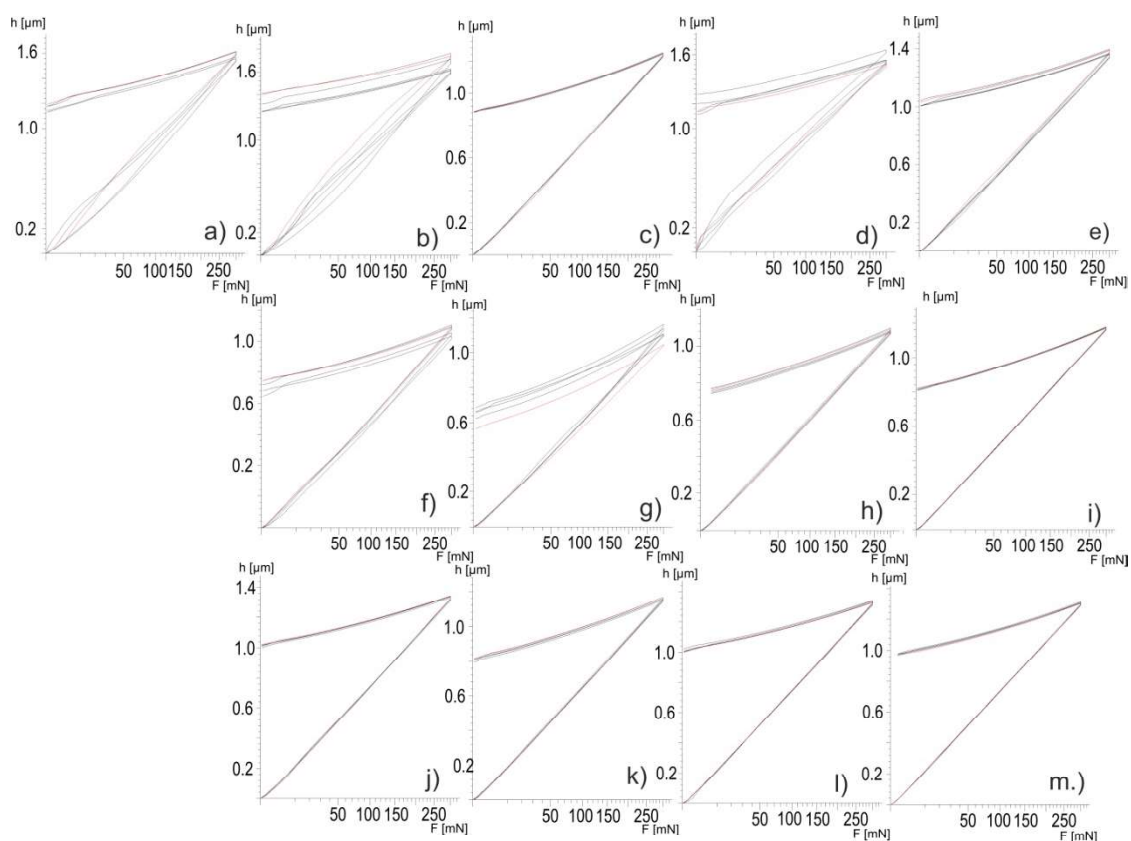
Rysunek 5. Krzywe obciążenie-odkształcenie dla nanokrystalicznego spieku Ta (a) oraz nanokrystalicznych spieków: Ta-5Nb (b), Ta-10Nb (c), Ta-20Nb (d), Ta-40Nb (e), Ta-5Mo (f), Ta-10Mo (g), Ta-20Mo (h), Ta-40Mo (i), Ta-5W (j), Ta-10W (k), Ta-20W (l) i Ta-40W (m) [37]

Dzięki modyfikacji składu chemicznego oraz mikrostruktury doszło do znaczącego zwiększenia twardości (Tabela 4). Rozdrobnienie mikrostruktury zgodnie z opisaną wcześniej zasadą Halla-Petcha skutkuje zwiększeniem twardości z około 346 HV dla

mikrokrystalicznego Ta do 583 HV dla nanokrystalicznego Ta. Wprowadzenie dodatków stopowych powoduje 2-3 krotny wzrost twardości. Największą twardość otrzymano dla stopów z układu Ta-Mo – 1481 HV dla Ta-10Mo. Bardzo dobre rezultaty otrzymano również dla stopów typu Ta-W. Moduł Younga dla wszystkich materiałów z wyjątkiem Ta-5Nb oraz Ta-20Nb wynosił powyżej 200 GPa, gdzie najwyższą wartość 343 GPa osiągnięto dla Ta-20Mo [37].

Tabela 4. Właściwości mechaniczne nanokrystalicznych stopów tantalu [37]

WŁAŚCIWOŚCI MECHANICZNE		
	HV	E_{IT} [GPa]
Ta micro	346,00±30,00	180,00±6,00
Ta nano	583,61±18,98	163,96±8,36
Ta-5Nb	509,30±46,31	170,77±6,09
Ta-10Nb	990,07±7,84	250,63±1,79
Ta-20Nb	592,79±35,64	188,58±10,33
Ta-40Nb	784,18±21,91	222,31±1,93
Ta-5Mo	940,73±48,25	245,62±12,44
Ta-10Mo	1481,58±158,17	230,17±21,78
Ta-20Mo	1317,83±29,52	343,13±4,56
Ta-40Mo	1121,66±6,48	285,22±2,36
Ta-5W	812,87±8,01	257,74±2,70
Ta-10W	1136,84±16,92	304,03±2,75
Ta-20W	818,84±9,69	263,66±4,93
Ta-40W	873,56±9,20	254,27±4,22

Bardzo dobre wyniki właściwości mechanicznych otrzymano również dla kompozytów (Rys. 6, Tabela 5). Pomiar nanotwardościomierzem materiałów wielofazowych o ultradrobnej- i nanostrukturze jest skomplikowany. Ważnym aspektem jest wybór miejsca pomiaru. Największe wartości twardości otrzymano dla kompozytów Ta-TaC. Najniższa wartość wyniosła 984 HV (Ta-5TaC), a najwyższa 1398 HV (Ta-10TaC). Wyznaczone wartości modułu sprężystości dla tych kompozytów wynosiły powyżej 300 GPa. Tak samo jak w przypadku stopów, dla kompozytów krzywe pomiarowe obciążenie-odkształcenie w większość charakteryzowały się jednorodnym rozkładem (Rys. 6). Rozrzut wyników pomiarów pojawiał się przy dużym udziale fazy ceramicznej (40%) [24].
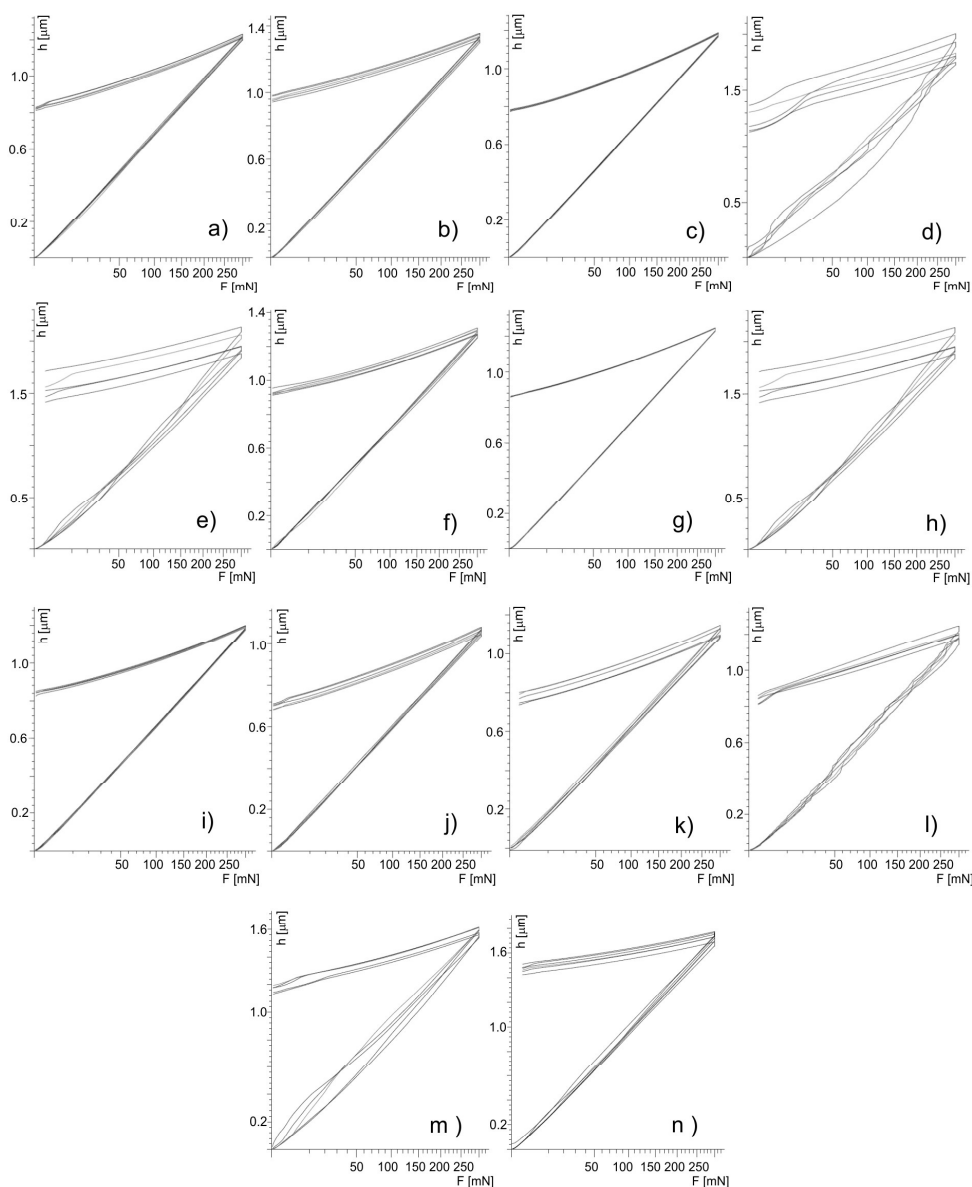
Rysunek 6. Krzywe obciążenie-odkształcenie dla nanokrystalicznych kompozytów Ta-5Y$_2$O$_3$ (a),
Ta-10Y$_2$O$_3$ (b), Ta-20Y$_2$O$_3$ (c),Ta-40Y$_2$O$_3$ (d), Ta-5ZrO$_2$ (e), Ta-10ZrO$_2$ (f), Ta-20ZrO$_2$ (g), Ta-40ZrO$_2$ (h),
Ta-5TaC (i), Ta-10TaC (j), Ta-20TaC (k), Ta-40TaC (l) oraz nanokrystaliczengo spieku Ta (m)
i mikrokrystalicznego spieku Ta (n) [24]

Tabela 5 Właściwości mechaniczne nanokrystalicznych kompozytów na bazie tantalu [24]

WŁAŚCIWOŚCI MECHANICZNE		
	HV	E$_{IT}$ [GPa]
Ta micro	346,00±30,00	180,00±6,00
Ta nano	583,61±18,98	163,96±8,36
Ta-5Y$_2$O$_3$	1055±23	248±2
Ta-10Y$_2$O$_3$	835±23	234±2
Ta-20Y$_2$O$_3$	1165±8	242±1
Ta-40Y$_2$O$_3$	436±52	114±10
Ta-5ZrO$_2$	821±24	231±4

|		
Ta-10ZrO$_2$	920±24	240±8
Ta-20ZrO$_2$	1003±3	246±1
Ta-40ZrO$_2$	366±44	115±3
Ta-5TaC	984±21	273±5
Ta-10TaC	1398±46	336±5
Ta-20TaC	1252±6	303±11
Ta-40TaC	994±48	346±12

7. Odporność na korozję

Istotną częścią badań były pomiary odporności na korozję [9,10,34]. Głównym zamierzeniem była ocena tendencji materiału do procesów korozji w środowisku agresywnym zawierającym jony chloru. Ma to znacznie nie tylko w przemyśle, ale również w kontekście aplikacji biomedycznych, gdzie takie materiały również są coraz częściej wykorzystywane. Tantal jest materiałem, który posiada bardzo dobrą odporność na korozję dzięki samoczynnie tworzącej się warstwie tlenku na jego powierzchni. Problemem może być nanostruktura, która przyczynia się do obniżenia odporności korozyjnej większości materiałów.

Odporność korozyjną wytworzonych materiałów badano w roztworze Ringera, w temperaturze pokojowej 21°C. Analizę wyników dokonano na podstawie krzywych polaryzacji poprzez dopasowanie stycznych Tafela. Rozdrobnienie mikrostruktury czystego Ta powoduje zwiększenie wartości gęstości prądu korozyjnego (I_{corr}) oraz przesunięcie wartości potencjału (E_{corr}) w kierunku wartości ujemnych (Rys. 7) [10]. Pogorszenie odporności korozyjnej nanokrystalicznego Ta jest bezpośrednio związane ze zwiększeniem udziału granic ziaren oraz dużej energii wewnętrznej materiałów nanokrystalicznych. Wprowadzenie dodatków stopowych do sieci krystalicznej powoduje obniżenie wartości gęstości prądu korozyjnego (wzrost odporności na korozję) oraz przesunięcie potencjału korozyjnego w kierunku wartości dodatnich. Otrzymane wyniki są porównywalne z wynikami dla mikrokrystalicznego Ta, a w większości przypadków nawet lepsze (niższe wartości gęstości prądu korozyjnego). Najlepszą odporność na korozję wykazuje stop Ta-5Mo [9,10,34].
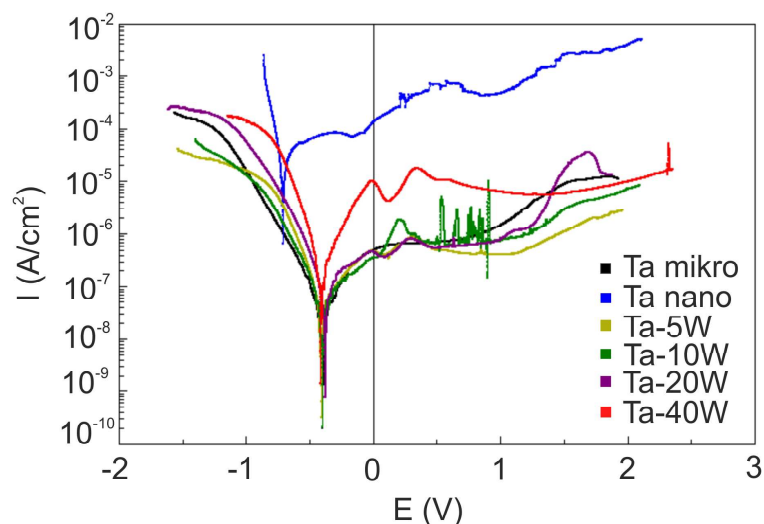
Rysunek 7. Przykładowe krzywe polaryzacji dla stopów Ta-W w porównaniu z mikrokrystalicznym i nanokrystalicznym Ta [10]

W taki sam sposób przeprowadzono badania dla nanokrystlicznych kompozytów. Wprowadzenie do struktury cząstek ceramicznych skutkuje znacznym polepszeniem parametrów korozyjnych w porównaniu do czystego nanokrystalicznego tantalu (Rys. 8). Różnice gęstości prądu korozyjnego pomiędzy nanokrystalicznym Ta, a stopami i kompozytami były znaczące i wahały się pomiędzy 3 a 5 rzędów wielkości. Ceramika podobnie jak dodatki stopowe powodują, że parametry korozyjne są porównywalne, a nawet lepsze w porównaniu do mikrokrystalicznego tantalu [10]. W przypadku kompozytu Ta-40Y$_2$O$_3$, zaobserwowano, że posiadał on właściwości izolacyjne, w związku z czym nie przewodził ładunku elektrycznego i pomiar odporności na korozję nie był możliwy.
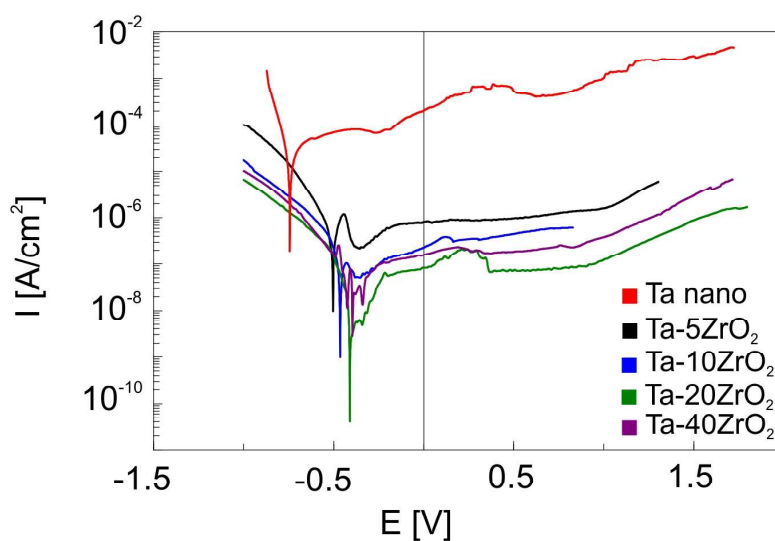
Rysunek 8. Przykładowe krzywe polaryzacji dla nanokrystalicznych kompozytów Ta-ZrO$_2$ w porównaniu z nanokrystalicznym Ta [9]

8. Stabilność temperaturowa

Ostatnia publikacja cyklu dotyczy analizy termograwimetrycznej (TGA) [1]. Badaniom zostało poddane zachowanie stopów i kompozytów w warunkach podwyższonej temperatury i atmosfery utleniającej. Jak donosi literatura stabilna warstwa tlenków tworzy się w temperaturze przekraczającej 400°C [39,40]. Jednakże przeprowadzając taki proces w atmosferze otoczenia często dochodzi do dyfuzji tlenu po granicach ziaren, gdzie tworzą się tlenki i równocześnie zaburzają strukturę materiału. Efektem jest kruszenie i łuszczenie, a w ostateczności dochodzi do oderwania warstwy tlenków. Z drugiej strony wytrącające się tlenki zapobiegają rozrostowi ziaren w podwyższonej temperaturze [38-40].

Materiały konstrukcyjne na bazie tantalu, ze względu na wysoką temperaturę topnienia, znajdują zastosowanie jako materiały żaroodporne i żarowytrzymałe. Problemem jest atmosfera utleniająca działająca w podwyższonej temperaturze i jednocześnie nanostruktura sprzyjająca dyfuzji [39]. Modyfikacja składu chemicznego dodatkami o właściwościach trudnotopliwych może zapewnić odpowiednią odporność na utlenianie wysokotemperaturowe [41].

Analizę TGA przeprowadzono w zakresie temperatury od 21°C do 900°C w atmosferze azotu. Drugim badaniem było wygrzewanie próbek w piecu przez dwie godziny w atmosferze otoczenia (powietrza) i azotu [1]. Z badań TGA wynika, że nanokrystaliczne stopy i kompozyty charakteryzują się dużo mniejszym przyrostem masy w porównaniu z mikrokrystalicznym tantalem (Rys. 9). Wśród stopów najmniejszy przyrost masy 105,34% (gdzie 100% stanowi wartość bazową) zaobserwowano dla Ta-10W. Jest to wynik o około 3% lepszy niż w przypadku czystego nanokrystalicznego Ta i zarazem najmniejszy dla wszystkich wytworzonych materiałów. Bardzo dobre rezultaty otrzymano dla kompozytów, gdzie najmniejszy przyrost masy wynosił 106,78%. Przyrost masy w przypadku sześciu materiałów był równy lub mniejszy niż dla nanokrystalicznego Ta. Najistotniejszy wydaje się fakt, iż wszystkie materiały mają lepszą stabilność temperaturową niż mikrokrystaliczny tantal (121,69%). Na podstawie wyników TGA wyznaczono kinetykę procesu oraz energię aktywacji [1].
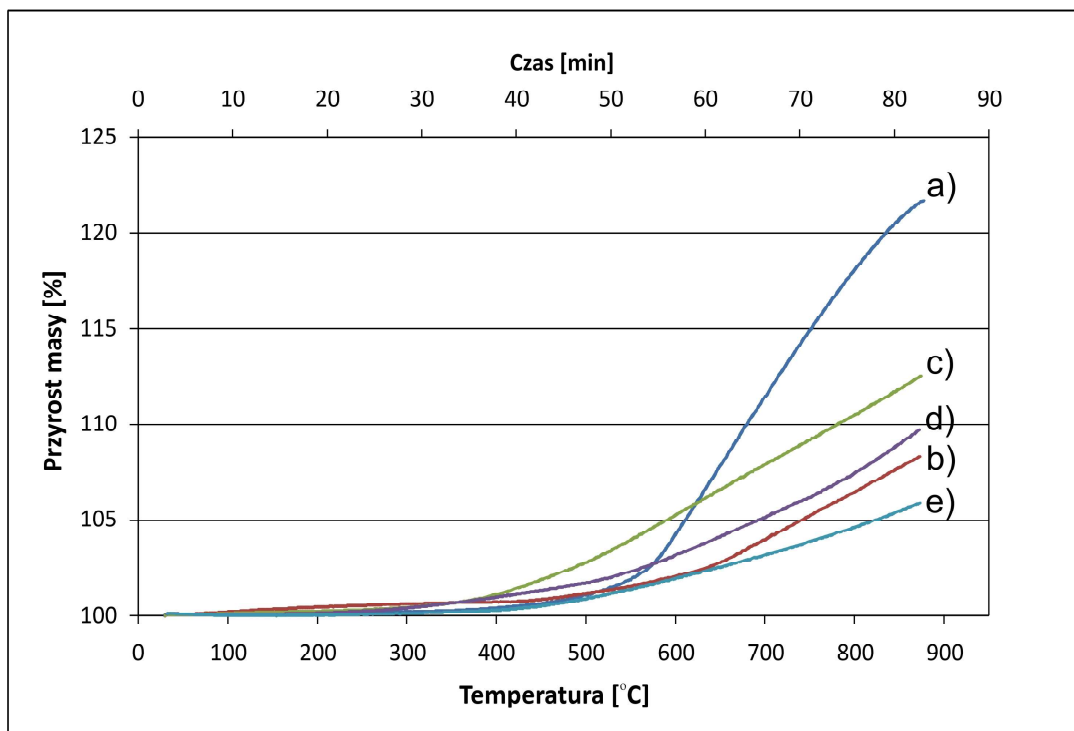
Rysunek 9. Przykładowe krzywe TGA dla mikrokrystalicznego Ta (a), nanokrystalicznego Ta (b), Ta-40Nb (c), Ta-40Mo (d), Ta-40W (e) [1]

Wygrzewanie próbek w 1000°C, w atmosferze powietrza prowadzi do powstania różnych tlenków co zaobserwować można na widmach XRD [1]. Ich rodzaj zależy od składu chemicznego materiału rodzimego. Głównym produktem utleniania jest β-Ta_2O_5. Według literatury jest to najstabilniejszy tlenek, który najczęściej powstaje w takich procesach [32,33]. Z analizy XRD wynika, że przy większej zawartości dodatków stopowych (20-40%) obecne są również ich tlenki takie jak MoO_2, Nb_2O_5, WO_3. W każdym przypadku warstwa tlenków słabo przylegała do podłoża. Zaobserwowano proces kruszenia i złuszczania powierzchni, co było efektem korozji gazowej.

Nanokrystaliczny tantal i jego stopy zachowują się w inny sposób jeżeli wygrzewanie przeprowadzi się w atmosferze azotu. Z analizy metalograficznej przekroju powierzchni zgładu wynika, że dochodzi do wytworzenia dyfuzyjnej warstwy azotków. Świadczy o tym charakterystyczny złoty kolor powierzchni próbek. Przeprowadzone badania strukturalne potwierdzają obecności azotków. Po przypisaniu refleksom danych z bazy ICDD-JCPDS zidentyfikowano kilka ich rodzajów. Były to głownie: TaN oraz NbN, Mo_2N, W_2N. Wykonano obrazy przekrojów powierzchni zgładów metalograficznych z wykorzystaniem mikroskopii SEM, gdzie zaobserwowano warstwy azotków o grubości od około 40 μm do 150 μm (Rys. 10).
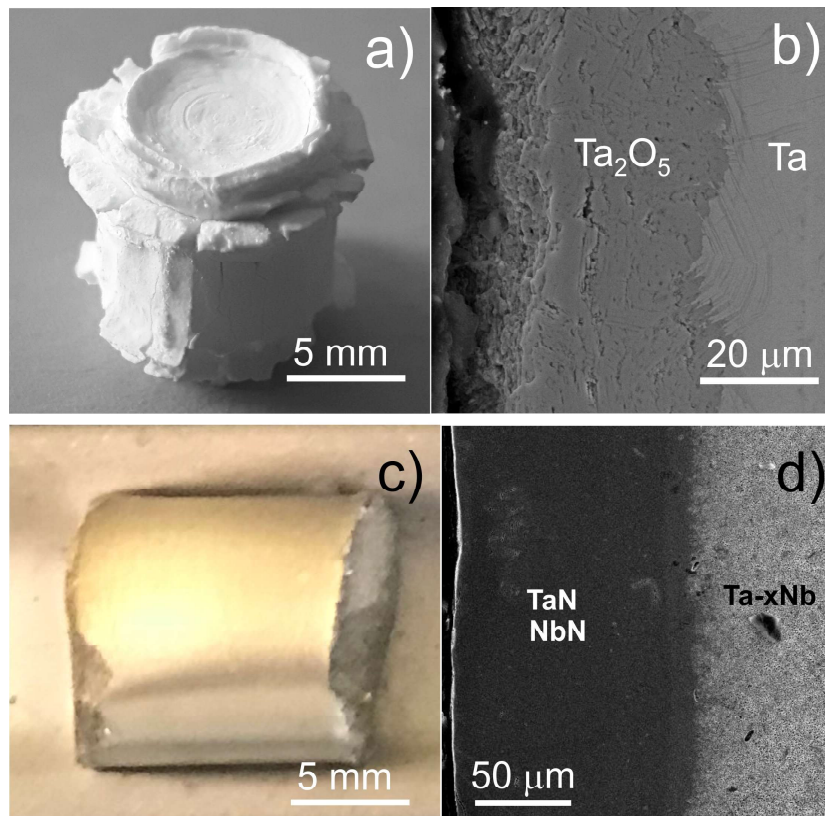
Rysunek 10. Obraz mikrokrystalicznego spieku Ta po utlenianiu (a), przekrój poprzeczny warstwy tlenkowej (b), obraz mikrokrystalicznego Ta po wygrzewaniu w azocie (c), przekrój poprzeczny warstwy azotowanej dla nanokrystalicznego spieku Ta-20Nb [1]

Jednoznacznie stwierdzono, że warstwy te są jednolite i silnie związane z podłożem. Nie zaobserwowano żadnych pęknięć lub złuszczeń co mogłoby spowodować odsłonięcie materiału rdzenia [1].

Proces azotowania jest obecnie jednym z intensywnie rozwijanych sposobów modyfikacji powierzchni. Otrzymane azotki tantalu i metali dodatków stopowych oraz podstawowa analiza ich właściwości jest bardzo dobrym wprowadzeniem do dalszych badań.

9. Podsumowanie

Przeprowadzone badania nad wytwarzaniem i właściwościami materiałów nanokrystalicznych/ultradrobnoziarnistych na bazie tantalu, pozwoliły na wysunięcie następujących wniosków:

– technologia metalurgii proszków złożona z procesu mechanicznej syntezy i prasowania na gorąco umożliwia wytworzenie nanokrystalicznych/ ultradrobnoziarnistych stopów i kompozytów na bazie tantalu.

- wprowadzenie do sieci krystalicznej dodatków stopowych skutkuje powstaniem roztworów stałych w układach Ta-Nb, Ta-Mo i Ta-W,

- po procesie mechanicznej syntezy proszków Ta z udziałem fazy ceramicznej otrzymano materiały wielofazowe,

- mechaniczna synteza prowadzi do otrzymania materiałów o średniej wielkości ziaren w przedziale 31-87 nm, a proces prasowania na gorąco prowadzi do otrzymania litych spieków o wielkości ziaren w przedziale 43-195 nm. Przykładowo najmniejsze ziarna uzyskano w spiekach Ta-5W: 47 nm i kompozytach Ta-40Y_2O_3: 43 nm,

- rozdrobnienie mikrostruktury czystego tantalu skutkuje pogorszeniem odporności na korozję (I_{corr}=1,198·10^{-5} A/cm^2). Zastosowanie dodatków stopowych i kompozytowych prowadzi do obniżenia gęstości prądu korozyjnego co świadczy o polepszeniu odporności korozyjnej (I_{corr} dla najlepszego stopu Ta-5Mo: 1,173·10^{-8} A/cm^2 oraz kompozytu Ta-20Y_2O_3: 4,064·10^{-9} A/cm^2). W większości przypadków otrzymano wyniki zbliżone, a nawet lepsze w porównaniu do mikrokrystalicznego Ta (I_{corr}= 3,108·10^{-8} A/cm^2),

- rozdrobnienie mikrostruktury oraz zastosowanie dodatków stopowych i kompozytowych znacząco wpływa na poprawienie właściwości mechanicznych materiałów. Nastąpił wzrost twardości od 346 HV dla mikro Ta do 1481 HV dla stopu Ta-10Mo oraz 1398 HV dla kompozytu Ta-10TaC,

- badania termograwimetryczne pozwoliły na określenie przyrostu masy i kinetyki procesu utlenienia. Najmniejszy przyrost masy wystąpił w przypadku stopu Ta-10W i wynosił 105,35% w porównaniu do mikrokrystalicznego Ta dla którego przyrost masy wynosił 121,69%,

- wygrzewanie w wysokiej temperaturze w atmosferze otoczenia powoduje utlenienie powierzchni i wytworzenie warstwy tlenków, która jest słabo związana z podłożem. W przypadku nagrzewania w atmosferze azotu na powierzchni nanokrystalicznych materiałów na bazie tantalu powstają głównie azotki tantalu silnie związane z podłożem poprawiające właściwości i tworzące warstwę ochronną,

10. Literatura

1. M. Sopata, M. Sadej, J. Jakubowicz, *High temperature resistance of novel tantalum-based nanocrystalline refractory compounds*, Journal of Alloys and Compounds 788 (2019) 476-484.
2. R. A. Silva, M. Walls, B. Rondot, M. Da Cunha Belo, R. Guidoin, *Electrochemical and microstructural studies of tantalum and its oxide films for biomedical applications in endovascular surgery*, Journal of Materials Science: Materials in Medicine 13 (2002) 495-500.
3. R.W. Buckmann, *New applications for tantalum and tantalum alloys*, JOM 52 (2000) 40-41.
4. B.E. Schuster, J.P. Ligda, Z.L. Pan, Q. Wei, *Nanocrystalline refractory metals for extreme condition applications*, JOM 63 (2011) 27-31.
5. T.E. Mitchell, P.L. Raffo, *Mechanical properties of some tantalum alloys*, Canadian Journal of Physics 45 (1967) 1047-1062.
6. F.F. Schmidt, D.J. Maykuth, H.R. Ogden, *Tantalum alloys for elevated-temperature service*, JOM 13 (1961) 487-489.
7. S.M. Cordonne, P. Kumar, C.A. Michaluk, H.D. Schwartz, *Tantalum and its alloys*, International Journal of Refractory Metals and Hard Materials 13 (1995) 187-194.
8. F. Cardarelli, *Materials handbook. A concise desktop reference*, Springer International Publishing, 2018, ISBN 978-3-319-38923-3.
9. M. Sopata, G. Adamek, J. Jakubowicz, *Microstructure and electrochemical properties of refractory $Ta-Y_2O_3$ and $Ta-ZrO_2$ nanocomposites*, International Journal of Electrochemical Science 13 (2018) 9583-9591.
10. J. Jakubowicz, G. Adamek, M. Sopata, J.K. Koper, T. Kachlicki, M. Jarzębski, *Microstructure and electrochemical properties of refractory nanocrystalline tantalum-based alloys*, International Journal of Electrochemical Science 13 (2018) 1956-1975.
11. Y. Kim, E.-P. Kim, J.-W. Noh, S.H. Lee, Y.-S. Kwon, I.S. Oh, *Fabrication and mechanical properties of powder metallurgy tantalum prepared by hot isostatic pressing*, International Journal of Refractory Metals and Hard Materials 48 (2015) 211-216.
12. R. Morales, R.E. Aune, O. Grinder, S. Seetharaman, *The powder metallurgy processing of refractory metals and alloys*, JOM 55 (2003) 20-23.
13. K-H. Sim, G. Wang, T-J. Kim, K-S. Ju, *Fabrication of a high strength and ductility Ta-22Al-25Nb alloy srom high energy ball-milled powder by spark plasma sintering*, Journal of Alloys and Compounds 741 (2018) 1112-1120.
14. J.R. Groza, A.K. Zavaliangos, *Sintering activation by external electrical field*, Material Science 28 (2000) 171-177.
15. P. Angerer, E. Neubauer L.G. Yu, K.A. Khor, *Texture and structure evolution of tantalum powder samples during spark-plasma-sintering (SPS) and conventional hot-pressing*, International Journal of Refractory Metals and Hard Materials 25 (2007) 280-285.
16. Q. Wei, Z.L. Pan, X.L. Wu, B.E. Schuster, L.J. Kecskes, R.Z. Valiev, *Microstructure and mechanical properties at different length scales and strain rates of nanocrystalline tantalum produced by high-pressure torsion*, Acta Materialia 59 (2011) 2423-2436.
17. Y.S. Zhang, L.C. Zhang, H.Z. Niu, X.F. Bau, S. Yu, X.Q. Ma, Z.T. Yu, *Deformation twinning and localized amorphization in nanocrystalline tantalum induced by sliding friction*, Materials Letters 127 (2014) 4-7.

18. J. Jakubowicz, M. Sopata, *Structure and microstructure of high-energy ball-milled nanocrystalline tantalum*, 4th Annual International Conference on Materials Science, Metals & Manufacturing (M3 2017) 1-6.
19. J. Jakubowicz, M. Sopata, G. Adamek, J.K. Koper, *Properties of high-energy ball-milled and hot pressed nanocrystalline tantalum*, GSTF Journal of Engineering Technology (JET) 4 (2017) 124-131.
20. V. Kentheswaran, S. Dine, D. Vrel J.–P. Couziné, G. Dirras, *Synthesis of nanometric refractory alloys powders in the MoNbW system*, Journal of Alloys and Compounds 679 (2016) 80-87.
21. M.A. Mayers, A. Mishra, D.J. Benson, *Mechanical properties of nanocrystalline materials*, Progress in Materials Science 51 (2006) 427-556.
22. D. Jia, K.T. Ramesh, E. Ma, *Effects of nanocrystalline and ultrafine grain sizes on constructive behavior and shear bands in iron*, Acta Materialia 51 (2003) 3495-3509.
23. Y.M. Wang, E. Ma, *Strain hardening, strain sensitivity and ductility of nanostructured metals*, Materials Science and Engineering A 375-377 (2004) 46-52.
24. J. Jakubowicz, M. Sopata, G. Adamek, P. Siwak, T. Kachlicki, *Formation and properties of the Ta-Y_2O_3, Ta-ZrO_2 and Ta-TaC nanocomposites*, Advances in Materials Science and Engineering (2018) 2085368.
25. A.H. Chokshi, A. Rosen, J. Karch, H. Gleiter, *On the validity of the hall-petch relationship in nanocrystalline materials*, Scripta Metallurgica 23 (1989) 1679-1683.
26. M. Bischof, S. Mayer, H. Leitner, H. Clemens, P. Staron, E. Geiger, A. Voiticek, W. Knabl, *On the development of grain growth resistant tantalum alloys*, International Journal of Refractory Metals and Hard Materials 24 (2006) 437-444.
27. D. Gambale, *Tantalum surface alloys prevent corrosion*, Advanced Materials and Processes 168 (2010) 23-25.
28. K.A. de Souza, A. Robin, *Influence of concentration and temperature on the corrosion behavior of titanium, titanium-20 and 40% tantalum alloys and tantalum in sulfuric acid solutions*, Materials Chemistry and Physics 103 (2007) 351-360.
29. K.A. de Souza, A. Robin, *Preparation and characterization of Ti-Ta alloys for application in corrosive media*, Materials Letters 57 (2003) 3010-3016.
30. A. Robin, J.L. Rosa, *Corrosion behavior of niobium, tantalum and their alloys in hot hydrochloric and phosphoric acid solutions*, International Journal of Refractory Metals and Hard Materials 18 (2000) 13-21.
31. C. Hertl, L. Koll, T. Schmitz, E. Werner, U. Gbureck, *Structural characterisation of oxygen diffusion hardened alpha-tantalum PVD-coatings on titanium*, Materials Sciance and Engineering C 41 (2014) 28-35.
32. G. Xu, X. Shen, Y. Hu, P. Ma, K. Cai, *Fabrication of tantalum oxide layers onto titanium substrates for improved corrosion resistance and cytocompatibility*, Sufrace and Coating Technology 272 (2015) 58-65.
33. Y-Y. Chang, H-L. Huang, C-H. Lai, C-Y. Wen, *Antibacterial properties and cytocompatibility of tantalum oxide coatings*, Surface and Coatings Technology 259 (2014) 193-198.
34. M. Sopata, J.K. Koper, J. Jakubowicz, *Odporność korozyjna prasowanych na gorąco nanokrystalicznych stopów tantalu*, Ochrona Przed Korozją 11 (2017) 365-367.
35. J. Jakubowicz, G. Adamek, M. Sopata, J.K. Koper, P. Siwak, *Hot pressing of nanocrystalline tantalum using high frequency induction heating and pulse plasma sintering*, 6th Global Conference on Materials Science and Engineering, IOP Conf. Series: Materials Science and Engineering 283 (2017) 012001.
36. J. Jakubowicz, G. Adamek, M. Sopata, *Characterization of high-energy ball-milled and hot-pressed nanocrystalline tantalum*, 2nd Interantional Conference on Civil

Engineering and Materials Science, IOP Conf. Series: Materials Science and Engineering 216 (2017) 012006.

37. M. Sopata, P. Siwak, G. Adamek, J. Jakubowicz, *The analysis of mechanical properties of nanocrystalline tantalum alloys*, Protection of Metals and Physical Chemistry of Surfaces – wysłana do opublikowania, w recenzji.

38. J.R. DiStefano, B.A. Pint, J.H. DeVan, *Oxidation of refractory metals in air and low pressure oxygen gas*, International Journal of Refractory Metals and Hard Materials 18 (2000) 237-243.

39. B. Gorr, F. Muller, M. Azim, H.-J. Christ, T. Muller, H. Chen, A. Kauffmann, M. Heilmaier, High-temperature oxidation behavior of refractory nanocrystalline tantalum-based alloys: effect of alloy composition, Oxidation of Metals 88 (2017) 339-349.

40. P. Kofstad, High temperature oxidation of metals, John Wiley & Sons, New York 1966.

41. S. Majumdar, P. Sengupta, G.B. Kale, I.G. Sharma, *Development of multilayer oxidation resistant coatings on niobium and tantalum*, Surface & Coatings Technology 200 (2006) 3713-3718.

Podziękowania

11. Artykuły będące przedmiotem jednotematycznego cyklu publikacji.

[1] J. Jakubowicz, G. Adamek, **M. Sopata**, *Characterization of high-energy ball-milled and hot-pressed nanocrystalline tantalum*, 2nd International Conference on Civil Engineering and Materials Science, IOP Conf. Series: Materials Science and Engineering 216 (2017) 012006, DOI:10.1088/1757-899X/216/1/012006 – **w bazie WoS, 15 pkt. MNiSW.**

[2] J. Jakubowicz, G. Adamek, **M. Sopata**, J.K. Koper, P. Siwak, *Hot pressing of nanocrystalline tantalum using high frequency induction heating and pulse plasma sintering*, 6th Global Conference on Materials Science and Engineering, IOP Conf. Series: Materials Science and Engineering 283 (2017) 012001, DOI:10.1088/1757-899X/283/1/012001 – **w bazie WoS, 15 pkt. MNiSW.**

[3] **M. Sopata**, J.K. Koper, J. Jakubowicz, Odporność korozyjna prasowanych na gorąco nanokrystalicznych stopów tantalu, Ochrona Przed Korozją 11 (2017) 365-367, DOI:10.15199/40.2017.11.2 – **12 pkt. MNiSW.**

[4] J. Jakubowicz, **M. Sopata,** G. Adamek, P. Siwak, T. Kachlicki, *Formation and properties of the Ta-Y_2O_3, Ta-ZrO_2 and Ta-TaC nanocoposites*, Advances in Materials Science and Engineering (2018) 2085368, DOI:10.1155/2018/2085368 – **w bazie WoS, 20 pkt. MNiSW, IF=1,372.**

[5] J. Jakubowicz, G. Adamek, **M. Sopata**, J.K. Koper, T. Kachlicki, M. Jarzębski, *Microstructure and electrochemical properties of refractory nanocrystalline tantalum-based alloys*, International Journal of Electrochemical Science 13 (2018) 1956-1975, DOI:10.20964/2018.02.67 – **w bazie WoS, 25 pkt. MNiSW, IF=1,369.**

[6] **M. Sopata**, G. Adamek, J. Jakubowicz, *Microstructure and electrochemical properties of refractory Ta-Y_2O_3 and Ta-ZrO_2 nanocomposites*, International Journal of Electrochemical Science 13 (2018) 9583-9591, DOI:10.20964/2018.10.20 **w bazie WoS, 25 pkt. MNiSW, IF=1,369.**

[7] **M. Sopata**, M. Sadej, J. Jakubowicz, *High temperature resistance of novel tantalum-based nanocrystalline refractory compounds*, Journal of Alloys and Compounds 788 (2019) 476-484, DOI:10.1016/j.jallcom.2019.02.230 – **w bazie WoS, 35 pkt. MNiSW, IF=3,779.**

1

Characterization of High-Energy Ball-Milled and Hot-Pressed Nanocrystalline Tantalum

J Jakubowicz[1,2], G Adamek[1] and M Sopata[1]
[1]Poznan University of Technology, Institute of Material Science and Engineering
Jana Pawla II, 24, 61-138 Poznan, Poland

[2]E-mail: jaroslaw.jakubowicz@put.poznan.pl;

Abstract. The paper shows a comparison of nanocrystalline and microcrystalline tantalum sinters. The nanocrystalline tantalum was made using high-energy ball milling. The sinters were made using hot pressing with high frequency induction heating. The structure and microstructure of the powders and sinters were investigated. After 48 hour milling, the microcrystalline tantalum transformed into nanocrystalline powder. The hot pressing resulted in a formation of bulk tantalum with ultrafine grains and hardness as high as 1067 HV. The nanostructure supports the densification process at lower sintering temperature in comparison to microcrystalline tantalum. The average crystallite size in nanocrystalline bulk materials reached 170 nm.

1. Introduction

Tantalum is a very promising material for different technical applications [1, 2]. Tantalum is a refractory material used as base for alloys used in air and space, chemical, energy and biomedical applications. However, the main downside of tantalum is its high cost and relatively hard processing because of its high melting point. Tantalum can be composed with other alloying elements such as Ti [3] as well as other refractory elements [4-6] to form alloys of very high resistance to temperature and corrosion. The Ta is relatively plastic but its combination with other alloying elements results in strengthening through solid solutioning, precipitating or dispersing [4]. The formation of nanostructure results in significant changes in the properties of materials [7, 8]. A reduction of grain size results in an increase in the grain boundaries. These microstructural elements cause an increase in the material strength following the grain refinement. Nanocrystalline powders can be successfully used for preparation of bulk materials [9]. The powder metallurgy processes are typical processes leading to their densification [10]. The nanocrystalline powders should be consolidated at lighter pressing and sintering conditions, i.e. temperature, pressure and time in comparison to microcrystalline counterparts. Thus, conventional powder metallurgy followed by pressureless sintering is not appropriate due to high temperature, long time and no pressure during sintering. The hot pressing, on the other hand, can minimize grain growth, thus preserving the nanostructure after the process, providing high mechanical properties.
In this work the formation of bulk nanocrystalline tantalum sinters was studied and compared to the microcrystalline ones. The authors used hot pressing in order to reduce the grain growth during consolidation.

2. Experimental details

In this work, nanocrystalline Ta sinters were made starting from high-energy ball milling followed by hot pressing. The tantalum powder of the mesh size of 325 (<44 μm) and the purity of 99.97% was

purchased at Alfa Aesar (Germany). During all the processing stages, the powder was kept in high purity inert atmosphere (argon). The powder handling was conducted in a Labmaster 130 glove box (MBraun, Germany). The milling procedure was done in a hardened steel vial mounted inside the SPEX 8000M shaker Mixer/Mill (Spex SamplePrep, USA). The mill was run for 48h at a room temperature with the frequency of 875 cycles/minute. 5g of Ta powder and 7 hardened steel balls were placed inside the vial. The ball to powder weight ratio was 3. The obtained powders were then axially hot-pressed at 10^{-2} Pa vacuum using graphite die and tungsten stamps. The pressing temperature was established experimentally and the process was done at 1500°C and 1000°C for microcrystalline and nanocrystalline powders, respectively. The pressure was 50 MPa and the sintering time at a constant temperature was 5s after 120s and 100s temperature rising to 1500°C and 1000°C, respectively. The BN spray was applied to prevent the powder material sticking to the die and ensure easier stamp moving. The structure analysis was controlled by Empyrean XRD (Panalytical, The Netherlands). The investigation was done using CuKα radiation at the voltage of 45 mV and the anode current of 40 mA. The angular 2θ range was 30-120 deg., the step size was 0.0167 deg. and the time per step was 12.54 s/step. The crystallite size was estimated using the Scherrer method. The microstructure was analyzed using Vega 5135 SEM (Tescan, Czech Republic). Additionally, Q-Scope 250 AFM (Quesant, USA) working in tapping mode was applied for the microstructure and grain size analysis. The surface was scanned by a SSS-NCLR Nanosensors probe. Based on the AFM images, a particle size dimension distribution histogram was developed. For microscopic observations, the bulk samples were grinded on a sandpaper, polished in a diamond suspension and finally etched in a H_2SO_4 + HNO_3 +HF mixture to reveal the grain boundaries. Vickers hardness HV3.0 was measured using a Nexus hardness tester (Innovatest).

3.   Results and discussion

Microcrystalline tantalum (figure 1a) was intensely milled for 48h (figure 1b). The high-energy ball-milling resulted in a reduction of the crystallite size to below 20 nm, nanostructure formation and significant material amorphization (figure 1b). Intense milling resulted in a strong deformation and stress introduction resulting in an increase of the lattice constant and the volume of the unit cell (figure 2). During HEBM, the initial Ta particles (figure 3a) undergo not only a reduction of the crystallite size, but also cold welding and plastic deformation, which can result in a formation of relatively large particles (figure 3b). These particles, however, are composed of nanocrystals (figure 4a). The strain hardening is the main factor leading to the size reduction of final powders and the crystallites. The particles after HEBM stuck together and formed larger agglomerates (figure 3b).
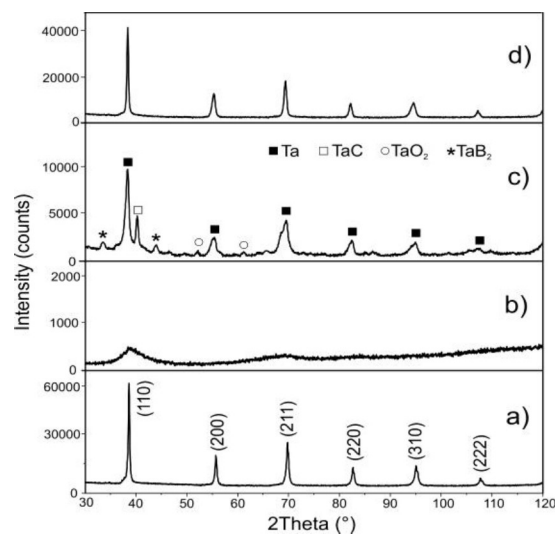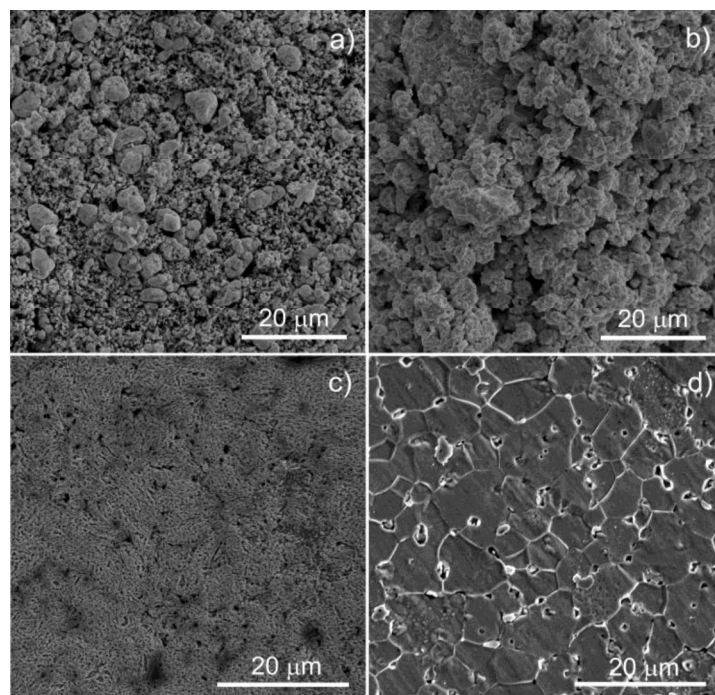

Figure 1. XRD spectra of tantalum: microcrystalline 325 mesh powder (a), nanocrystalline powder obtained after 48h of HEBM (b), nanocrystalline sinter (c) and microcrystalline sinter (d)
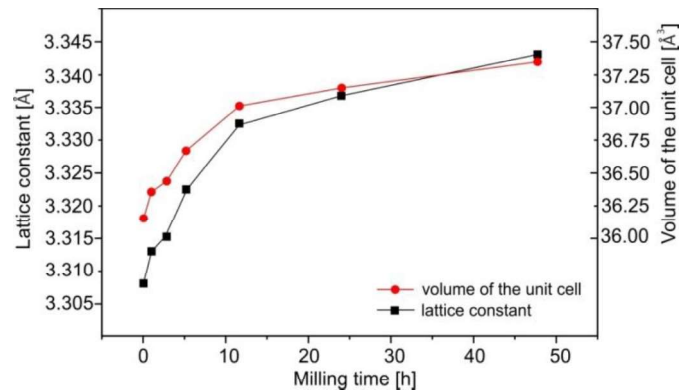
Figure 2. Lattice constant and the volume of the unit cell changes during HEBM

The hot-pressing process was done in a very short time and at a relatively low temperature. For nanocrystalline tantalum we have found that the temperature of 1500°C is too high in contrast to microcrystalline tantalum, which is why, for nanocrystalline material, the pressing was done at 1000°C. Due to the high reactivity of the nanocrystalline powder, the material reacts with graphite die and boron nitride covering the die and the stamp. As a result, small amounts of additional hard precipitations (TaC, TaB$_2$) appear in the structure of the compacts as well as TaO$_2$ due to high reactivity with oxygen (figure 1c). For comparison, the parent, much bigger microcrystalline powder does react with the above-mentioned die materials (figure 1d). The hot-pressing process results in a limited grain growth in comparison to conventional powder metallurgy. Low temperature and short time at a given temperature lead to inhibiting the grain growth of the compact (figure 4b). The compacting leads to the obtainment of uniform grains in the case of nanocrystalline material of a spherical shape (figure 4b), while in the case of microcrystalline materials it is typical polyhedral grains (figure 4c). In both cases, for nanocrystalline and microcrystalline materials, an over 95% density was obtained without significant pores (figure 3c,d and figure 4b,c). Small pits observed in figure 3c,d are a result of the polished sample etching in order to reveal the grain boundaries.
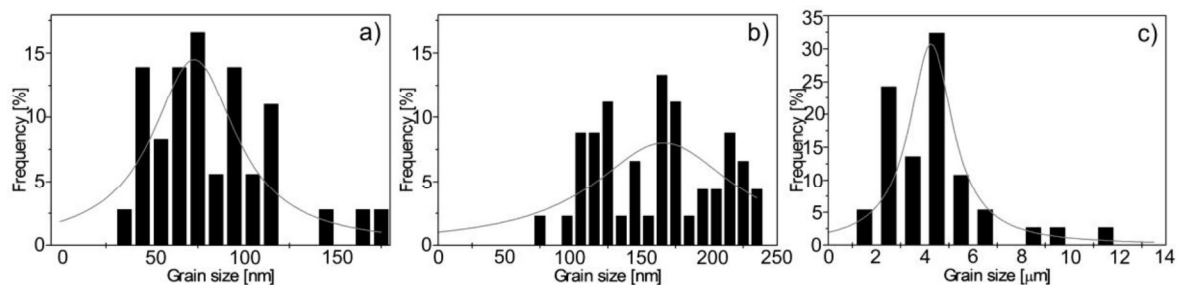

Figure 3. SEM images of tantalum: microcrystalline powder (a), nanocrystalline powder after 48h of HEBM (b), nanocrystalline sinter (c) and microcrystalline sinter (d)
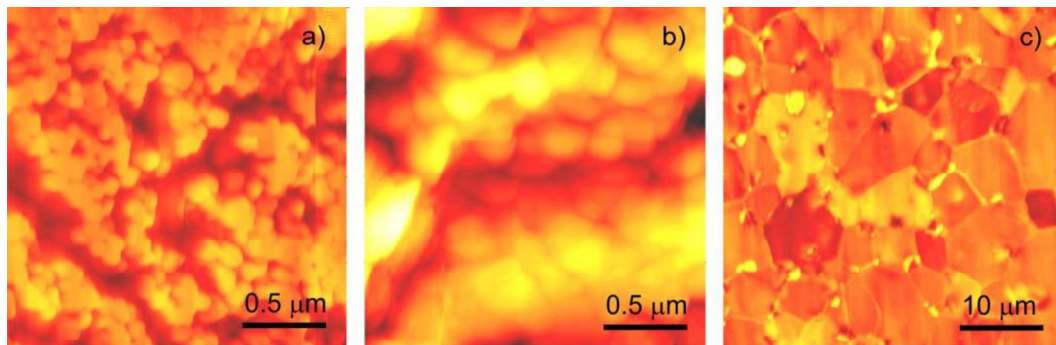
Figure 4. AFM images of tantalum: nanocrystalline powder after 48h of HEBM (a), nanocrystalline sinter (b) and microcrystalline sinter (c)

The grain size distribution was calculated taking into account the AFM data. The average grain size after 48h of HEBM reaches 70 nm (Figure 5a), while after sintering, it increases up to 170 nm (figure 5b). For comparison, when the microcrystalline particles were sintered, the average grain size reached 4.3 µm (figure 5c). In all cases, the grains have a wide range of distribution.

Figure 5. Grain size distribution of the: nanocrystalline powder after 48h of HEBM (a), nanocrystalline sinter (b) and microcrystalline sinter (c)

In the case of both, nanocrystalline and microcrystalline hot-pressed materials hardness was measured using the Vickers tester. The microcrystalline material had a hardness of 357 ± 6.6 HV and the nanocrystalline material due to small grains and hard precipitations reached 1067 ± 78 HV. For comparison, the hardness was also measured on commercial bulk sintered tantalum, which reached the value of 101 ± 2.2 HV.

4.   Conclusions

This work discussed the formation of hot-pressed nanocrystalline tantalum in comparison to the microcrystalline ones. HEBM results in a reduction of the crystallite size up to the average value of approx. 70 nm. The hot pressing of the nanocrystalline tantalum results in a limited grain growth and an average crystal size of approx. 170 nm. For comparison, microcrystalline powders were compacted, giving standard microcrystalline sinters with crystal size of approx. 4.3 µm. The nanocrystalline material showed additional hard precipitations, that derived from the graphite die and lubricant, forming during a reaction with the nanocrystalline material. The hardness of the ultrafine tantalum is very high and reaches 1067 HV.

This work constitutes preliminary studies for further research of nanocrystalline tantalum alloys and composites prepared by mechanical alloying followed by densification process.

5.   Acknowledgements

6.   References

[1]   Buckman R W 2000 *JOM* **52** 40
[2]   Silva R A, Walls M, Rondot B, Cunha Belo M and Guidoin R 2002 *J. Mater. Sci. Mat. Med.* **13** 495
[3]   Souza K A and Robin A 2007 *Mat. Chem. Phys.* **103** 351
[4]   Cardonne S M, Kumar P, Michaluk C A and Schwartz H D 1995 *Int. J. Refract. Met. Hard Mat.* **13** 187
[5]   Robin A and Rosa J L 2000 *Int. J. Refract. Met. Hard Mat.* **18** 13
[6]   Schuster B E, Ligda J P, Pan Z L and Wei Q 2011 *JOM* **63** 27
[7]   Tang Y, Bringa E M and Meyers M A 2013 *Mat. Sci. Eng.* A **580** 414
[8]   Ligda J, Scotto D'antuono D, Taheri M L, Schuster B E and Wei Q 2016 *JOM* **68** 2832
[9]   Maglia F, Tredici I G and Anselmi-Tamburini U 2013 *J. Euro. Ceramic Soc.* **33** 1045
[10]   Morales R, Aune R E, Seetharaman S and Grinder O 2003 *JOM* **55** 20

2

Hot pressing of nanocrystalline tantalum using high frequency induction heating and pulse plasma sintering

J Jakubowicz[1*], G Adamek[1], M Sopata[1], J K Koper[1] and P Siwak[2]

[1]Institute of Materials Science and Engineering, Poznan University of Technology, Poznan, Poland
[2]Institute of Mechanical Technology, Poznan University of Technology, Poznan, Poland
*E-mail: jaroslaw.jakubowicz@put.poznan.pl

Abstract. The paper presents the results of nanocrystalline powder tantalum consolidation using hot pressing. The authors used two different heating techniques during hot pressing: high-frequency induction heating (HFIH) and pulse plasma sintering (PPS). A comparison of the structure, microstructure, mechanical properties and corrosion resistance of the bulk nanocrystalline tantalum obtained in both techniques was performed. The nanocrystalline powder was made to start from the microcrystalline one using the high-energy ball milling process. The nanocrystalline powder was hot-pressed at $1000\,^{\circ}$ C, whereas, for comparison, the microcrystalline powder was hot pressed up to $1500\,^{\circ}$ C for proper consolidation. The authors found that during hot pressing, the powder partially reacts with the graphite die covered by boron nitride, which facilitated punches and powder displacement in the die during densification. Tantalum carbide and boride in the nanocrystalline material was found, which can improve the mechanical properties. The hardness of the HFIH and PPS nanocrystalline tantalum was as high as 625 and 615 HV, respectively. The microstructure was more uniform in the PPS nanomaterial. The corrosion resistance in both cases deteriorated, in comparison to the microcrystalline material, while the PPS material corrosion resistance was slightly better than that of the HFIH one.

1. Introduction

Many components used in advanced industry require high-tech materials that are resistant to high temperature, corrosive media or radiation. These components are usually made using, inter alia, refractory elements. However, refractory metals, alloys and composites based on Ta, W, Nb, oxides and nitrides [1-5] are technologically problematic materials that require high temperature processing, i.e. high sintering temperature. These materials are usually made using powder metallurgy [6,7]. In terms of powder metallurgy, the conventional process is usually based on the following stages: (1) preparation of a powder of required composition, size and shape, (2) high pressure compaction for green compact formation and (3) sintering for green compact consolidation [8]. To provide good mechanical properties of sintered material, i.e. strength and low porosity, high pressure and high temperature are required, which is unfavorable in terms of the grain growth at elevated temperature and high requirements for the pressing/sintering equipment. The conventional powder metallurgy process can be successfully used for microcrystalline powders. For nanocrystalline powders, however, other processing routes are required such as hot pressing [8], in which the stages of pressing and

sintering are carried out simultaneously. Thus, the process has many advantages including lower pressure, temperature and shorter sintering time. Finally, the hot-pressed material has a greater density, lower porosity and smaller grain size, which ensure better mechanical properties. The hot pressing process has many possible variants of heating. One of them is high frequency induction heating (HFIH), resistance heating (RH), spark plasma sintering (SPS) or pulse plasma sintering (PPS) [1,9-11]. The PPS is a relatively new technique [11,12] developed for the consolidation of high melting temperature compounds [13]. The PPS technique for fast powder heating during pressing, utilizes the pulses of high electric current generated by discharging high voltage capacitors. This allows acceleration of the heating to the steady temperature and shortening the time of sintering. The process is useful in the obtainment of high-density and fine-grained materials [13]. Tantalum can be used in different technical elements, which works in hard conditions [14] and it is very resistant in acidic environments. High corrosion resistance is a consequence of a passive Ta_2O_5 oxide film [15]. Tantalum is an unfavourably expensive element used in very hard operating conditions: in aviation and in the space industry, for chemical, energy-related and biomedical applications. Beside the high cost, which limits its widespread use, one of the downsides of tantalum is its high melting point and difficulties during processing. The powder metallurgy applied to tantalum is a good choice for the production of bulk elements, however, high sintering temperature leads to an increase in the size of the grains. It is commonly known that, according to the Hall-Petch equation, the smaller grain size leads to material strengthening [16]. Therefore, small grains of nanometer size, before the consolidation stage, are much desired to limit the final grain size in the consolidated materials after the sintering process. The formation of nanostructure tantalum can be promising in terms of its strengthening. Decrease of the grain diameter leads to larger volume of the boundaries between them. The nanostructure tantalum powder can be successfully consolidated to form bulk parts of high density, close to the theoretical value. The application of hot pressing limits the grain growth at elevated temperatures (which is lower in hot pressing compared to a conventional sintering process) and should provide nanocrystalline or ultrafine tantalum of greater strength in comparison to microcrystalline counterparts.

The first study of the nanocrystalline tantalum sintering was carried out in 1999 by Yoo *et al* [17]. They found that large surface area of the nanoparticles improves the densification process in comparison to the microcrystalline powder. At high strain rates, tantalum nanograins exhibit ductile deformation behavior without significant fracture and the tantalum nanograins tend to get softer [17]. Ductility and flow stress increase significantly as the initial particle size is reduced below 100 nm. Thus, the nanocrystalline tantalum not only has better mechanical properties but is more susceptible to process in comparison to microcrystalline powder.

The nanocrystalline tantalum was investigated by other researchers [18,19], however, the material still needs further investigation. In this work, we compare properties of HFIH and PPS hot-pressed nanocrystalline tantalum. This is a preliminary study for further preparation of nanocrystalline tantalum based alloys. The new methods of nanomaterials formation can provide new data and properties useful in extending theirs application. Different techniques were successfully used for tantalum nanopowders consolidation [8,10]. The work attempted to determine whether the applied method of hot pressing affects the properties of tantalum.

2. Experimental data

The nanocrystalline tantalum was produced in the process of high energy ball milling (HEBM). The milled powders were next hot pressed. The starting Ta powder (AlfaAesar, Germany) has a size <44 µm. The impurities do not exceed 0.03%. The powder was stored and handled in Unilab glove box (MBraun, Germany). The HEBM process was run using SPEX8000M mill (SpexSamplePrep, USA). Milling time was set experimentally at 48 h. Room temperature (RT) was a standard condition of the process. Powders after HEBM were hot-pressed in vacuum ($<10^{-2}$ Pa). The consolidation was done using graphite equipment (die as well as upper and lower punches), which were covered by BN layer (HeBoCoat, Germany). The BN layer improves punches moving and powders consolidation. The

authors used two different heating modes during consolidation: high-frequency induction heating (HFIH) and pulse plasma sintering (PPS). The consolidation temperature was 1500°C and 1000°C for micro- and nanocrystalline powders, respectively. The time of sintering at a constant temperature was 5 s. The lower temperature of hot pressing was choosing for nanocrystalline material, which has better sinterability and to avoid its excessive grain growth [17,20]. The pressure exerted on the powder had a value of 50 MPa. In the PPS process the pulses of high electric current going through the die and the powder. The current pulses in the module are generated by discharging of a 250 F capacitor, charged to a voltage of maximum 8 kV. The pulse duration during sintering process is automatically controlled due to a temperature measurement by a pyrometer direct on the upper punch. Voltage, pulse frequency, force, temperature, and real-time vacuum were automatically controlled during the sintering procedure.

The structure was checked using Empyrean XRD (Panalytical, The Netherlands) with a crystallographic database ICDD-JCPDS. The investigations were performed using CuK radiation (45 mV, 40 mA). The crystallite size was calculated by the Scherrer's equation.

The microstructure was recorded by SEM (Tescan, Czech Republic), operated at 20 kV in the secondary electrons mode as well as by AFM (Quesant, USA). The AFM works in the wavemode (SSS-NCLR premounted Nanosensors probe, 145 kHZ probe frequency, and scan speed 3 lines/s, total 1024 lines for image formation). For the microstructure evaluation the hot-pressed samples were grinded, polished and chemically etched in a $H_2SO_4 + HNO_3 + HF$ mixture.

The mechanical properties were measured using Picodentor HM500 (Fischer, USA) nanoindentation tester. The HV – Vickers hardness and E_{IT} – indentation modulus were measured at loading. The indentations were made using diamond indenter at the force of 300 mN acting for 20 s.

The corrosion resistance was measured on hot-pressed materials using Solartron 1285 Potentiostat (Solartron Analytical, England). The potentiodynamic mode was applied, starting at -0.5 V and finishing at 3 V vs OCP. The scan speed was 0.5 mV/s. The bulk tantalum was the working electrode, graphite was the counter electrode and $Ag/AgCl/Cl^-$ was the reference electrode. The corrosion resistance was measured in the Ringer's solution containing the following ion concentrations: 147.2 mmol l^{-1} Na^+, 4.0 mmol l^{-1} K^+, 2.2 mmol l^{-1} Ca^{2+}, 155.7 mmol l^{-1} Cl^-.

3. Results and discussion

The microcrystalline tantalum powder shows a cubic-type Im-3m structure (reference code 01-089-4901). The material is single-phase (figure 1(a)). During high-energy ball milling for 48 h (figure 1(b)) a significant decrease of the crystallite size to 20 nm occurred. The reduction of intensity of peaks and their broadening points formation of nanostructure or even partial amorphization (figure 1(b)). The ball-powder-ball hits results in the introduction of material stress, formation of dislocations and subgrains. These finally lead to cold strengthening, material crushing and nanostructure formation. During hot pressing, a significant relaxation of stress occurs and the provided energy results in grain growth (figures 1(c) and 1(d)). Because of high reactivity of the amorphous/nanocrystalline metallic material, high temperature and residual gases under vacuum, the powder partially reacts with the gases as well as the graphite die (figures 1(c) and 1(d)) and forms intermetallic phases. However, given their properties, these Ta-C, Ta-O or Ta-B type compounds can have a positive effect on the final properties of the bulk nanocrystalline tantalum. The precipitations can strengthening of the tantalum as well as inhibit grain growth at elevated temperature [5,7,8]. In the case of the PPS material, the XRD peaks for additional phases are smaller, indicating that the PPS process does not significantly support the reaction of Ta with the B, C or O elements as is in the case of the HFIH material. The microcrystalline hot-pressed material (figure 1(e)) shows no additional phases, for both HFIH and PPS hot-pressed samples (due to the same spectrum for both PPS and HFIH materials, for comparison, figure 1(e) shows the HFIH sample only).
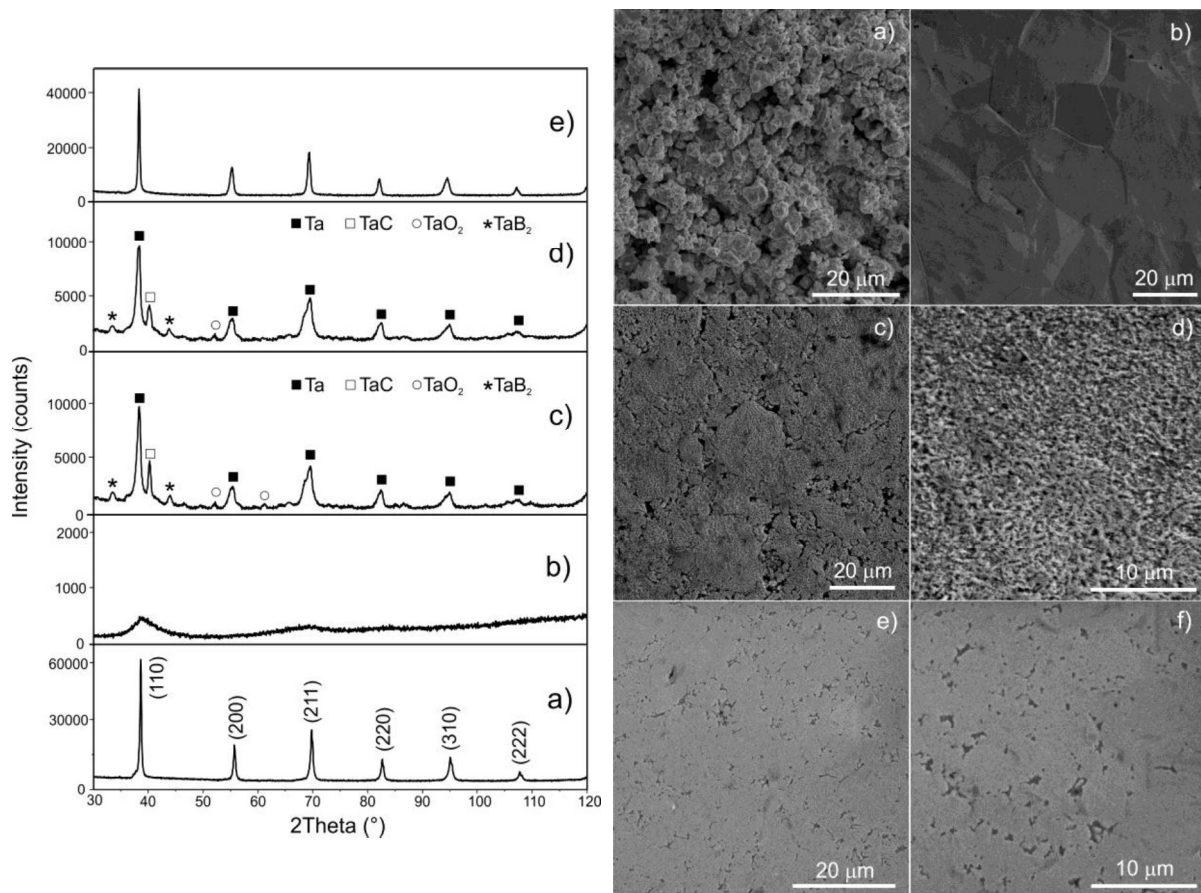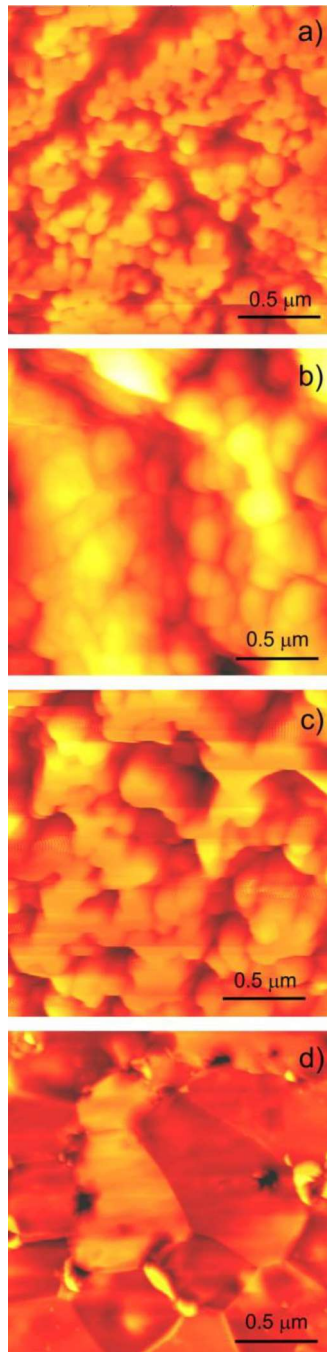
Figure 1. X-ray diffraction data for Ta: microcrystalline powder (a), nanocrystalline powder after mechanical milling (b), nanocrystalline hot-pressed using HFIH (c) nanocrystalline hot-pressed using PPS (d) and microcrystalline hot-pressed using HFIH (e).
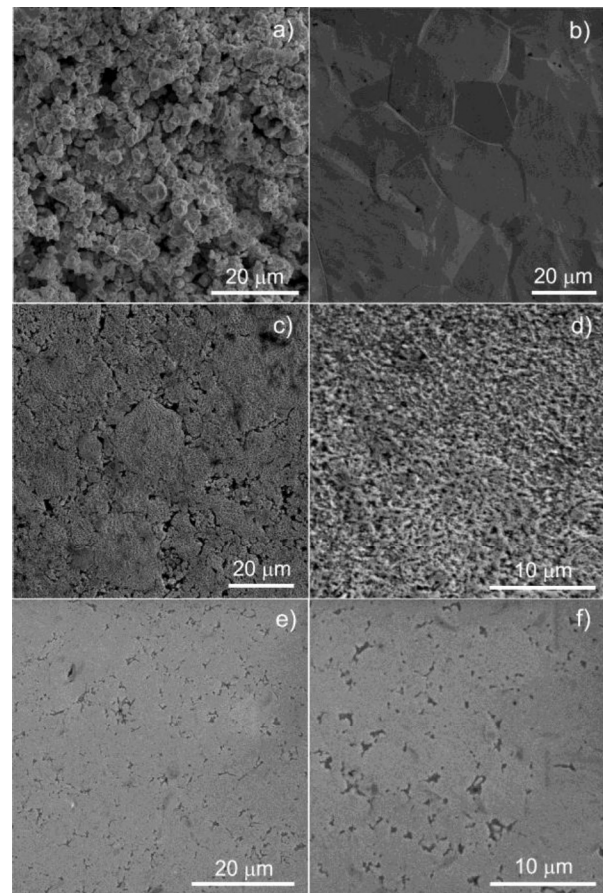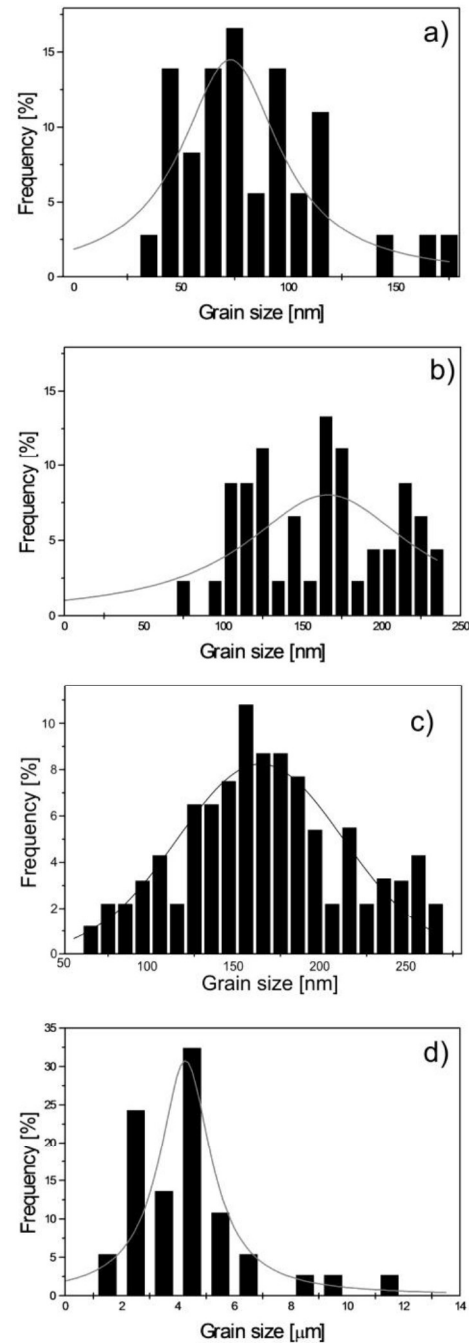
Figure 2. SEM image of tantalum: nanocrystalline powder after mechanical milling (a), microcrystalline hot-pressed (b) nanocrystalline hot-pressed using HFIH (c, d — different magnification) and nanocrystalline hot-pressed using PPS (e,f — different magnification).

In the HEBM process, the tantalum powder undergoes a grain size reduction, however, the powder during milling undergoes not only crushing but strong plastic deformation and cold welding (the powder particles are hit and trapped between the balls and the wall of the milling vial), which results in the formation of powder agglomerates of relatively large size (figure 2(a)). The agglomerates are composed of smaller particles, hence the SEM image (figure 2(a)) shows agglomerate particles (composed of nanograins) rather than nanoparticles. The XRD shows (peaks broadening and decreasing their intensity) that the material after intense milling transforms into nanocrystalline. As the reference material, the authors chose hot-pressed microcrystalline 325-mesh powder. The obtained consolidated microcrystalline sample has large grain size of the average value of 15 µm and low porosity (figure 2(b)). After mechanical milling, the nanocrystalline powders were hot-pressed using HFIH (figure 2(c) and 2(d)) and PPS (figures 2(e) and 2(f)). The hot-pressed nanomaterials have a slightly larger porosity following the pressing of the agglomerates, however, due to limited time of the hot pressing and a relatively low temperature, the metastable nanocrystalline material has insufficient energy for significant grain growth. After the HFIH slight porosity forms around the hot-pressed agglomerates (figure 2(c)). The higher magnification shows ultrafine structure (figure 2(d)). The PPS process results in a lower porosity and more uniform microstructure. The density of hot-pressed

microcrystalline tantalum was 15.6 g/cm^3, whereas for HFIH and PPS hot-pressed nanocrystalline tantalum was 14.9 g/cm^3 and 15.3 g/cm^3, respectively. These densities are 95%, 91% and 93% of the theoretical value, respectively.


Figure 3. AFM images of tantalum: nanocrystalline powder after mechanical milling (a), nanocrystalline hot-pressed using HFIH (b), nanocrystalline hot-pressed using PPS (c) and microcrystalline hot-pressed (d).

Figure 4. AFM grain size histogram of tantalum in the nanocrystalline powder after mechanical milling (a), nanocrystalline hot-pressed using HFIH (b), nanocrystalline hot-pressed using PPS (c) and microcrystalline hot-pressed (d).

The nanocrystalline materials were investigated using AFM. For comparison, the microcrystalline was also checked. Taking into account the AFM images (figures 3(a)-3(d)), grain size histograms were calculated (figures 4(a)-4(d)). For grain size analysis, we take the AFM pictures of 12 m^2 summarized area. The analysis was done on the pictures recorded on 3 different places to avoid sample inhomogeneity. The mechanically milled tantalum powders are shown in figure 3(a). The presented image shows agglomerated particles of relatively high homogeneity. However, the measured grain size distribution has a relatively broad range from approx. 30 to above 180 nm. The calculated average grain size is 70 nm (figure 4(a)). The hot pressing using HFIH results in the grain growth (figure 3(b)), but the grains are not larger than 230 nm (figure 4(b)). The calculated average grain size is 170 nm. The PPS process results in a smaller grain growth during the consolidation of the powders (figure 3(c)) and the average grain size is 165 nm (figure 4(c)). The microcrystalline sinter has large grains and, due to limited scan size, a relatively low surface area with only few grains in the frame was scanned (figure 3(d)). For the microcrystalline hot-pressed tantalum, the average grain size was calculated at 4.5 µm (figure 4(d)), however, the SEM image shows the average value of approx. 15 µm (figure 2(b)). The difference can be explained with the fact that AFM considered a lower amount of grains for the analysis and the smaller ones are better visibly compared to the SEM image.

The mechanical properties were measured using a nanoindentation tester (figure 5 and table 1). Figure 5 shows example load-displacement curves recorded for nanocrystalline tantalum. The results have a relatively broad spectrum of the curves that do not overlap one another, indicating some inhomogeneity and porosity of the hot-pressed material. The hardness of the nanocrystalline materials is twice as high compared to the microcrystalline and significantly higher than commercially available tantalum (100 HV for annealed and 200 HV for cold-worked). In both, HFIH and PPS nanomaterials, the mechanical properties are comparable. The high hardness in nanocrystalline tantalum can be attributed to the nanostructure as well as hard precipitations formed at elevated temperatures after contact with boron nitride-coated graphite die. The indentation modulus is comparable for all hot-pressed samples and is slightly lower in comparison to bulk commercial tantalum (186 GPa). Generally the porosity deteriorates the modulus.
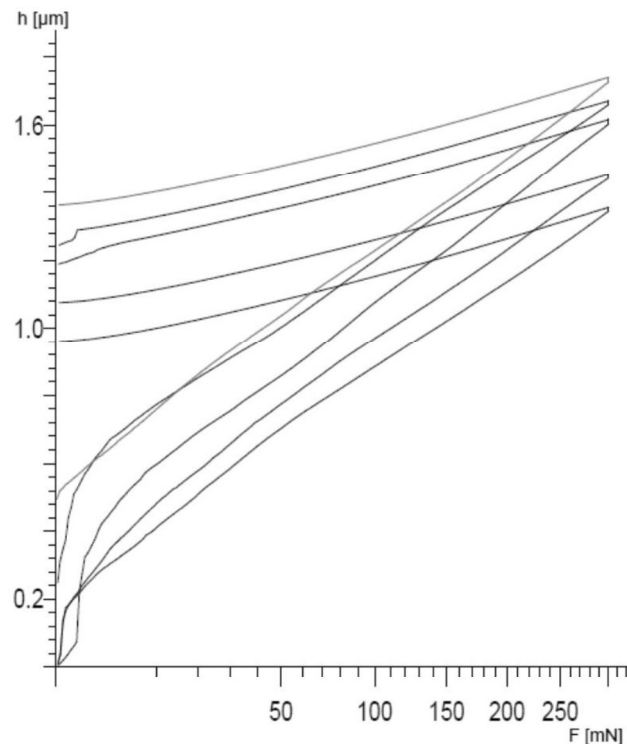

Figure 5. Example load-displacement curves recorded for nanocrystalline PPS tantalum.

Table 1. Mechanical properties of the hot-pressed microcrystalline and nanocrystalline tantalum

Parameter	Microcrystalline (HFIH)	Nanocrystalline (HFIH)	Nanocrystalline (PPS)
HV [HV]	346.4±29.8	625.2±132.1	615.2±149.5
E_{IT} [GPa]	180.3±5.8	180.4±22.8	182.2±23.1

The corrosion resistance was measured for microcrystalline and nanocrystalline hot-pressed materials. It is commonly accepted that the microcrystalline and single-phase structure favour better corrosion resistance in comparison to nanostructure of large volume grain boundaries (smaller grains) and multiphase materials [15,21]. It is, thus expected that nanomaterials have worse corrosion resistance in comparison to microcrystalline materials. The OCP (open circuit potential) and polarization curves are shown in figures 6A and 6B, respectively. OCP for the microcrystalline Ta (a) shows a significantly more negative value in comparison to the nanocrystalline Ta (b, c). The more positive value of OCP suggests a formation of a more stable passive layer. An increase in OCP to a more positive value with time indicates that the material undergoes overall corrosion (a), whereas constant OCP or its slight decrease denotes a stable passive layer (b, c).
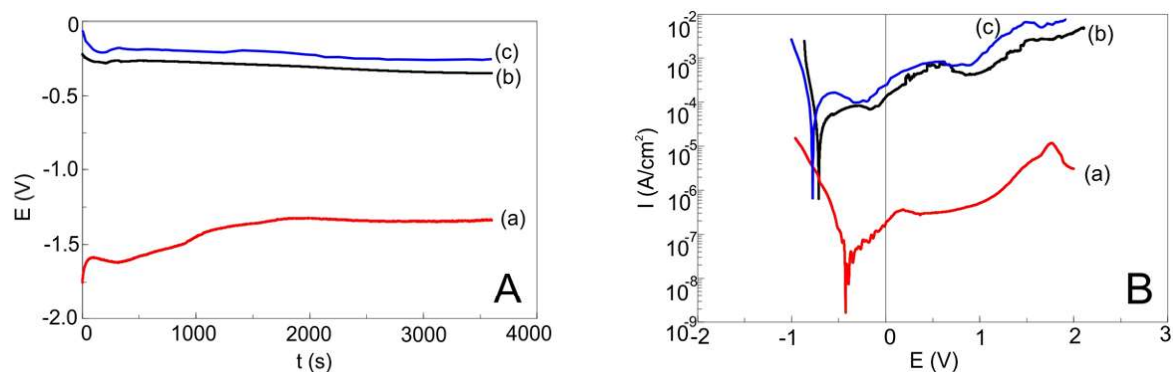
Figure 6. OCP (A) and polarization (B) curves for microcrystalline (a) and nanocrystalline HFIH (b) and PPS (c) tantalum.

The polarization curves shown in B point to better corrosion resistance of the microcrystalline Ta (a) in comparison to the nanocrystalline Ta (b, c). The microcrystalline Ta has a corrosion current density of $I_{corr} = 3.108 \cdot 10^{-8}$ A/cm^2, whereas for the hot-pressed nanocrystalline HFIH and PPS Ta, the $I_{corr} = 3.625 \cdot 10^{-5}$ A/cm^2 and $1.198 \cdot 10^{-5}$ A/cm^2, respectively. The lowest I_{corr} denotes better corrosion resistance. For the nanocrystalline Ta, the I_{corr} has a significantly higher I_{corr}. The high I_{coor} is related to greater volume of the grain boundaries and a smaller grain size. The current in the passive range is significantly higher for the case of nanocrystalline material.

4. Conclusions

The paper has shown the results of nanocrystalline tantalum consolidation using different heating techniques during hot pressing. To prevent excessive grain growth at elevated temperature, the nanocrystalline powders, made using HEBM process were hot-pressed applying induction heating and pulse plasma sintering. Both methods give comparable results, i.e. small average grain size in the range of 165-170 nm and good mechanical properties with the hardness of approx. 620 HV, twice higher compare to the hot-pressed microcrystalline Ta. PPS tantalum exhibits a slightly better corrosion resistance in comparison to HFIH tantalum, however, the microcrystalline tantalum has a best corrosion resistance.

Acknowledgments

References

[1]   Browning P N, Alagic S, Carroll B, Kulkarni A, Matson L and Singh J 2017 Room and ultrahigh temperature mechanical properties of field assisted sintered tantalum alloys *Mater. Sci. Eng.* **680** 141-51

[2]   Buckman R W 2000 New applications for tantalum and tantalum alloys *J. Min. Met. Mat. Soc.* **52** 40-1

[3]   Yong Q, Lin L and Li Ch 1998 Characterization of nanocrystalline tantalum nitride formed by solid-gas reaction during mechanical alloying *J. Alloys Comp.* **269** 238-40

[4]   Zhou J-Q, Akhtar S K, Cai R and Chen L 2006 Comperative study on constructive modeling of tantalum and tantalum tungsten alloy *Int. J. Iron Steel Res.* **13** 68-74

[5]   Cardonne S M, Kumar P, Michaluk C A and Schwartz H D 1995 Tantalum and its alloys *Int. J. Refract. Met. Hard Mater.* **13** 187-94

[6]   Kofstad P 1963 Studies of the oxidation of tantalum at 1000°-1300°C *J. Less Common Met.* **5** 158-70

[7]   Angerer P, Neubauer E, Yu L G and Khor K A 2007 Textur and structure evolution of tantalum powder samples during spark-plasma-sintering (SPS) and conventional hot-pressing *Int. J. Refract. Met. Hard Mater.* **25** 280-5

[8]   Kim Y, Kim E P, Noh J W, Lee S H, Kwon Y S and Oh I S 2015 Fabrication and mechanical properties of powder metallurgy tantalum prepared by hot isostatic pressing *Int. J. Refract. Metals Hard Mater.* **48** 211-6

[9]   Borodianska H, Demirskyi D, Sakka Y, Badica P and Vasylkiv O 2012 Grain boundary diffusion driven spark plasma sintering of nanocrystalline zirconia *Ceramic Inter.* **38** 4385-9

[10]   Dias M, Guerreiro F, Correia J B, Galatanu A, Rosinski M, Monge M A, Munoz A, Alves E and Carvalho P A 2015 Consolidation of W-Ta composites: Hot isostatic pressing and spark and pulse plasma sintering *Fusion Eng. Design* **98-99** 1950-5

[11]   Rosinki M, Ciupinska L, Grzonka J, Michalski A and Kurzydlowski K J 2012 Synthesis and characterization of the diamond/copper composites produced by the pulse plasma sintering (PPS) method *Diamond Related Materials* **27-28** 29-35

[12]   Atkinson V H and Davies S 2000 Fundamental aspects of hot isostatic pressing: An overview *Metall. Mater. Trans.* **31** 2981-3000

[13]   Bischof M, Mayer S, Leitner H, Clemens H, Staron P, Geiger E, Voiticek A and Knabl W 2006 On the development of grain growth resistant tantalum alloys *Int. J. Refract. Met. Hard Mater.* **2** 437-44

[14]   Schuster B E, Ligda J P, Pan Z L and Wei Q 2011 Nanocrystalline refractory metals for extreme condition applications *Refract. Met. Alloys* **63** 27-31

[15]   Robin A and Rosa J L 2000 Corrosion behavior of niobium, tantalum and their alloys in hot hydrochloric and phosphoric acid solutions *Int. J. Refract. Met. Hard Mater.* **18** 13-21

[16]   Tang Y, Bringa E M and Meyers M A 2013 Inverse Hall-Petch relationship in nanocrystalline tantalum *Mater. Sci. Eng. A* **580** 414-26

[17]   Yoo S H, Sudarshan T S, Sethuram K, Subhash G and Dowding R J 1999 Consolidation and high strain rate mechanical behavior of nanocrystalline tantalum powder *Nanostruct. Mater.* **12** 23-8

[18]   Zhang Y S, Zhang L C, Niu H Z, Bai X F, Yu S, Ma X Q and Yu Z T 2014 Deformation twinning and localized amorphization in nanocrystalline tantalum induced by sliding friction *Mater. Lett.* **127** 4-7

[19]   Brar L K, Singla G, Kaur N and Pandey O P 2015 Thermal stability and structural properties of Ta nanopowder synthesized via simultaneous reduction of Ta_2O_5 by hydrogen and carbon *J.*

*Therm. Anal. Calo*r. **119** 175-82

[20]   Fang Z, Maheshwari P, Wang X, Sohn H Y, Griffo A and Riley R 2005 An experimental study
of the sintering of nanocrystalline WC–Co powders, *Int. J. Refract. Met. Hard Mater.* **23** 249-57

[21]   Bermudez M D, Carrion F J, Martinez-Nicolas G and Lopez R 2005 Erosion-corrosion of
stainless steels, titanium tantalum and zirconium *Wear* **258** 693-700

3

MATEUSZ SOPATA
JEREMIASZ K. KOPER
JAROSŁAW JAKUBOWICZ

Politechnika Poznańska, Instytut Inżynierii Materiałowej, ul. Jana Pawła II 24, 61-138 Poznań

Odporność korozyjna prasowanych na gorąco nanokrystalicznych stopów tantalu

Corrosion resistance of the hot pressed nanocrystalline tantalum alloys

W pracy zaprezentowano wyniki badań odporności korozyjnej nanokry-stalicznego tantalu oraz jego stopów. Dodatkami stopowymi były niob, molibden oraz wolfram. Materiałem wyjściowym były proszki metali, które poddano mechanicznej syntezie. Po 48 h mechanicznej syntezy materiał sprasowano na gorąco. Przeprowadzono badania odporności korozyjnej w trybie potencjodynamicznym, w płynie Ringera. Na posta-wie krzywych polaryzacji określono, że najgorszą odpornością korozyj-ną charakteryzuje się stop tantalu z niobem, a najlepszą stop tantalu z molibdenem. Bardzo dobre właściwości korozyjne zmierzono również dla stopów Ta-W. Wyniki porównano z czystym tantalem nanokrystalicz-nym, który charakteryzuje się gęstością prądu korozyjnego o 2–3 rzędy wielkości większą (gorszą odpornością korozyjną) od najlepszych nanokrystalicznych stopów Ta-Mo oraz Ta-W.

Słowa kluczowe: tantal, nanokrystaliczny tantal, stopy tantalum, praso-wanie na gorąco, wysoce odporne metale, odporność korozyjna

The paper describes the results of corrosion resistance study of the nano-crystalline tantalum and its alloys. Alloying additives were niobium, mo-lybdenum and tungsten. The starting materials were in the form of the metal powders which were then used in mechanical alloying synthesis. After 48 h of synthesis materials were hot pressed. The corrosion resis-tance was measured using the potentiodynamic mode in Ringer's solu-tion. The polarization curves show that the worst resistance has tanta-lum-niobium alloys and the best resistance has tantalum-molybdenum alloys. Significantly good properties for Ta-W alloy were measured. The results were compared with pure nanocrystalline tantalum which is characterized by 2–3 orders of magnitude higher corrosion current density (worst corrosion resistance) than the best nanocrystalline Ta-Mo and Ta-W alloys.

Keywords: tantalum, nanocrystalline tantalum, tantalum alloys, hot pressing, refractory metals, corrosion resistance

1. Wstęp

Tantal jest metalem o bardzo dobrych właściwościach fizyko-chemicz-nych. Do jego głównych zalet zalicza się odporność na działanie moc-nych kwasów. Posiada również wysoką temperaturę topnienia – 3017°C. Dzięki tym właściwościom zastosowanie znalazł w wielu gałęziach prze-mysłu. Tantal może być również stosowany jako biomateriał, dla przykła-du w elementach sztucznych stawów biodrowych. Bardzo często porów-nywany jest do tytanu. Można wzbogacać go o dodatki stopowe takie jak niob, wolfram, węgiel, azot, molibden w celu polepszenia jego właściwo-ści. Jedną z głównych wad tego materiału jest jego wysoka cena [2].

Materiały o nanostrukturze są obecnie coraz częściej stosowane w prze-myśle i medycynie. Mogą one występować w postaci czystych metali lub ich stopów [5]. Różnią się one również właściwościami mechanicznymi, biologicznymi, fizykochemicznymi. Materiały o strukturze nanokrysta-licznej można wytwarzać między innymi poprzez zastosowanie dużych odkształceń plastycznych (metody wyciskania lub skręcania). Jednak obecnie bardzo częstym sposobem wytworzenia takich materiałów jest wysoko-energetyczne mielenie kulowe (ang. High-Energy Ball Milling, HEBM lub proces mechanicznej syntezy (ang. Mechanical Alloying, MA). Do syntezy wykorzystuje się reaktory, w których znajdują się proszki wraz z kulami mielącymi instalowane w specjalistycznych młynkach [3–6, 8].

Ważną cechą każdego materiału jest odporność korozyjna. Jest ona istotna jeżeli materiał pracuje w środowisku agresywnym. W takim przy-padku powierzchnia jest narażona na działanie czynników niszczących. O ile korozja równomierna jest możliwa do przewidzenia i łatwa w zapo-bieganiu, to korozja lokalna stanowi większe zagrożenie [5]. Tantal i jego stopy zaliczany jest do najbardziej odpornych materiałów metalowych pracujących w szczególnie agresywnych środowiskach. Podobnie jak tytan nie jest odporny na działanie kwasu fluorowodorowego. W przeci-wieństwie do tytanu jest odporny na działanie zarówno kwasów o właści-wościach redukujących jak i utleniających [1, 7].

Coraz częściej stosowane materiały nanokrystaliczne wymagają po-znania ich odporności korozyjnej. Dotyczy to także materiałów na bazie tantalu, gdyż duża powierzchnia granic ziaren może tą odporność po-garszać.

W prezentowanej pracy do określenia odporności korozyjnej nanokry-stalicznego tantalu i jego stopów wykorzystano metodę elektrochemicz-ną stosując tryb potencjodynamiczny pomiaru krzywych polaryzacji.

2. Metodologia

Materiałem wyjściowym był tantal w postaci proszku o czystości 99,97% i rozdrobnieniu 325 mesh (< 44 μm) oraz proszki metali (< 44 μm) jako dodatki stopowe. Wytworzono nanokrystaliczne stopy tantalu Ta-xNb, Ta-xMo, Ta-xW, gdzie x = 5, 10, 20 i 40 wag. %. Dla celów porów-nawczych wytworzono również metodą HEBM czysty tantal nanokrysta-liczny. Strukturę nanokrystaliczną wytworzono w procesie mechanicznej syntezy w młynkach SPEX 8000M. Synteza trwała 48 godzin dla każdej z próbek, z częstotliwością reaktora 875 cykli/minutę. Proszki przygoto-wywano w komorze rękawicowej (Unilab MBraun), w której zastosowano atmosferę ochronną w postaci argonu.
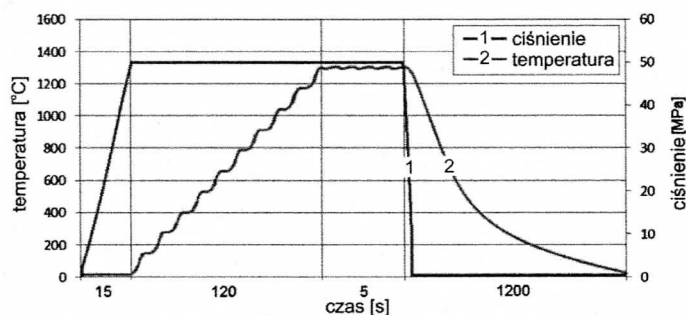
Otrzymane proszki zostały jednoosiowo sprasowane na gorąco z uży-ciem metody PPS (ang. Pulse Plasma Sintering – spiekanie impulsowo plazmowe). Zastosowano prasę firmy Elbit. Proces przeprowadzono z użyciem matryc grafitowych. Proces PPS prowadzono w próżni (4 Pa) zgodnie ze schematem (Rys. 1).

Z otrzymanych spieków wykonano zgłady metalograficzne, które szlifowano na papierach o gradacji do 1000, a następnie polerowano w zawiesinie Al$_2$O$_3$ celem uzyskania jednolitej, gładkiej powierzchni dla pomiarów korozyjnych. Strukturę określono stosując dyfraktometr rent

■ Kontakt z Autorem:
Mateusz Sopata, e-mail: mateusz.m.sopata@doctorate.put.poznan.pl

Rys. 1. Schemat procesu prasowania na gorąco

Fig. 1. The hot pressing process scheme

Rys. 3. Przykładowy obraz AFM (a) i rozkład wielkości (b) ziaren nanokrystalicznego stopu Ta-10W

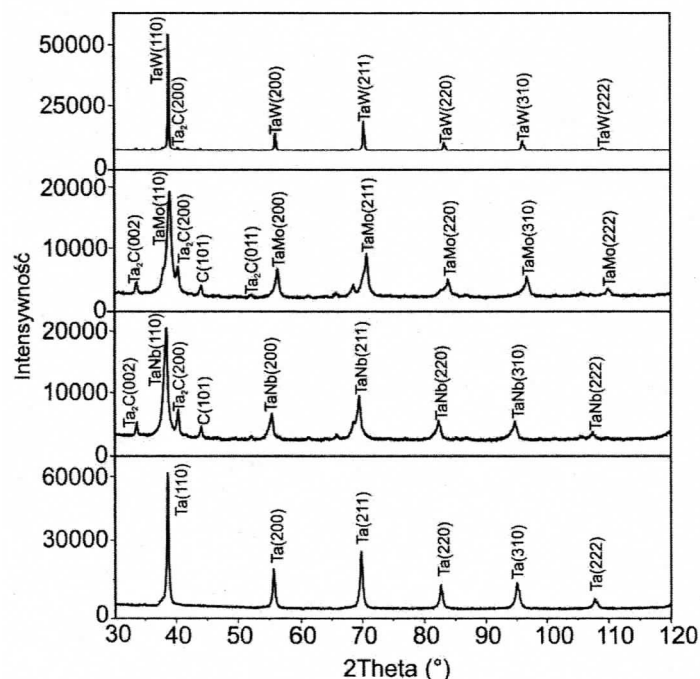Fig. 3. Example AFM picture (a) and grain size distribution (b) of the nanocrystalline Ta-10W alloy

genowski XRD (Panalytical) z promieniowaniem CuKα. Ponadto zastosowano mikroskop sił atomowych (AFM) Q-Scope 250 (Quesant) celem zbadania mikrostruktury i określenia wielkości ziaren.

Badania odporności korozyjnej zostały przeprowadzone z wykorzystaniem potencjostatu Solartron 1285. Zastosowano tryb potencjodynamiczny w zakresie od -2 V do 3 V wzgl. OCP (potencjału obwodu otwartego). Prędkość skanowania wynosiła 0,5 mV·s^{-1}. Przeciwelektrodą był grafit, a ogniwo Ag/AgCl elektrodą odniesienia model ERPt-11 (Hydromet). Pomiar przeprowadzono w elektrolicie, którym był płyn Ringera o składzie chemicznym: 147,2 mmol·l^{-1} Na$^+$, 4,0 mmol·l^{-1} K$^+$, 2,2 mmol·l^{-1} Ca^{2+}, 155,7 mmol·l^{-1} Cl$^-$. Elektrolit był odtleniony poprzez przedmuchiwanie azotem. Zastosowano mieszanie mieszadłem magnetycznym.

3. Wyniki badań i dyskusja

Wytworzone spieki charakteryzują się nanokrystaliczną strukturą i dużą jednorodnością (Rys. 2, Rys. 3). Gęstość spieków wynosi ok. 95% wartości teoretycznej.

W stopach występuje niewielkie zanieczyszczenie węglem oraz węglikami Ta$_2$C pochodzącymi od reakcji nanokrystalicznego materiału z matrycą grafitową (Rys. 2). Główną fazę tworzą roztwory stałe różnowęzłowe, odpowiednie dla danego dodatku stopowego (TaNb, TaMo, TaW). Średnia wielkość ziaren wyniosła od 50 do 190 nm w zależności od rodzaju stopu (najmniejsze ziarna dla stopów Ta-W a największe dla Ta-Nb). Przykładową nanostrukturę i rozkład wielkości ziaren przedstawiono na rys. 3.

Wyniki pomiarów odporności korozyjnej przedstawiono na rys. 4–7 oraz w tabeli 1. Rysunek 4 przedstawia krzywe polaryzacji dla stopu z 5% zawartością dodatku stopowego, oraz dla porównania nanokrystalicznego Ta, rysunek 5 stop z 10%, rysunek 6 z 20% zawartością dodatku, a rysunek 7 z 40% dodatku stopowego. W tabeli 1 zamieszczono zmierzone wartości (program CorrView) gęstości prądu (I_{corr}) i potencjału korozyjnego (E_{corr}). Z porównania wynika, że stopy Ta-Mo oraz Ta-W charakteryzują się znacznie lepszą odpornością korozyjną w stosunku do czystego nanokrystalicznego tantalu. Zmierzono dla nich wartości gęstości prądu o dwa i trzy rzędy wielkości mniejsze niż w przypadku tantalu nanokrystalicznego.

Rys. 4. Krzywe polaryzacji dla stopów tantalu: Ta-5Nb (a), Ta-5Mo (b), Ta-5W (c); dla porównania nanokrystaliczny Ta (d)

Fig. 4. Polarization curves of tantalum alloys: Ta-5Nb (a), Ta-5Mo (b), Ta-5W (c); for comparison nanocrystalline Ta (d)

Rys. 2. Widma XRD materiałów po procesie MA+PPS: nanokrystalicznego Ta (a) oraz nanokrystalicznych stopów Ta-10Nb (b), Ta-10Mo (c) oraz Ta-10W (d)
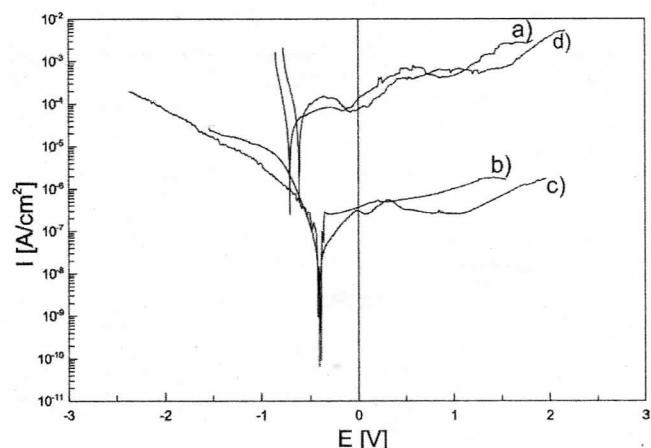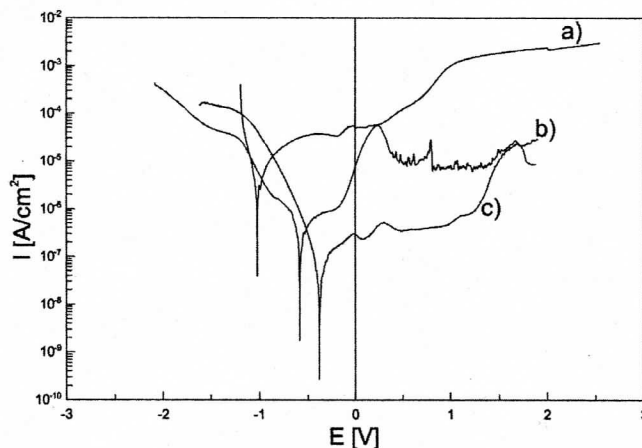
Fig. 2. XRD spectra after MA+PPS: nanocrystalline Ta (a) and nanocrystalline alloys Ta-10Nb (b), Ta-10Mo (c) and Ta-10W (d)
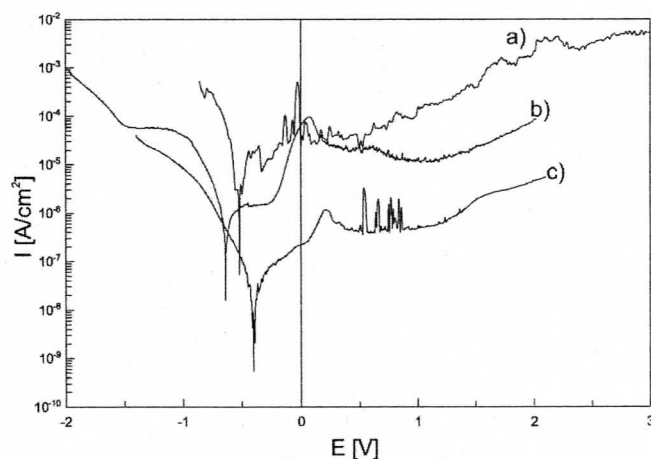
Rys. 5. Krzywe polaryzacji dla stopów tantalu: Ta-10Nb (a), Ta-10Mo (b), Ta-10W (c).

Fig. 5. Polarization curves of tantalum alloys: Ta-10Nb (a), Ta-10Mo (b), Ta-10W (c).

Rys. 6. Krzywe polaryzacji dla stopów tantalu: Ta-20Nb (a), Ta-20Mo (b), Ta-20W (c)
Fig. 6. Polarization curves of tantalum alloys: Ta-20Nb (a), Ta-20Mo (b), Ta-20W (c)
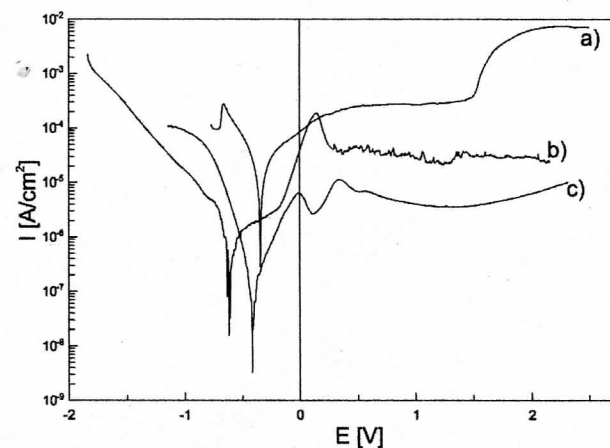
Rys. 7. Krzywe polaryzacji dla stopów tantalu: Ta-40Nb (a), Ta-40Mo (b), Ta-4[
Fig. 7. Polarization curves of tantalum alloys: Ta-40Nb (a), Ta-40Mo (b), Ta-40[

Tabela 1. Wartości gęstości prądu korozyjnego I_{corr} oraz potencjału korozyjnego E_{corr} dla badanych nanokrystalicznych stopów tantalu

Table 1. The values of corrosion current density I_{corr} and corrosion potential E_{corr} of the nanocrystalline tantalum alloys

Próbka	I_{corr} [A/cm^2]	E_{corr} [V]
Ta nano	$1,198 \cdot 10^{-5}$	-0,711
Stopy tantalu		
Ta-5Nb	$9,084 \cdot 10^{-5}$	-0,615
Ta-10Nb	$5,852 \cdot 10^{-6}$	-0,519
Ta-20Nb	$9,182 \cdot 10^{-6}$	-1,023
Ta-40Nb	$3,123 \cdot 10^{-5}$	-0,342
Ta-5Mo	$1,173 \cdot 10^{-8}$	-0,401
Ta-10Mo	$4,201 \cdot 10^{-7}$	-0,635
Ta-20Mo	$1,778 \cdot 10^{-7}$	-0,587
Ta-40Mo	$7,967 \cdot 10^{-7}$	-0,607
Ta-5W	$7,138 \cdot 10^{-8}$	-0,410
Ta-10W	$7,416 \cdot 10^{-8}$	-0,400
Ta-20W	$9,629 \cdot 10^{-8}$	-0,379
Ta-40W	$8,726 \cdot 10^{-8}$	-0,414

Zwiększanie zawartości dodatków stopowych nie zmienia istotnie odporności korozyjnej. Większy wpływ ma rodzaj zastosowanego dodatku stopowego. Stopy zawierające niob posiadają zbliżone właściwości do tantalu nanokrystalicznego – gęstość prądu korozyjnego około 10^{-5} A/cm^2. Świadczy to o braku wpływu na zwiększenie ochrony korozyjnej przez ten dodatek stopowy. Najmniejszą wartość gęstości prądu korozyjnego, a co za tym idzie najlepszą odporność wykazuje stop Ta-5Mo ($I_{corr} = 1,173 \cdot 10^{-8}$ A/cm^2). Dla stopów z dodatkiem wolframu zmierzono gęstość prądu korozyjnego także na poziomie 10^{-8} A/cm^2 i jest ona mniej więcej stała, niezależnie od składu chemicznego.

4. Wnioski

W pracy przedstawiono właściwości korozyjne nanokrystalicznych stopów tantalu z Nb, Mo oraz W, wytworzonych w procesie mechanicznej syntezy i prasowania na gorąco, odniesione do czystego nanokrystalicznego tantalu.

Stosując dodatki stopowe w postaci molibdenu oraz wolframu [
mujemy stopy nanokrystaliczne o 2÷3 rzędy wielkości większej odp[
ści korozyjnej w porównaniu do stopów Ta-Nb i nanokrystaliczne[
Brak wpływu na ochronę korozyjną zauważono w przypadku stos[
niobu jako dodatku stopowego do tantalu. Pierwiastek ten nie po[
w znaczący sposób właściwości względem czystego tantalu o stru[
nanokrystalicznej. Stopy z molibdenem i wolframem charakteryz[
najwyższą odpornością korozyjną, w szczególności Ta-5Mo oraz][
Najwęższy rozkład wyników gęstości prądu korozyjnego uzyskar[
stopów z wolframem.

LITERATURA

[1] De Souza K.A., A. Robin. 2003. „Preparation and characterization of Ti-Ta[
for application in corrosive media". *Mater Lett* 57 : 3010–3016.

[2] Huang Y., N. Maury, N.X. Zhang, T.G. Langdon. 2014. Microstructures a[
chanical properties of pure tantalum processed by high-pressure torsi[
Conf. Series: Materials Science and Engineering 63 012100.

[3] Jakubowicz J., G. Adamek, M. Sopata. 2017. Characterization of High-[
Ball-Milled and Hot-Pressed Nanocrystalline Tantalum, IOP Conf. Series[
rials Science and Engineering 216 012006.

[4] Jakubowicz J., M. Sopata. 2017. Structure and microstructure of high-[
ball-milled nanocrystalline tantalum. Conf. Proc. Annual International [
rence on Materials Science Metal and Manufacturing Singapore : 1–6.

[5] Jurczyk M., J. Jakubowicz. 2008. Bionanomateriały, wyd. Politechnika P[
ska. ISBN: 978-83-7143-373-3.

[6] Kim Y., E.P. Kim, J.W. Noh, S.H. Lee, Y.S. Kwon, I.S. Oh. 2015. „Fabrication a[
chanical properties of powder metallurgy tantalum prepared by hot is[
pressing". *Int. J. Refract Met. Hard Mater.* 48 : 211–216.

[7] Lee U.J., T.H. Lee, D.Y. Kim, H.H. Nersisyan, M.H. Han, K.S. Kang, K.K. [
Shin, J.H. Lee. 2013. „Microstructural and corrosion characteristic of ta[
coatings prepared by molten salt electrodeposition". *Surface and Coating[
nology* 235 : 819–826.

[8] Morales R., R.E. Aune, O. Grinder, S. Seetharaman. 2003. The powder met[
processing of refractory metals and alloys, JOM 55 : 20–23.

4

Research Article

Formation and Properties of the Ta-Y$_2$O$_3$, Ta-ZrO$_2$, and Ta-TaC Nanocomposites

J. Jakubowicz [ID],[1] M. Sopata,[1] G. Adamek,[1] P. Siwak,[2] and T. Kachlicki[1]

[1]*Institute of Materials Science and Engineering, Poznan University of Technology, Jana Pawla II 24, 61-138 Poznan, Poland*
[2]*Institute of Mechanical Technology, Poznan University of Technology, Piotrowo 3, 60-965 Poznan, Poland*

Correspondence should be addressed to J. Jakubowicz; jaroslaw.jakubowicz@put.poznan.pl

The nanocrystalline tantalum-ceramic composites were made using mechanical alloying followed by pulse plasma sintering (PPS). The tantalum acts as a matrix, to which the ceramic reinforced phase in the concentration of 5, 10, 20, and 40 wt.% was introduced. Oxides (Y$_2$O$_3$ and ZrO$_2$) and carbides (TaC) were used as the ceramic phase. The mechanical alloying results in the formation of nanocrystalline grains. The subsequent hot pressing in the mode of PPS results in the consolidation of powders and formation of bulk nanocomposites. All the bulk composites have the average grain size from 40 nm to 100 nm, whereas, for comparison, the bulk nanocrystalline pure tantalum has the average grain size of approximately 170 nm. The ceramic phase refines the grain size in the Ta nanocomposites. The mechanical properties were studied using the nanoindentation tests. The nanocomposites exhibit uniform load-displacement curves indicating good integrity and homogeneity of the samples. Out of the investigated components, the Ta-10 wt.% TaC one has the highest hardness and a very high Young's modulus (1398 HV and 336 GPa, resp.). For the Ta-oxide composites, Ta-20 wt.% Y$_2$O$_3$ has the highest mechanical properties (1165 HV hardness and 231 GPa Young's modulus).

1. Introduction

Refractory materials of the melting point higher than 3000°C are the most desired in design and manufacturing of heavy load-bearing components where resistance to high temperature and wear plays a crucial role. Additionally, these materials usually have high corrosion resistance in very aggressive environments as well as high mechanical properties [1]. The examples of refractory materials are pure metals such as Ta, W, or Mo and theirs alloys [2]. Other most commonly used refractory materials are ceramics such as oxides (ZrO$_2$ and Y$_2$O$_3$), carbides (TaC, ZrC, and WC), or nitrides (TiN and Si$_3$N$_4$) [3–5]. Both types of refractory materials, that is, metals and ceramics have found applications in the design of bulk parts or coatings. Due to their high hardness, refractory materials (particularly ceramics) are brittle. Both materials can be joined together in the form of composites, which usually constitutes a combination of

the best properties of both the metals and the ceramics [6–8]. Particularly, the high brittleness of ceramics can be limited by the addition of a metallic phase and vice versa, and the addition of ceramic phase into the metallic matrix leads to the improvement of the hardness and wear resistance of refractory metals. Refractory materials require high temperature processes for the formation of materials and products. For example, powder metallurgy requires the sintering temperature of at least 1500°C (usually above 2000°C) for proper microcrystalline powder consolidation [9]. Conventional high temperature and longtime sintering processes can be applicable for coarse-grained materials of micrometer size grains. Nanomaterials, compared to microcrystalline ones, can be consolidated for a shorter time and at significantly lower temperatures to achieve optimum properties. The consolidation processes used for nanocrystalline powders are usually different than conventional powder metallurgy used for microcrystalline powders. For

example, for the consolidation of nanomaterials, the hot pressing working in the heating mode of the spark plasma sintering (SPS) or pulse plasma sintering (PPS) gives the best results [10, 11]. In these processes of consolidation, both the pressure and the temperature increase simultaneously, which results in a shortening of the time for which the material is kept at a given high sintering temperature, and this process can be done at a significantly lower consolidation temperature compared to conventional pressureless sintering [12]. Both factors (temperature and time) are crucial for the reduction of the grain growth and the maintenance of the nanostructure or ultrafine structure [13]. Differences in the absence of wetting and the densities of the melted metal and ceramic components result in their segregation, which requires special casting techniques [14]. Therefore, powder metallurgy is very useful for the formation of homogeneous composites [15]. In the process of preparation of the refractory composites, the powders of metallic and ceramic components of the designed chemical composition are mixed together and then consolidated using hot pressing, SPS, PPS, or other relevant techniques [16–18]. For the formation of nanocomposite powders, the mechanical alloying process can be applied, in which the reduction of microcrystalline into nanocrystalline grains is provided by high-energy impacts of the balls in the milling vial [19]. In the mechanical alloying process, the final powders' mixture comes in the form of agglomerates of the micrometer or submicrometer size composed of nanometer size grains of metallic as well as ceramic phases uniformly distributed in the entire volume of the material [20].

New prospects for refractory nanomaterials are related to their outstanding mechanical properties [21], whereas high-temperature applications are limited due to excess grain growth at elevated temperatures [22]. At high temperatures, the nanostructure is unstable and grows up, which leads to deterioration of the mechanical properties.

In this work, the authors focus on the preparation and properties of tantalum-based nanocomposites, reinforced by ceramic Y_2O_3, ZrO_2, and TaC. Ta has the melting point of $3017°C$ and the density of $16.4\,g/cm^3$. The ceramics have the melting point of 2690, 2715, and $3985°C$ for Y_2O_3, ZrO_2, and TaC, respectively. The density of ceramics is 5.03, 5.68, and $14.5\,g/cm^3$ for Y_2O_3, ZrO_2, and TaC, respectively. The nanocomposites having 5, 10, 20, and 40 wt.% of the ceramic phase were formed using mechanical alloying and PPS. The paper studies the formation of nanocomposites and their structure, microstructure, and mechanical properties.

2. Materials and Methods

In this work, nanocrystalline $Ta-xY_2O_3$, $Ta-xZrO_2$, and $Ta-xTaC$ composites ($x = 5$, 10, 20, and 40 wt.% of the ceramic phase) were synthesized using mechanical alloying (MA) followed by hot pressing in the mode of pulse plasma sintering (PPS). In the MA process, the tantalum powder ($<44\,\mu m$, purity > 99.97%; Alfa Aesar) was intensely mixed and milled with the Y_2O_3 powder ($<50\,nm$, purity > 99.9%; Sigma-Aldrich) as well as the ZrO_2 powder ($0.1-2\,\mu m$, stabilized

with 5.4% of Y_2O_3; Goodfellow) and TaC ($<45\,\mu m$, purity > 99.5%; Goodfellow). The mixture of a total of 5.5 g of the metallic and ceramic powders was loaded and reloaded into the milling vial in the Unilab glove box (MBraun) providing a high purity Ar 5.0 atmosphere. For each composite composition, several syntheses were performed to provide material for 5 consolidated samples with 8 mm in diameter and 4 mm in height. In the mechanical alloying process (SPEX 8000M Mixer/Mill; SpexSamplePrep), the two types of powders (Ta + selected ceramic one) were high-energy mixed and milled for 48 h at the room temperature in the Ar 5.0 atmosphere. The steel-hardened vial with ball bearings (>62 HRC) was used for proper mixing. Due to the milling of the ceramic phase, the Fe impurity was introduced to the nanocomposites, but, its content did not exceed 2 wt.%. The as-milled powders were axially hot-pressed (Elbit) at 4 Pa vacuum. The graphite die and the graphite movable punches were coated by boron-nitride lubricant spray (HeBoCoat) during the process. The pressure of the punches directed at the powder was 50 MPa. The pulse plasma sintering mode (PPS) was used for the heating. The heating rate, sintering temperature, and time were set at $650°C/min$, $1300°C$, and 5 s. The other setup parameters for the PPS process were automatically selected to maintain proper heating rate and sintering temperature.

For comparison, the nanocrystalline pure tantalum was made using high-energy ball-milling (HEBM) and PPS. In the MA process, at least two different powders (Ta and ceramic powders) are mixed and milled together, whereas in HEBM, only the one component (Ta powder) is mixed and milled. Both processes were conducted in SPEX mill at the same conditions.

The structure and microstructure were investigated using Empyrean XRD (Panalytical) with CuKα radiation, SEM Vega 5135 (Tescan) with EDS PGT Prism 200 Avalon (Princeton Gamma-Tech), AFM Q-Scope 250 (Quesant), and TEM CM 20 Super Twin (Philips). For the AFM and SEM observations, all the bulk samples were grinded up to 1000 grit, polished in the Al_2O_3 suspension, and etched in an $H_2SO_4 + HNO_3 + HF$ mixture to reveal the grain morphology. More details regarding the above equipment used by the authors have been provided in [23].

The mechanical properties were measured using a Picodentor HM500 (Fischer) nanoindentation tester. The following parameters were measured: HV, Vickers hardness; E_{IT}, indentation modulus; C_{IT}, indentation creep; W_t, total mechanical work of indentation; and N_{plast}, plastic deformation portion. The indentation force load was 300 mN for 20 s. The load-displacement curves were recorded. For the measurement of the mechanical properties, the authors used unetched samples to avoid incorrect measurement results.

3. Results

The tantalum metal of a cubic structure (Figures 1(a), 2(a), and 3(a)) was mixed and milled with ceramic Y_2O_3 (cubic), ZrO_2(monoclinic), and TaC(cubic) powders (Figures 1(b), 2(b), and 3(b), resp.) of different crystallographic parameters. During the intense milling, the ceramic phase is
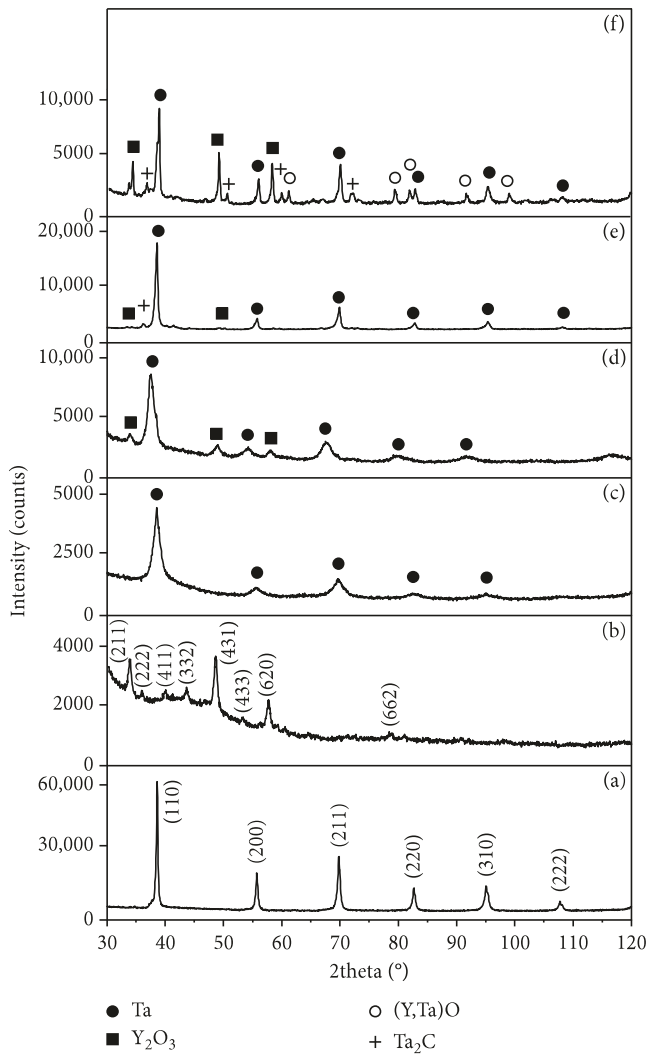
FIGURE 1: XRD of the pure Ta (a) and Y_2O_3 (b) powders; Ta-5Y_2O_3 (c) and Ta-40Y_2O_3 (d) nanocomposites' powder mixture after mechanical alloying; and Ta-5Y_2O_3 (e) and Ta-40Y_2O_3 (f) bulk nanocomposites after consolidation.

FIGURE 2: XRD of the pure Ta (a) and ZrO_2 (b) powders; Ta-5ZrO_2 (c) and Ta-40ZrO_2 (d) nanocomposites' powder mixture after mechanical alloying; and Ta-5ZrO_2 (e) and Ta-40ZrO_2 (f) bulk nanocomposites after consolidation.

homogenously distributed in the mixture of powders. For the Ta composites of low ceramic content (Figures 1(c), 2(c), and 3(c)), the MA process results mainly in the formation of a solid solution or a highly dispersed ceramic phase in the tantalum matrix. No visible peaks of the oxide ceramic phase are present (Figures 1(c) and 2(c)); however, carbides are visible (Figure 3(c)). An increase in the content of the ceramic phase leads to a typical composite structure, showing peaks (tantalum and the ceramic phase) (Figures 1 (d), 2(d), and 3(d)). The consolidation process conducted at an elevated temperature in a graphite die can lead to additional carburization and formation of additional tantalum carbides (Figures 1(e) and 1(f)). High temperature can lead to diffusion of oxygen from the oxides and formation of (Y, Ta) O at a higher ceramic phase content (Figure 1(f)). The made materials are classified as composites, in which the metallic phase coexists with the ceramic phase.
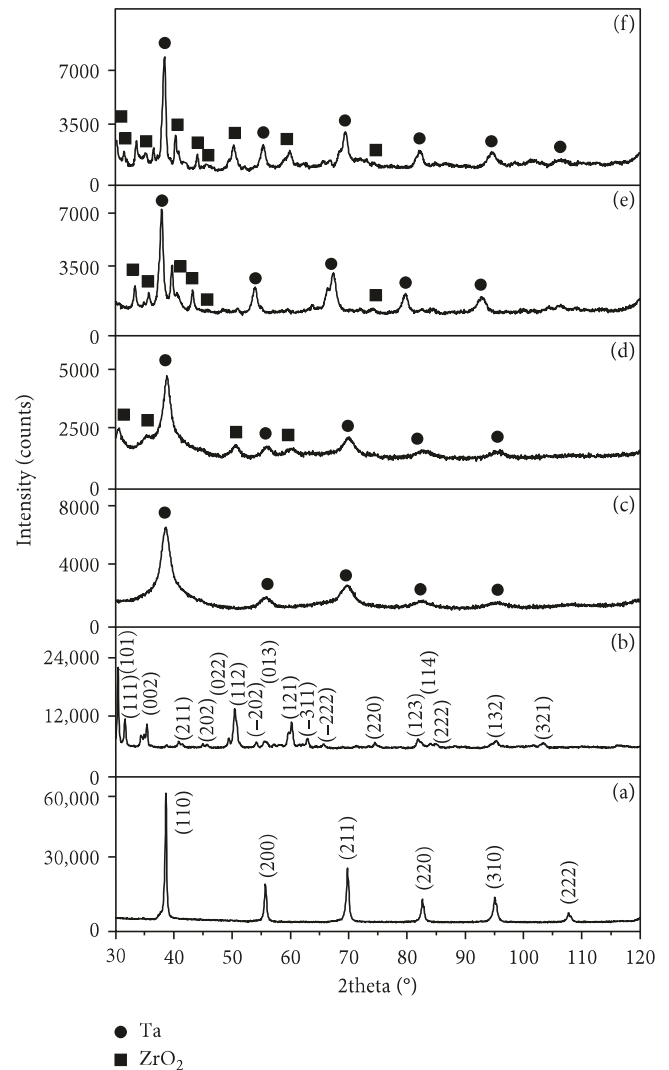
During the milling process, the ceramic phase affects the crystallographic parameters of the tantalum (Figure 4(a)) and vice versa—the tantalum affects the crystallographic parameters of the ceramic phase (Figure 4(b)). The ceramic phase has significantly different lattice parameters compared to tantalum. All the used materials have a cubic-type structure, but the lattice constant for the Ta, Y_2O_3, ZrO_2, and TaC is 3.306, 10.604, 5,065, and 4.456 Å, respectively. The volume of the unit cell for these materials is 35.127, 1192.365, 129.939, and 88.478 Å^3, respectively. Only Y_2O_3 of the highest lattice constant leads to an increase in the lattice and volume of the unit cell of the tantalum matrix, whereas ZrO_2 and TaC participate in a slight reduction of these parameters for tantalum (Figure 4(a)). Alternatively, the tantalum can affect the lattice constant of the ceramic phase (Figure 4(b)) leading to a decrease in the lattice constant and volume of the unit cell, especially for a high Y_2O_3 content.
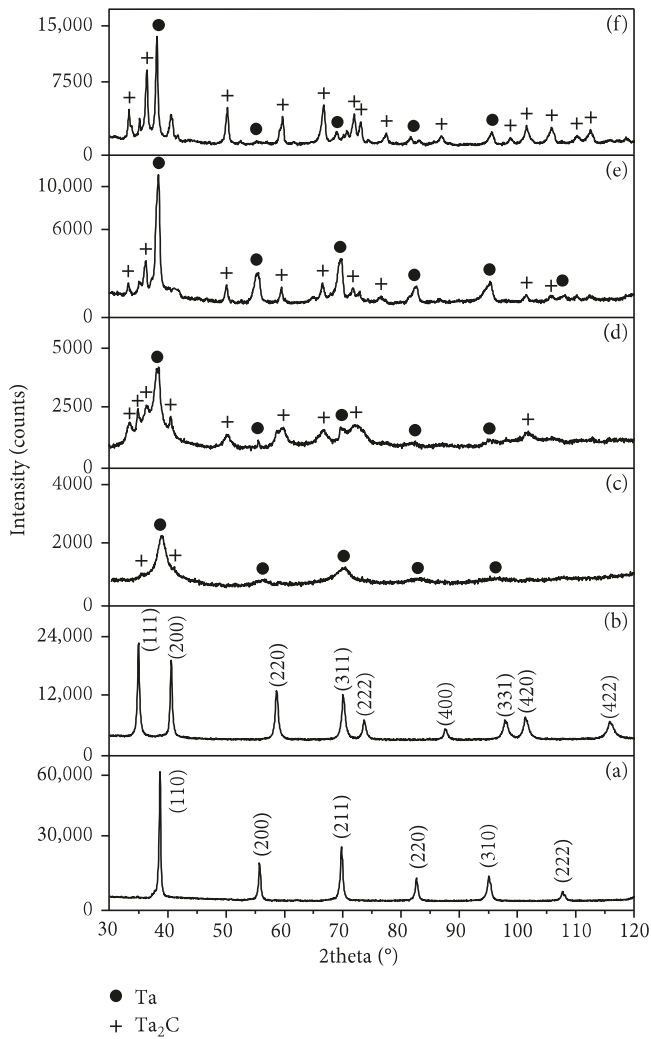
FIGURE 3: XRD of the pure Ta (a) and TaC (b) powders; Ta-5TaC (c) and Ta-40TaC (d) nanocomposites' powder mixture after mechanical alloying; and Ta-5TaC (e) and Ta-40TaC (f) bulk nanocomposites after consolidation.

FIGURE 4: The effect of the Y_2O_3, ZrO_2, and TaC content in the Ta-xY_2O_3, Ta-$xZrO_2$, and Ta-$xTaC$ composites on the Ta lattice constant and the Ta volume of the unit cell (after MA process) (a) and the effect of the Ta content in the Ta-xY_2O_3, Ta-$xZrO_2$, and Ta-$xTaC$ composites on the Y_2O_3, ZrO_2, and TaC lattice constant and the volume of the unit cell (b); $x = 0$, 5, 10, 20, and 40 wt.%.

The example TEM images of Ta and Ta-Y_2O_3 have been shown in Figure 5. The results confirm the two-phase nanostructure of the composite powders. Ta and the presented Ta-Y_2O_3 have a grain size of approximately 40–100 nm. The dark spots, clearly visible in Figures 5(b)–5(d), belong to the Y_2O_3 grains that are uniformly distributed in the Ta matrix. Generally, an increase in the Y_2O_3 content leads to a tantalum matrix grain size reduction.

The grain size reduction with the increased Y_2O_3 content was confirmed in the AFM measurements (Figure 6). The grains of nanocrystalline Ta (170 nm) were estimated earlier [24]. The introduction of nanocrystalline Y_2O_3 significantly shifts the grain size towards lower values. For 5% Y_2O_3, the average grain size was estimated at 76 nm, whereas for 10, 20, and 40 wt.% of Y_2O_3 it changed to 55, 70, and 42 nm, respectively. The increases in the Y_2O_3 concentration lead to a narrower grain size distribution as well as a smaller size of the largest grains.
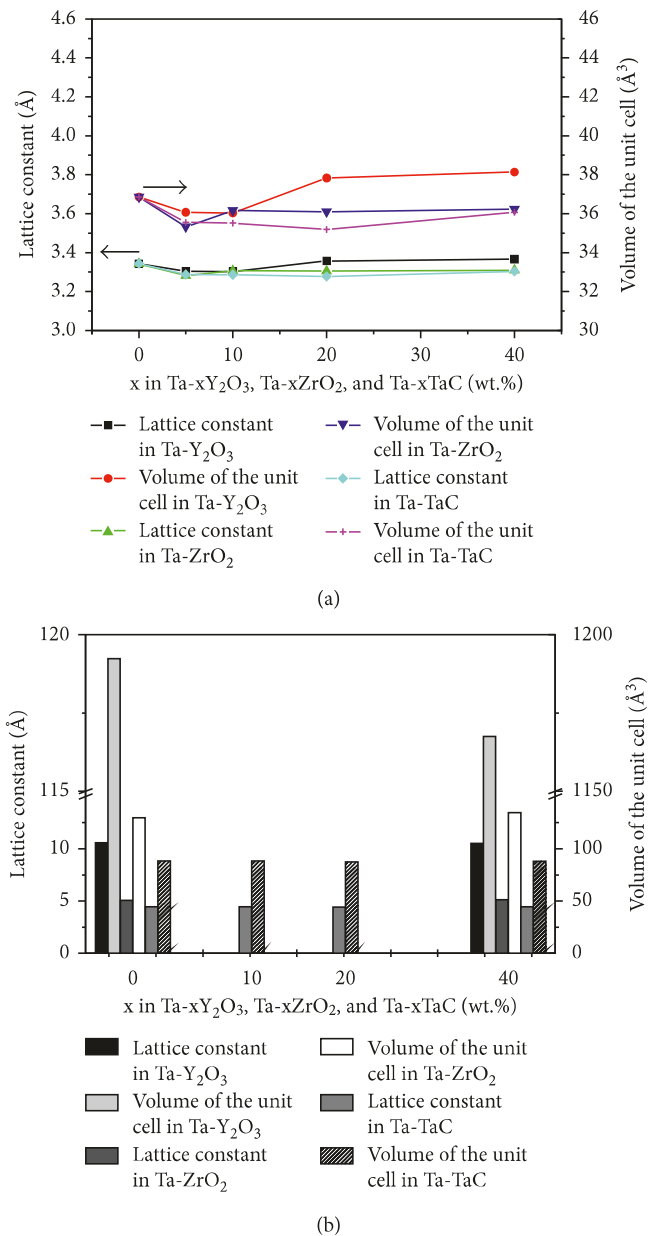
The comparison of the Ta-based composite microstructure with different ceramic phases (all 40 wt.% for Y_2O_3, ZrO_2, and TaC) has been shown in Figure 7. The smallest grains have their composites reinforced with nanocrystalline Y_2O_3 (a, b), whereas the largest grains have the composites reinforced with TaC (e, f), but are the most homogenous. As for the tantalum-based composites reinforced with ZrO_2, they are inhomogeneous and concentrated ZrO_2 precipitations are present (c).
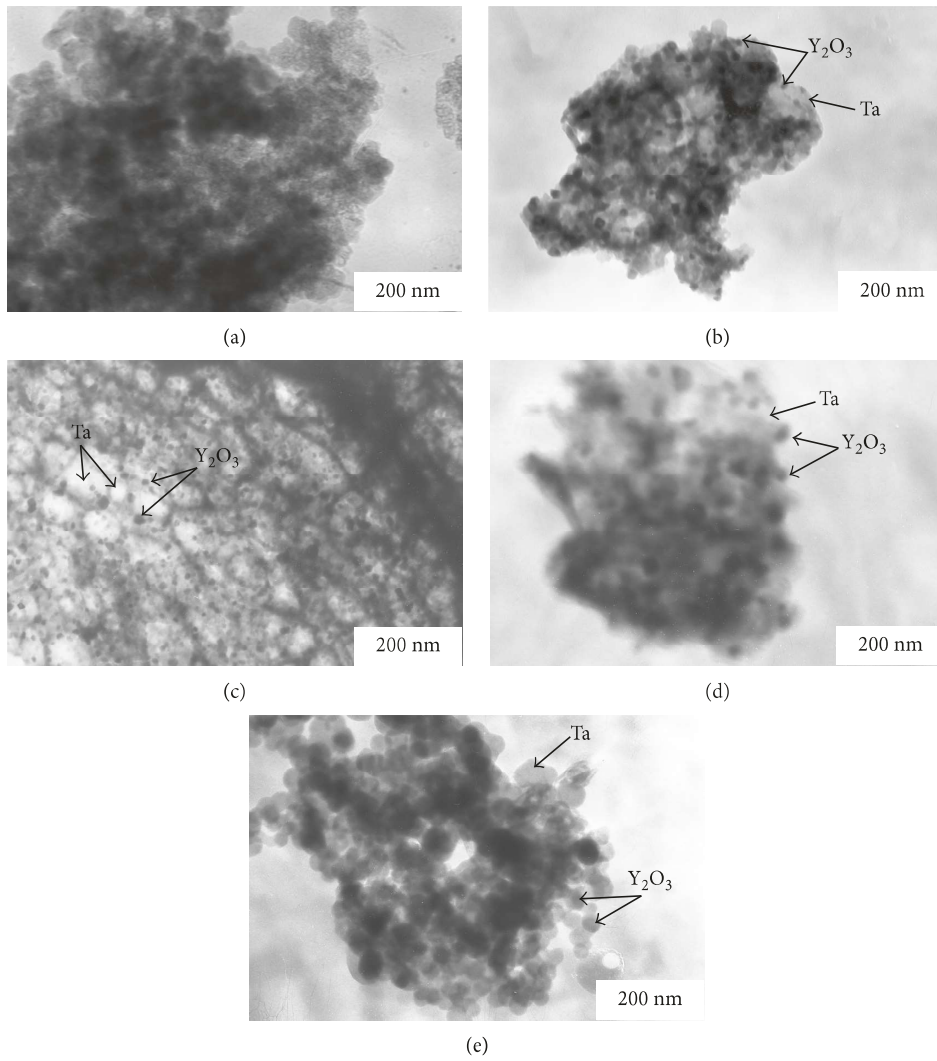
(a)

(b)

(c)

(d)

(e)

FIGURE 5: TEM images of the mechanically milled nanocrystalline Ta (a) and mechanically alloyed Ta-5Y$_2$O$_3$ (b), Ta-10Y$_2$O$_3$ (c), Ta-20Y$_2$O$_3$ (d), and Ta-40Y$_2$O$_3$ (e) nanocomposite powders; the smaller and darker particles correspond to ceramic phase, whereas bigger and lighter to tantalum matrix; the example grains are marked.
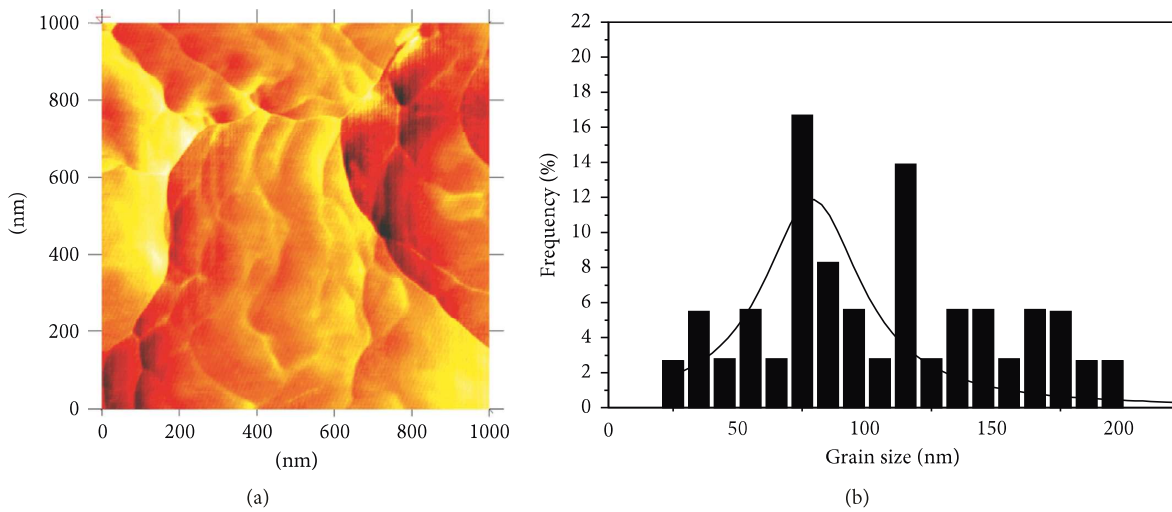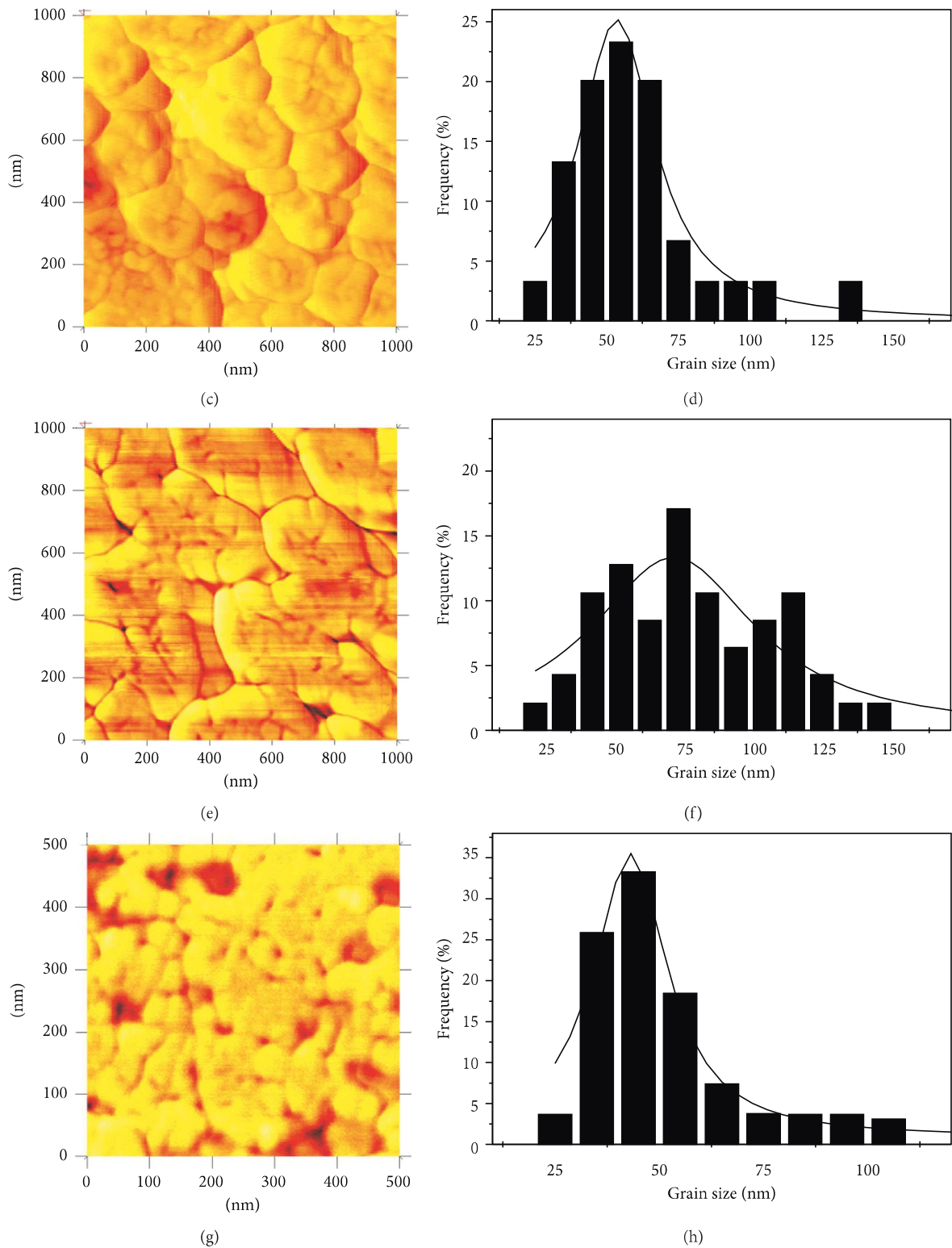

(a)

(b)

FIGURE 6: Continued.

(c)

(d)

(e)

(f)

(g)

(h)

FIGURE 6: AFM pictures (a, c, e, g) and grain size distribution (b, d, f, h) of the mechanically alloyed and consolidated bulk nanocomposites: Ta-5Y$_2$O$_3$ (a, b), Ta-10Y$_2$O$_3$ (c, d), Ta-20Y$_2$O$_3$ (e, f), and Ta-40Y$_2$O$_3$ (g, h).
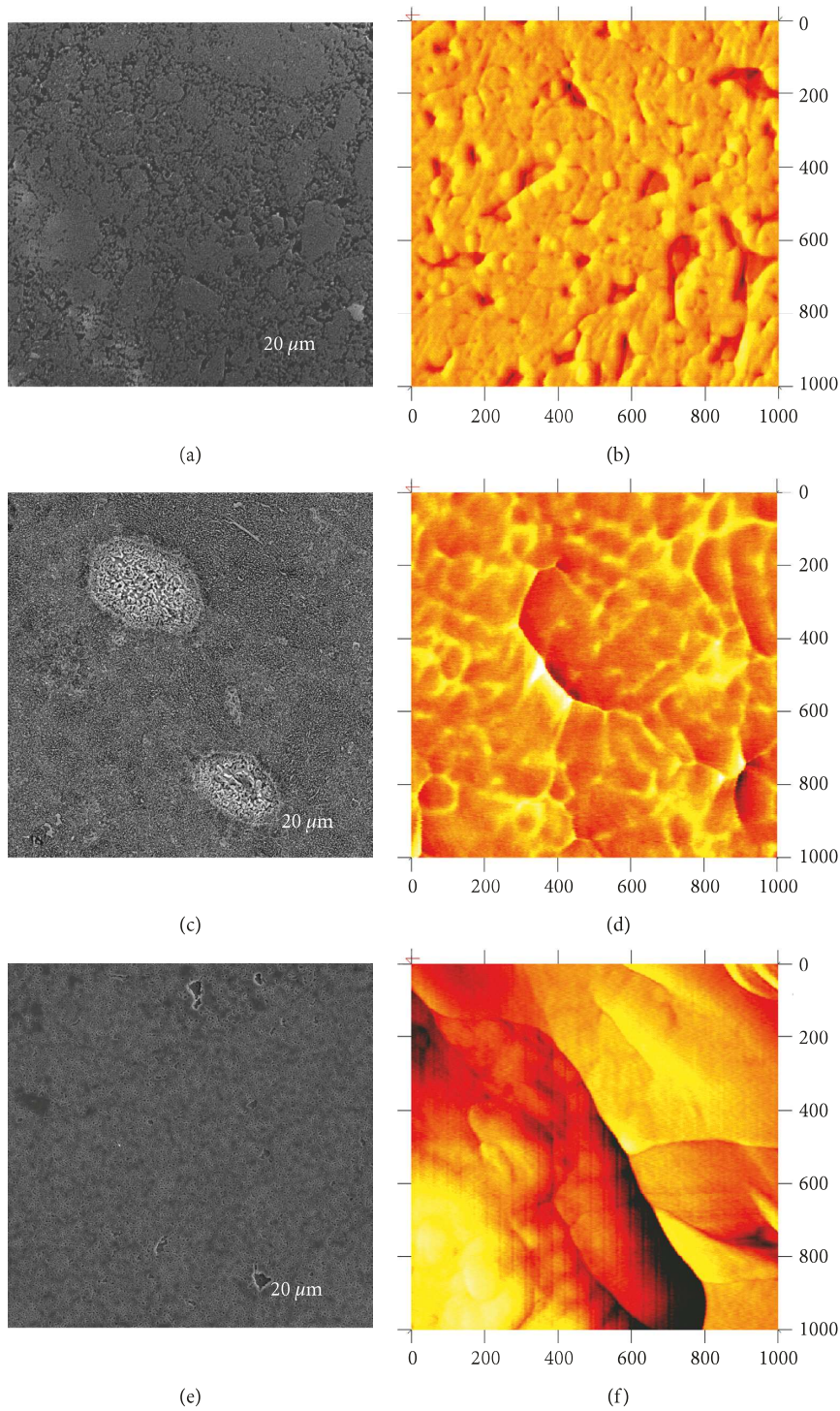
Figure 7: Example of SEM (a, c, e) and AFM (b, d, f) images of the consolidated bulk Ta-40Y$_2$O$_3$ (a, b), Ta-40ZrO$_2$ (c, d), and Ta-40TaC (e, f) nanocomposites.

The average grain size (estimated using AFM) of all the investigated bulk composites has been shown in Figure 8. In all the composites, the grains are smaller in comparison to pure nanocrystalline tantalum. The smallest grains have the composites reinforced with Y$_2$O$_3$ and ZrO$_2$. Generally, the majority of the composites have the grain size significantly below 100 nm.

The ceramic phase grains are well visible on the TEM images of the powders (Figure 5) and are well identified by AFM in the bulk samples (Figure 9). The example
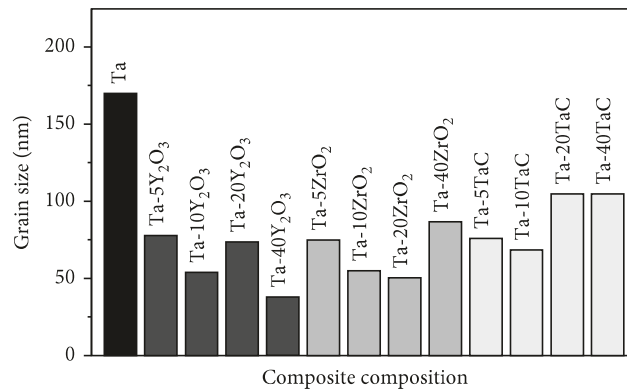
FIGURE 8: Average grain size for the Ta-xY$_2$O$_3$, Ta-xZrO$_2$, and Ta-xTaC bulk nanocomposites ($x = 0, 5, 10, 20,$ and 40 wt.%); data measured using AFM (not all AFM images and grain size distributions have been shown in this paper).

microstructure of the Ta-20ZrO$_2$ bulk nanocomposite shows two-phase morphology (Figure 9(a)), with slightly larger Ta grains (Figure 9(b)) compared to the ZrO$_2$ grains (Figure 9(c)). The corresponding EDS spectra show the grain composition of both the metallic and the ceramic phases. On the lower magnified image (Figure 9(a)), the ceramic phase grains are well visible, because after chemical etching, they are flatter compared to the Ta grains (the samples for the microscopic observations were grinded, polished, and chemically etched to reveal the grains, hence, the etched craters among the sintered agglomerate particles).

The mechanical properties (Figure 10, Table 1) show that the nanocrystalline materials have high strength. The hardness of pure microcrystalline Ta (447 HV) is lower compared to pure nanocrystalline Ta (584 HV). An introduction of the reinforced ceramic phase results in an increase in the hardness up to 1398 HV for Ta-10TaC. Up to the 20 wt.% content of the ceramic phase, the hardness remains very high for all the investigated materials: the highest for the Ta-TaC and the lowest for the Ta-ZrO$_2$ composites. As for the composites of the 40 wt.% content of the ceramic phase, their content is too high to achieve full material integration at the sintering temperature of 1300°C (this needs further investigation at a higher consolidation temperature); therefore, the hardness is significantly lower compared to other composites. Young's modulus increases from 164 GPa for nanocrystalline Ta to the highest value of 346 GPa for Ta-40TaC nanocomposites. The other parameters for composites (W_t, total mechanical work of indentation; N_{plast}, plastic deformation portion; and C_{IT}, indentation creep) are the highest for the 40 wt.% content of the ceramic phase, pointing to the too low sintering temperature (or time) to achieve full integrity of the samples (especially in the case of oxide-reinforced composites). The load-displacement curves (5 indents made on each sample at different spots) in most cases overlap one another indicating very good homogeneity of the microstructure and uniform material deformation during force loading-unloading. Consequently, the mechanical properties have a low value of standard deviation. At the highest oxide ceramic phase content, the curves have a relatively broad spectrum, which

is reflected in the low mechanical properties of these composites.

4. Discussion

The mechanical alloying applied to the tantalum and the ceramic phase particles leads to the formation of nanocrystalline mixture of both tantalum and ceramic grains. The grains have the size of several nanometers. The hot pressing in the PPS mode (performed at an elevated but relatively low temperature) leads to diffusion processes, which is necessary for strong particle bonding. The elevated temperature, however, is also the driving force for the grain growth. The relatively fast heating rate, short sintering time, and low sintering temperature result in a limited grain growth. The large volume of the grain boundaries of the nanocrystalline material should improve the densification process through the sliding mechanism. The agglomerates (formed in the mechanical alloying), which have significant voids between them work against high densification [25]. The pressure acting on the powders when the temperature increases (to the constant sintering temperature) improves the densification and reduces the voids between the consolidated powders. In general, for the densification of the nanocrystalline material, the consolidation temperature can be significantly lower compared to the microcrystalline material [13, 25]. The ceramic phase in the tantalum-based composites can suppress grain growth during consolidation. Hence, all the nanocomposites have a significantly lower grain size compared to pure nanocrystalline tantalum. The higher content (40 wt.%) of the oxide phase acts as a diffusion barrier; thus, in the Ta-40ZrO$_2$ and Ta-40Y$_2$O$_3$ composites, full microstructure integration during hot pressing at given conditions was not obtained. This is reflected in the mechanical properties, which are the worst for the Ta-40ZrO$_2$ and Ta-40Y$_2$O$_3$ composites. The high affinity of tantalum to oxygen leads to the formation of grain boundary oxides that cause embrittlement and grain size growth and the high temperature intensifies this effect [26]. In the case of the Ta-40TaC composite, the aforementioned process is limited. The high-temperature contact of the Ta-based powders with the graphite die and the punches leads to the diffusion of carbon and the
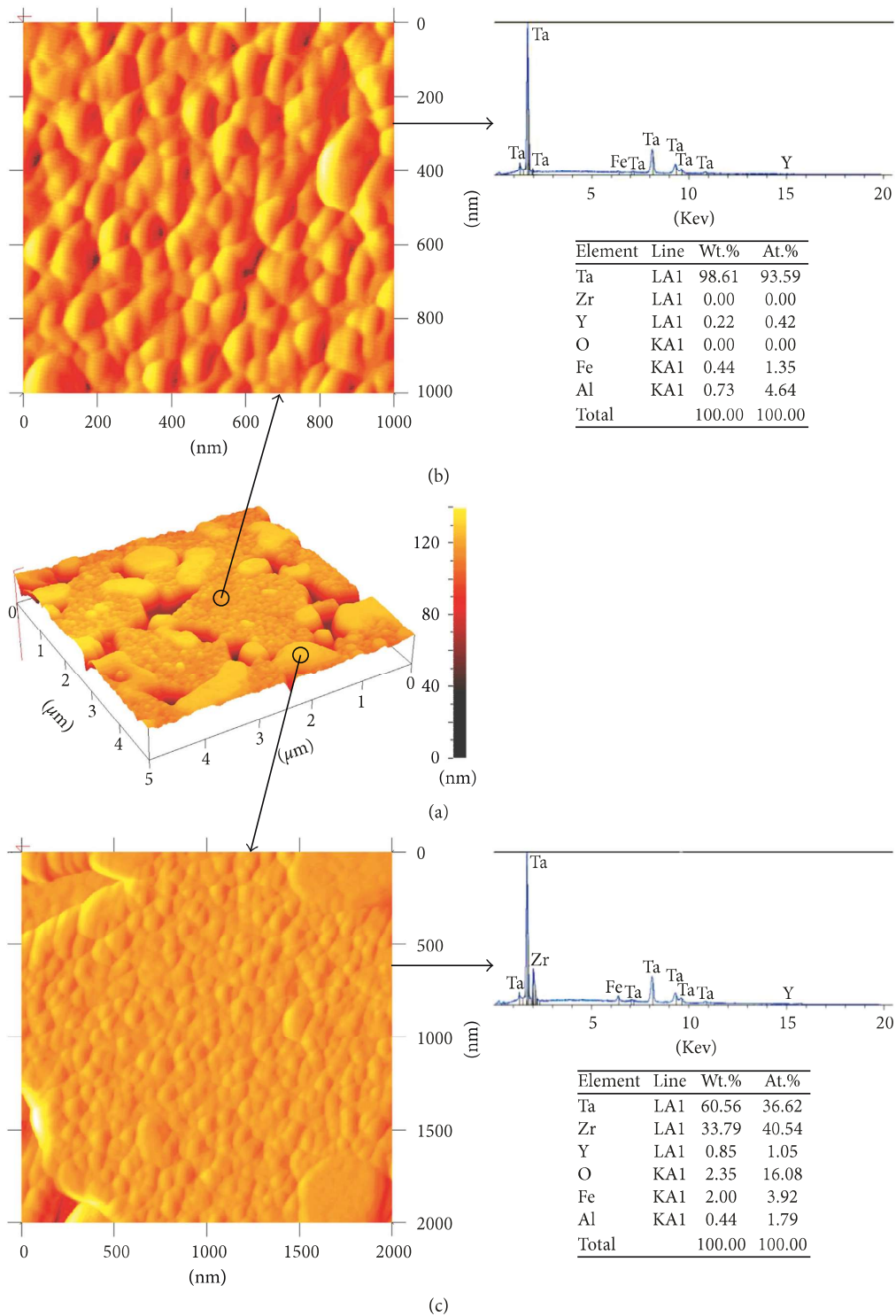
FIGURE 9: Example AFM images and EDS analysis showing the phase distribution in the consolidated bulk Ta-20ZrO$_2$ nanocomposite: larger area view (a), magnified area of the Ta grains (b), and ZrO$_2$ grains (c) with the corresponding EDS analysis.

formation of tantalum carbides, which was also observed by other authors [27].

The nanocomposites (composed of refractory tantalum as the metal matrix with the embedded refractory ceramic phase such as Y$_2$O$_3$, ZrO$_2$, and TaC) have very high mechanical properties, particularly the nanocrystalline Ta-TaC materials, which are promising in terms of heavy load conditions.

5. Conclusions

In this work, nanocomposites based on the Ta matrix reinforced by the ceramic phase of the Y$_2$O$_3$, ZrO$_2$, and TaC particles were developed. The mechanical alloying followed by hot pressing working in the pulse plasma sintering mode was applied for the bulk nanocomposite formation. We
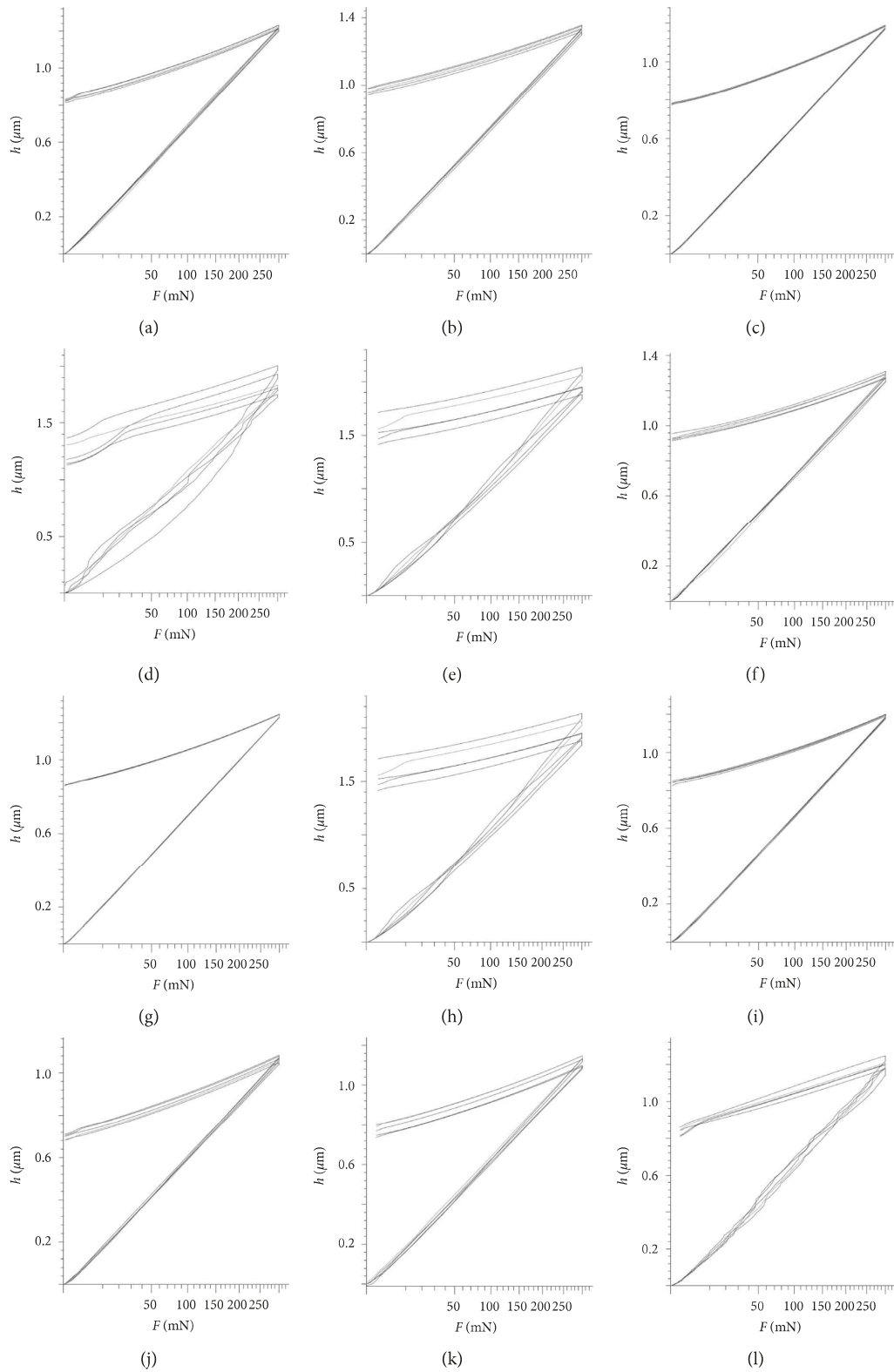
(a)

(b)

(c)

(d)

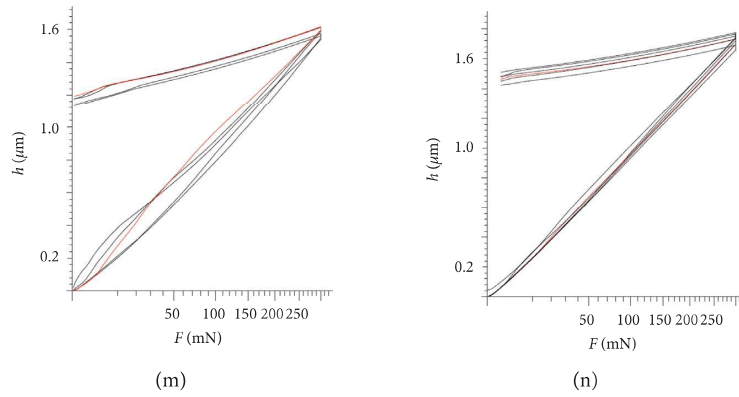(e)

(f)

(g)

(h)

(i)

(j)

(k)

(l)

Figure 10: Continued.

FIGURE 10: Load-displacement curves for consolidated bulk nanocrystalline composites: Ta-5Y$_2$O$_3$ (a), Ta-10Y$_2$O$_3$ (b), Ta-20Y$_2$O$_3$ (c), Ta-40Y$_2$O$_3$ (d), Ta-5ZrO$_2$ (e), Ta-10ZrO$_2$ (f), Ta-20ZrO$_2$ (g), Ta-40ZrO$_2$ (h), Ta-5TaC (i), Ta-10TaC (j), Ta-20TaC (k), and Ta-40TaC (l); for comparison bulk consolidated nanocrystalline Ta (m) and microcrystalline Ta (n).

TABLE 1: Mechanical properties of the investigated hot-pressed Ta-ceramic nanocomposites (data for micro- and nanocrystalline Ta for comparison).

	Mechanical properties				
	HV	E_{IT} (GPa)	W_t (μJ)	N_{plast} (%)	C_{IT} (%)
Ta micro	447 ± 17	211 ± 5	0.17 ± 0.01	81.6 ± 0.5	1.92 ± 0.08
Ta nano	584 ± 19	164 ± 8	0.16 ± 0.01	71.1 ± 2.5	1.54 ± 0.19
Ta nanocomposites:					
Ta-5Y$_2$O$_3$	1055 ± 23	248 ± 2	0.12 ± 0.01	63.6 ± 0.7	1.14 ± 0.08
Ta-10Y$_2$O$_3$	835 ± 23	234 ± 2	0.14 ± 0.01	68.7 ± 0.5	1.56 ± 0.07
Ta-20Y$_2$O$_3$	1165 ± 8	242 ± 1	0.12 ± 0.01	60.0 ± 0.2	1.26 ± 0.03
Ta-40Y$_2$O$_3$	436 ± 52	114 ± 10	0.20 ± 0.04	70.3 ± 3.5	1.70 ± 0.48
Ta-5ZrO$_2$	821 ± 24	231 ± 4	0.14 ± 0.01	69.6 ± 1.0	1.66 ± 0.08
Ta-10ZrO$_2$	920 ± 24	240 ± 8	0.13 ± 0.01	67.3 ± 0.5	1.72 ± 0.09
Ta-20ZrO$_2$	1003 ± 3	246 ± 1	0.13 ± 0.01	64.7 ± 0.1	1.30 ± 0.03
Ta-40ZrO$_2$	366 ± 44	115 ± 3	0.21 ± 0.02	75.5 ± 2.6	2.15 ± 0.17
Ta-5TaC	984 ± 21	273 ± 3	0.13 ± 0.01	67.8 ± 0.4	1.29 ± 0.05
Ta-10TaC	1398 ± 46	336 ± 5	0.11 ± 0.01	61.6 ± 0.9	1.01 ± 0.05
Ta-20TaC	1252 ± 69	303 ± 11	0.12 ± 0.01	63.5 ± 1.2	1.17 ± 0.07
Ta-40TaC	994 ± 48	346 ± 12	0.12 ± 0.01	70.1 ± 1.6	2.17 ± 0.69

HV, Vickers hardness; E_{IT}, indentation modulus; W_t, total mechanical work of indentation; N_{plast}, plastic deformation portion; C_{IT}, indentation creep.

made Ta composites with addition of up to 40% of the ceramic phase. The nanocomposite materials have the average grain size of approximately 40–100 nm, significantly lower than nanocrystalline Ta (170 nm). The lowest grain size has the composites reinforced by oxides. Both reinforced factors, the fine-grained nanostructure and the ceramic phase, lead to significant increase in the hardness as well as Young's modulus. For Ta-10TaC, the hardness and the Young's modulus reach 1398 HV and 336 GPa, respectively. For comparison, pure nanocrystalline Ta has the value of 584 HV and 164 GPa, respectively, whereas microcrystalline Ta has the value of 447 HV and 211 GPa, respectively. The combination of the MA and PPS processes has a potential in developing nanocomposites of high mechanical properties.

Data Availability

The original data files are the property of the Poznan University of Technology and are located in its repository. Access will be considered by the corresponding author upon request.

Conflicts of Interest

The authors declare that there are no conflicts of interest regarding the publication of this paper.

Acknowledgments

References

[1] G. Samsono, *Handbook of Refractory Compounds*, Springer-Verlag, New York, NY, USA, 2012.

[2] C. L. Briant, "The properties and uses of refractory metals and their alloys," *MRS Proceedings*, vol. 322, pp. 305–314, 1993.

[3] H. O. Pierson, *Handbook of Refractory Carbides and Nitrides. Properties, Characteristics, Processing and Applications*, Noyes Publ., New York, NY, USA, 1996.

[4] S. A. Ghaffari, M. A. Faghihi-Sani, F. Golestani-Fard, and M. Nojabayy, "Diffusion and solid solution formation between the binary carbides of TaC, HfC, ZrC," *International Journal of Refractory Metals and Hard Materials*, vol. 41, pp. 180–184, 2013.

[5] E. P. Simonenko, N. P. Simonenko, Y. S. Ezhov, V. G. Sevastyanov, and N. T. Kuznetsov, "Study of the synthesis of nanocrystalline mixed tantalum–zirconium carbide," *Physics of Atomic Nuclei*, vol. 78, no. 12, pp. 1357–1365, 2015.

[6] L. Xu, S. Wei, J. Li, G. Zhang, and B. Dai, "Preparation, microstructure and properties of molybdenum alloys reinforced by in-situ Al_2O_3 particles," *International Journal of Refractory Metals and Hard Materials*, vol. 30, no. 1, pp. 208–212, 2012.

[7] F. Xiao, L. Xu, Y. Zhou et al., "Preparation, microstructure, and properties of tungsten alloys reinforced by ZrO_2 particles," *International Journal of Refractory Metals and Hard Materials*, vol. 64, pp. 40–46, 2017.

[8] M. Battabyal, R. Schäublin, P. Spätig, and N. Baluc, "W-2 wt.% Y_2O_3 composite: microstructure and mechanical properties," *Materials Science and Engineering A*, vol. 538, pp. 53–55, 2012.

[9] S. A. Ghaffari, M. A. Faghihi-Sani, F. Golestani-Fard, and S. Ebrahimi, "Pressureless sintering of Ta0.8Hf0.2C UHTC in the presence of $MoSi_2$," *Ceramics International*, vol. 39, no. 2, pp. 1985–1989, 2013.

[10] M. A. Hussein, C. Suryanarayana, and N. Al-Aqeeli, "Fabrication of nano-grained Ti–Nb–Zr biomaterials using spark plasma sintering," *Materials and Design*, vol. 87, pp. 693–700, 2015.

[11] A. Michalski and D. Siemiaszko, "Nanocrystalline cemented carbides sintered by the pulse plasma method," *International Journal of Refractory Metals and Hard Materials*, vol. 25, no. 2, pp. 153–158, 2007.

[12] R. Chaim, "Superfast densification of nanocrystalline oxide powders by spark plasma sintering," *Journal of Materials Science*, vol. 41, no. 23, pp. 7862–7871, 2006.

[13] Z. Fang, P. Maheshwari, X. Wang, H. Y. Sohn, A. Griffo, and R. Riley, "An experimental study of the sintering nanocrystalline WC-co powders," *International Journal of Refractory Metals and Hard Materials*, vol. 25, no. 4–6, pp. 249–257, 2005.

[14] M. K. Surappa and P. K. Rohatgi, "Preparation and properties of cast aluminium-ceramic particle composites," *Journal of Materials Science*, vol. 16, no. 4, pp. 983–993, 1981.

[15] L. Olmos, C. L. Martin, and D. Bouvard, "Sintering of mixtures of powders: experiments and modelling," *Powder Technology*, vol. 190, no. 1-2, pp. 134–140, 2009.

[16] R. Orrù, R. Licheri, A. M. Locci, A. Cincotti, and G. Cao, "Consolidation/synthesis of materials by electric current activated/assisted sintering," *Materials Science and Engineering R*, vol. 63, no. 4–6, pp. 127–287, 2009.

[17] M. S. Yurlova, V. D. Demenyuk, Y. L. Lebedev, D. V. Dudina, E. G. Grigoryev, and E. A. Olevsky, "Electric pulse consolidation: an alternative to spark plasma sintering," *Journal of Materials Science*, vol. 49, no. 3, pp. 952–985, 2014.

[18] J. Q. Li, W. A. Sun, W. Q. Ao, K. M. Gu, and P. Xiao, "Al_2O_3–FeCrAl composites and functionally graded materials fabricated by reactive hot pressing," *Composites Part A*, vol. 38, no. 2, pp. 615–620, 2007.

[19] S. S. Nayak, M. Wollgarten, J. Banhart, S. K. Pabi, and B. S. Murty, "Nanocomposites and an extremely hard nanocrystalline intermetallic of Al–Fe alloys prepared by mechanical alloying," *Materials Science and Engineering A*, vol. 527, no. 9, pp. 2370–2378, 2010.

[20] G. Zhang and D. Gu, "Synthesis of nanocrystalline TiC reinforced W nanocomposites by high-energy mechanical alloying: microstructural evolution and its mechanism," *Applied Surface Science*, vol. 273, pp. 364–371, 2013.

[21] O. B. Zgalat-Lozinskii, "Nanocomposites based on refractory compounds, consolidated by rate-controlled and spark-plasma sintering (review)," *Powder Metallurgy and Metal Ceramics*, vol. 53, no. 1-2, pp. 19–30, 2014.

[22] T. Niu, W.-W. Chen, H.-W. Cheng, and L. Wang, "Grain growth and thermal stability of nanocrystalline Ni–TiO_2 composites. Transactions of Nonferrous Metals," *Society of China*, vol. 27, no. 10, pp. 2300–2309, 2017.

[23] J. Jakubowicz, G. Adamek, M. Sopata, J. K. Koper, T. Kachlicki, and M. Jarzebski, "Microstructure and electrochemical properties of refractory nanocrystalline Tantalum-based alloys," *International Journal of Electrochemical Science*, vol. 13, pp. 1956–1975, 2018.

[24] J. Jakubowicz, G. Adamek, and M. Sopata, "Characterization of high-energy ball-milled and hot-pressed nanocrystalline tantalum," *IOP Conference Series: Materials Science and Engineering*, vol. 216, p. 012006, 2017.

[25] S. H. Yoo, T. S. Sudarshan, K. Sethuram, G. Subhash, and R. J. Sowding, "Consolidation and high strain rate mechanical behavior of nanocrystalline tantalum powder," *Nanostructured Materials*, vol. 12, no. 1–4, pp. 23–28, 1999.

[26] M. Bischof, S. Mayer, H. Leitner et al., "On the development of grain growth resistant tantalum alloys," *International Journal of Refractory Metals and Hard Materials*, vol. 24, no. 6, pp. 437–444, 2006.

[27] Y. Kim, E. P. Kim, J. W. Noh, S. H. Lee, Y. O. Kwon, and I. S. Oh, "Fabrication and mechanical properties of powder metallurgy tantalum prepared by hot isostatic pressing," *International Journal of Refractory Metals and Hard Materials*, vol. 48, pp. 211–216, 2015.

5

Microstructure and Electrochemical Properties of Refractory Nanocrystalline Tantalum-based Alloys

J. Jakubowicz[1,*], G. Adamek[1], M. Sopata[1], J.K. Koper[1], T. Kachlicki[1], M. Jarzebski[3]

[1] Poznan University of Technology, Institute of Materials Science and Engineering, Jana Pawla II, 24, 61-138 Poznan, Poland
[2] Life Sciences University, Department of Physics, Wojska Polskiego 38/42, 60-637 Poznan, Poland
[*]E-mail: jaroslaw.jakubowicz@put.poznan.pl

The nanocrystalline refractory tantalum alloys were made using mechanical alloying. The tantalum alloys were modified by niobium, molybdenum and tungsten in the concentration of 5, 10, 20 and 40 wt.%. The nanocrystalline powders were consolidated (hot-pressed) using the pulse plasma sintering mode. The hot pressing at the temperature of $1300^{o}C$ results in an increase of the grain size, in comparison to mechanically alloyed powders. However, the lowest grain size (significantly below 100 nm) was achieved for Ta-W alloys (approximately 40-60nm). The grain size was confirmed by XRD, TEM and AFM. The most uniform microstructure is also exhibited by the Ta-W alloys. The corrosion resistance was measured using the potentiodynamic mode in a chloride solution. The nanocrystalline Ta-Mo and Ta-W alloys achieved the same level of corrosion resistance as microcrystalline pure tantalum and 3 orders of magnitude better than pure nanocrystalline tantalum. Among all the prepared nanocrystalline tantalum alloys, the most promising properties exhibit those having 10% of the tungsten addition.

1. INTRODUCTION

Tantalum is a refractory element of high melting point and toughness. It belongs to a group of materials of many possible applications, from temperature resistant to biomedical ones [1-3]. The material is very resistant to corrosive agents as well high temperature and radiation [4, 5]. The limits for its application are related mainly to its high cost and difficult processing. The material is promising

for future applications conditional upon its technological progress. Tantalum constitutes a base for its refractory alloys and composites [6-8]. It can also be used for coating other materials [9]. Tantalum is a ductile bcc metal of high melting point that can be strengthened through grain size reduction and alloying without brittle fracture. The alloying elements, which can modify the properties of tantalum, can be derived into interstitial or substitutional elements, such as C, N or W, Mo, Nb and Ti, respectively. Tungsten, for example, has a high melting point, strength and corrosion resistance, yet brittle material. Combination of different elements with tantalum results in solid solution and/or precipitation strengthening [6]. A solute-solution softening is possible resulting in a decreased yield stress [10]. Tantalum exhibits significant strain hardening, which is a function of the strain rate and pre-straining. In the form of nanostructure, tantalum tends to get softer at high strain rates [11]. Ductility and flow stress increase when the grain size is lower than 100 nm.

Beside solid solutions, intermetallic phases lead to the strengthening of the microstructure. It is very difficult to prepare uniform alloys using conventional melting processes (for example, vacuum arc melting or electron beam melting) and casting, especially if the melted components have significantly different melting temperatures (high melting temperature of $3017^{\circ}C$ for Ta) and densities (high density of 16.4 g/cm^3 for Ta).

In conventionally cast tantalum, the microstructure contains large columnar and highly textured grains [12, 13]. Subsequent plastic deformation of the textured microstructure is often hampered by a non-uniform flow [14, 15]. The texture requires many processing routes to its elimination and uniformization [12-15]. The conventional melting processes of refractory alloys require equipment capable of maintaining a very high temperature. To overcome these problems, the refractory compounds can be made using unconventional processes, leading to the formation of powders, bulks or coatings often in the form of nanomaterials [16, 17].

The formation of tantalum alloys in the form of nanopowders can be done through intensive milling of the elemental powder mixture in the process of mechanical alloying (MA). The problem related to nanocrystalline powders is their transformation into bulk consolidated material as well as the oxidation process. The high consolidation temperature leads to grain growth, which is why conventional powder metallurgy including conventional high-temperature and long-time sintering has limited applications. Several processes useful for nanomaterials consolidation have been developed, in which the consolidation temperature and time are limited [18-23]. The nanocrystalline powders have better sinterability and require lower consolidation temperature in comparison to the microcrystalline ones [11, 24]. The lowest useful consolidation temperature is limited by excess high porosity and low mechanical strength of the final product, whereas the highest consolidation temperature is limited by the excess grain growth. The large surface area of the nanoparticles improves the densification process. Unfortunately, the large and highly reactive surface area of the active metals exposed to oxygen (even residual oxygen at vacuum or inert atmosphere) leads to fast oxidation and reduction of mechanical properties [25].

Due to lack of information regarding nanostructural tantalum alloys, this work shows the results of the formation and properties of nanocrystalline Ta-based alloys modified by refractory Nb, Mo and W elements. The alloys were produced in a mechanical alloying process and the consolidation

was performed by the Pulse Plasma Sintering (PPS) process. The structural and electrochemical properties of the alloys were described.

2. MATERIAL AND METHODS

In this work, nanocrystalline Ta-Nb, Ta-Mo and Ta-W alloys, containing 5, 10, 20 and 40 wt.% of Nb, Mo and W were synthesized, marked as Ta-xNb, Ta-xMo and Ta-xW, where x is 5, 10, 20 or 40 wt.%, respectively. The nanocrystalline tantalum alloy powders were produced by mechanical alloying (MA). The tantalum powder of the 325 mesh size (<44 μm) and the purity >99.97% was provided by Alfa Aesar (Germany). The niobium powder <45 μm size and purity >99.8% as well as tungsten powder of the size range 0.1-1μm and purity >99.9% were provided by Sigma-Aldrich (Germany). The molybdenum powder of the size <5 μm and purity >99.8% was provided by Goodfellow (England). The mixture of a total of 5.5g of the powders was loaded and reloaded into the milling vial in the Labmaster and Unilab glove boxes (MBraun, Germany) providing high purity inert atmosphere (argon) of controlled oxygen and moisture content (<2 ppm). For each alloy several syntheses were performed to provide material for 5 consolidated samples of each designed composition. The MA process was performed in a proprietary hardened steel vial (>62 HRC) mounted in the SPEX 8000M Mixer/Mill (Spex SamplePrep, USA). The milling time was set experimentally at 48h and the mill ran with the frequency of 875 cycles/minute. A room temperature was a standard condition of the MA process. The steel hardened ball bearings (>62 HRC) to powder weight ratio was 3. The atmosphere in the vial was inert, of the same purity as in the glove box.

The as-milled powders were then axially hot-pressed at vacuum (about 4 Pa) using graphite die and graphite movable punches. The pressure of the punches directed at the powder was 50 MPa. The boron-nitride spray (HeBoCoat, Germany) was applied to prevent the powder material from sticking to the die and to ensure easier motion of the punches. In the consolidation process, Pulse Plasma Sintering mode (PPS) was applied for heating with pulses of high electric current going through the die and the powder. The hot-pressed equipment including PPS module has been made by Elbit (Elbit, Koszyce Wielkie, Poland). The current pulses in the module were generated by discharging of a 250 μF capacitor, charged to 8 kV maximum voltage. The pulse duration in the sintering process was automatically controlled following a temperature measurement by a pyrometer aiming at the upper punch. Voltage, pulse frequency, force, temperature, and real-time vacuum were automatically controlled during the PPS procedure. The pressing temperature was set experimentally and the process was performed at 1300°C. The time of sintering at a constant temperature was 5 s. The hot-pressed bulk samples were 8 mm in diameter and 4 mm in height.

The structure analysis was performed on each step of the experiments using Empyrean XRD (Panalytical, The Netherlands) equipped with a crystallographic ICDD-JCPDS database. The investigations were carried out using CuKα radiation at the voltage of 45 mV and the anode current of 40 mA. The structure was investigated in 2θ range 30-120 deg., the step size was 0.0167 deg. and the time per step was 12.54 s/step. The grain size of the alloys was estimated by the Scherrer equation. For the XRD analysis, Panalytical HighScore software was used.

The microstructure and morphology of the powders and alloys was analyzed using Vega 5135 SEM (Tescan, Czech Republic), operating at 20 kV in the mode of secondary electrons. The SEM operates together with PGT Prism 200 Avalon EDS (Princeton Gamma-Tech, USA). The microstructure and grain size analysis was also performed using Q-Scope 250 AFM (Quesant, USA). The AFM worked in the tapping mode using a NanoandMore premounted SSS-NCLR Nanosensors probe of the frequency of 145 kHZ and the scan speed of 3 lines/s. A total of 1024 scan lines were fixed for image acquisition. For microstructural observations, all the bulk samples after hot pressing were grinded on a sandpaper (up to 1000 grit), polished in a Al_2O_3 suspension and finally etched in a H_2SO_4 + HNO_3 + HF mixture to reveal the grain boundaries (for the corrosion and XRD tests, the samples were not etched).

A CM 20 Super Twin TEM microscope (Philips, The Netherlands) of a 0.24 nm resolution at an acceleration voltage of 200 kV was applied for the powders characterization.

The hydrodynamic diameters of the particles after the MA process were obtained applying the dynamic light scattering technique (DLS) using Zetasizer Nano-ZS (Malvern Instruments Ltd, UK). Typically, a few mg of the prepared powders were suspended in 1mL of deionized water. Before the examinations, the dispersions were treated at the sonic bath for 2h. For the measurements, 100µL of the supernatant from the suspension was taken into 1000µL of water.

The corrosion resistance was measured on hot-pressed samples using a Solartron 1285 Potentiostat (Solartron Analytical, England). The potentiodynamic mode was applied, starting at −0.5V and finishing at 3V against OCP (open-circuit-potential). The scan rate was 0.5 mV/s. The sample was the working electrode, graphite was the counter electrode and Ag/AgCl was the reference electrode in the electrochemical EG&G electrochemical cell (Princeton Applied Research, USA). The corrosion resistance was measured in the Ringer's solution containing the following concentration of ions: 147.2 mmol· l^{-1} Na$^+$, 4.0 mmol· l^{-1} K$^+$, 2.2 mmol· l^{-1} Ca^{2+}, 155.7 mmol· l^{-1} Cl$^-$. The electrolyte was mixed with a magnetic stirrer and purged with nitrogen.

3. RESULTS

In the described work, nanocrystalline tantalum alloys were made utilizing the mechanical alloying (MA) process, followed by hot pressing using the pulse plasma sintering mode (PPS). For clear comparison of the effect of the alloying elements on the alloy properties, the authors made alloys of identical wt.% content of the Nb, Mo and W as the alloying element (i.e. 0, 5, 10, 20 and 40%). These are substitutional elements forming continuous solid solutions in the entire range of compositions and belong to a group of refractory metals. The main contamination of the elemental powders is oxygen (<1200 ppm), niobium (<50 ppm) and iron (<40 ppm). In the MA process, the powder mixture of desired composition was mechanically milled for 48h. The time of milling was set based on our previous research on the milling of pure Ta [26] as well as on the experiments of the current work for alloy formation. During intensive milling of the powders in the steel vial, the iron contamination was introduced into the alloy composition (Fig. 1). Oxygen and carbon in alloys

(introduced from the atmosphere and graphite die, respectively) were detected by EDS (not shown here), but their content cannot be properly determined using this method.
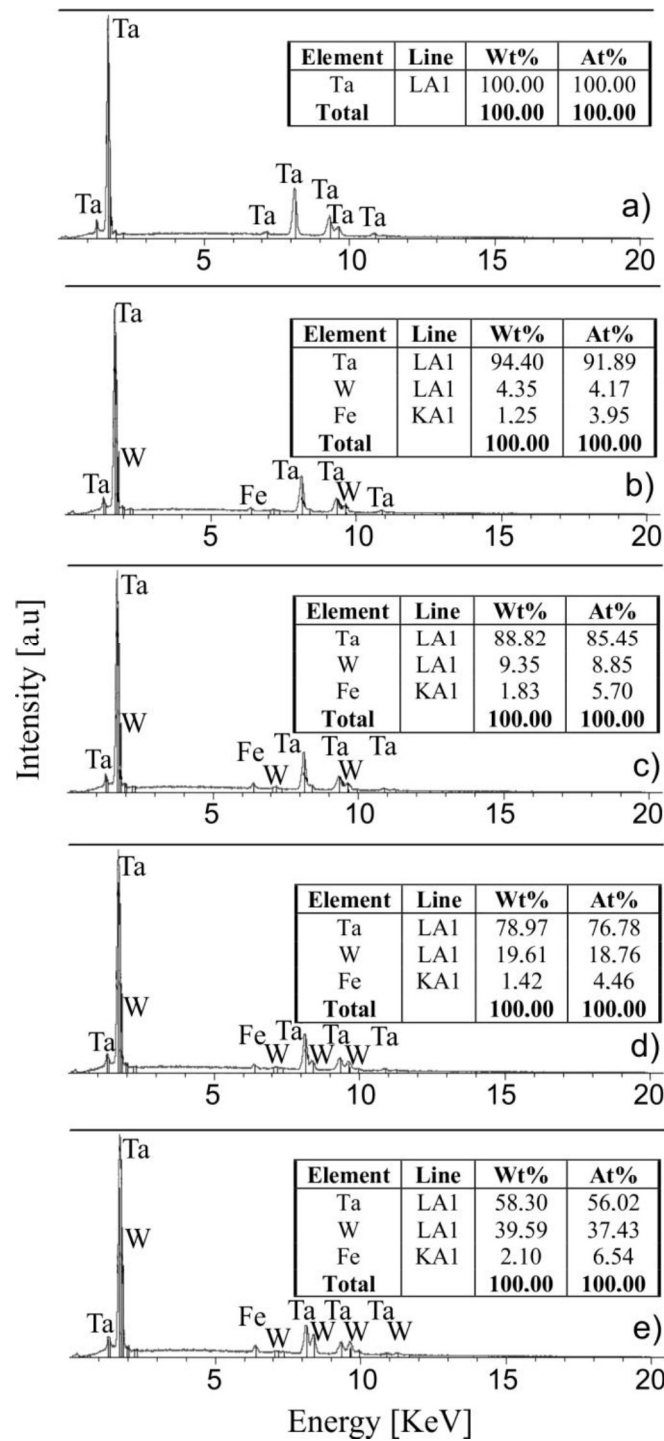

Figure 1. Example EDS analysis of the material after mechanical alloying and hot pressing for the: Ta (a), Ta-5W (b), Ta-10W (c), Ta-20W (d) and Ta-40W (e) designed compositions

In the process, the authors used Ar of 99.999% purity at all experimental stages, thus the oxygen content was limited. In the work [27] the authors used depth profiling AES analysis for chemical analysis of the mechanically alloyed powders. The thickness of the oxide layer reaches 5 nm,

whereas for iron and carbon it is approx. 10 nm, hence the powders in the mechanical alloying process are contaminated only in the surface layer [33]. The final alloy composition after mechanical alloying and hot pressing is slightly different from the design composition, because of the iron impurity (Fig. 1). In all the alloys, the Fe content does not exceed 2.1 wt.%.

Figure 2 shows the XRD spectra for microcrystalline Ta (a), example Ta-40Nb composition after the MA process (b) and examples of Ta-40Nb, Ta-40Mo and Ta-40W alloys of the highest alloying elements content after the MA and PPS processes (c, d, e). For all the investigated alloys the solid solutions are formed. The hot pressing of the mechanically alloyed powders leads to their densification and consolidation. The graphite die can partially react with the powder, forming carbides. The formation of carbides while pressing in the graphite die was also observed in [22]. The hot pressing in all the cases results in narrower and higher intensity XRD peaks, which means that the grain size increases during high temperature consolidation.
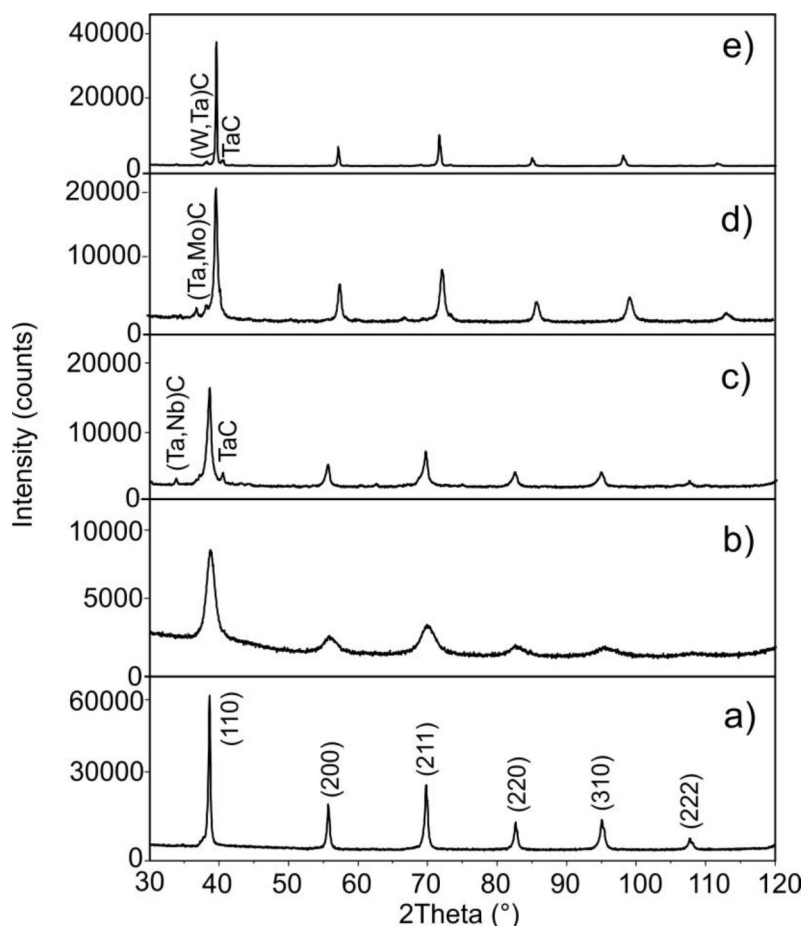
Figure 2. XRD of pure Ta (a), example Ta-40Nb after mechanical alloying (b), and example bulk alloys Ta-40Nb (c), Ta-40Mo (d) and Ta-40W (e) after mechanical alloying and PPS (c-e)

Mechanical alloying leads not only to alloy formation at a room temperature, but also to a significant reduction of the grain size (Figure 3; data obtained based on the XRD spectra using Panalytical HighScore software).
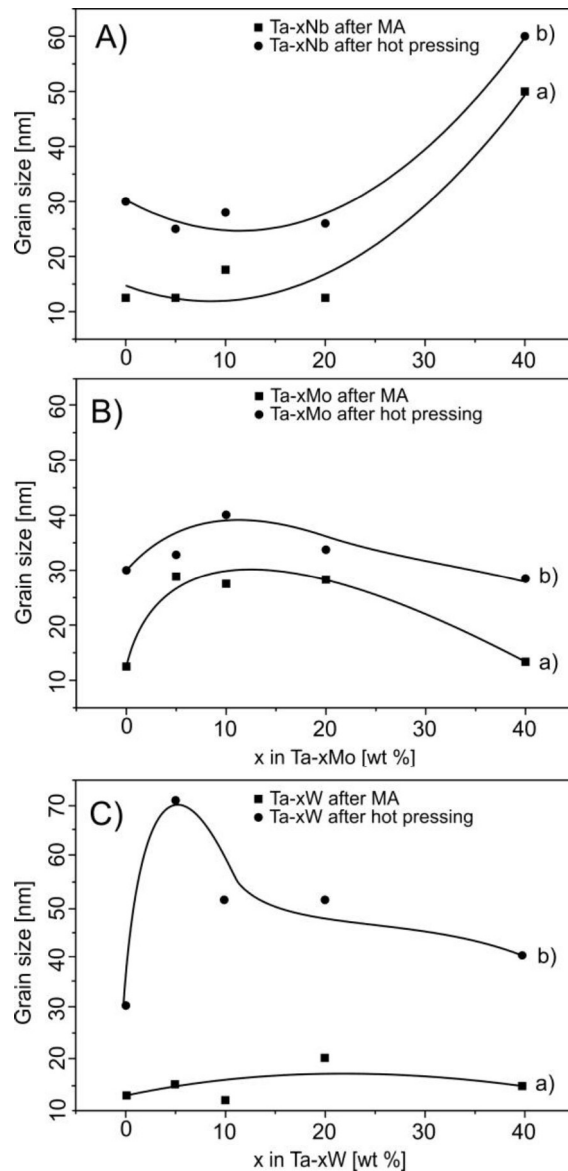
Figure 3. The effect of the Nb (A), Mo (B) and W (C) content on the grain size of the Ta-xNb, Ta-xMo and Ta-xW alloys after mechanical alloying (a) and hot pressing (b)

In all alloys a nanostructure was formed, i.e. there exist grains with the size significantly below 100 nm. In the Ta-Nb system, after the MA process, the grain size increases with the Nb content, and for Ta-40Nb reaches approx. 48 nm, whereas pure Ta after 48h milling has grains of approx. 13 nm (Fig. 3A). Hot pressing, as was shown on the XRD spectra, results in a grain size increase, and for pure nanocrystalline Ta and Ta-40Nb alloys, the values are 30 and 60 nm, respectively (Fig. 3A). For the Ta-Mo alloy system, the increase of the Mo content up to 10% initially leads to an increase in the grain size, whereas at a higher Mo content, the size decreases (Fig. 3B). The hot-pressed Ta-Mo alloys have a lower grain size in comparison to the Ta-Nb alloys (Fig. 3B). After hot pressing, the grain size does not exceed 40 nm. For the Ta-W alloy system, for all investigated tungsten contents, the MA process results in a grain size of the range of 12-20 nm (Fig. 3C). After hot pressing, the grain size

significantly increases for the Ta-5W alloy only and reaches 70 nm. For higher tungsten content, the material has a grain size of approx. 40-50 nm.

The hydrodynamic diameters of the particles (Fig. 4) after mechanical alloying were obtained with dynamic light scattering (DLS). The average values were obtained from 10 measurements and representative particle size distributions. In the mechanical alloying, due to the milling characteristic, mainly the agglomerates are formed composed of smaller grains (see later TEM results in Fig. 5).
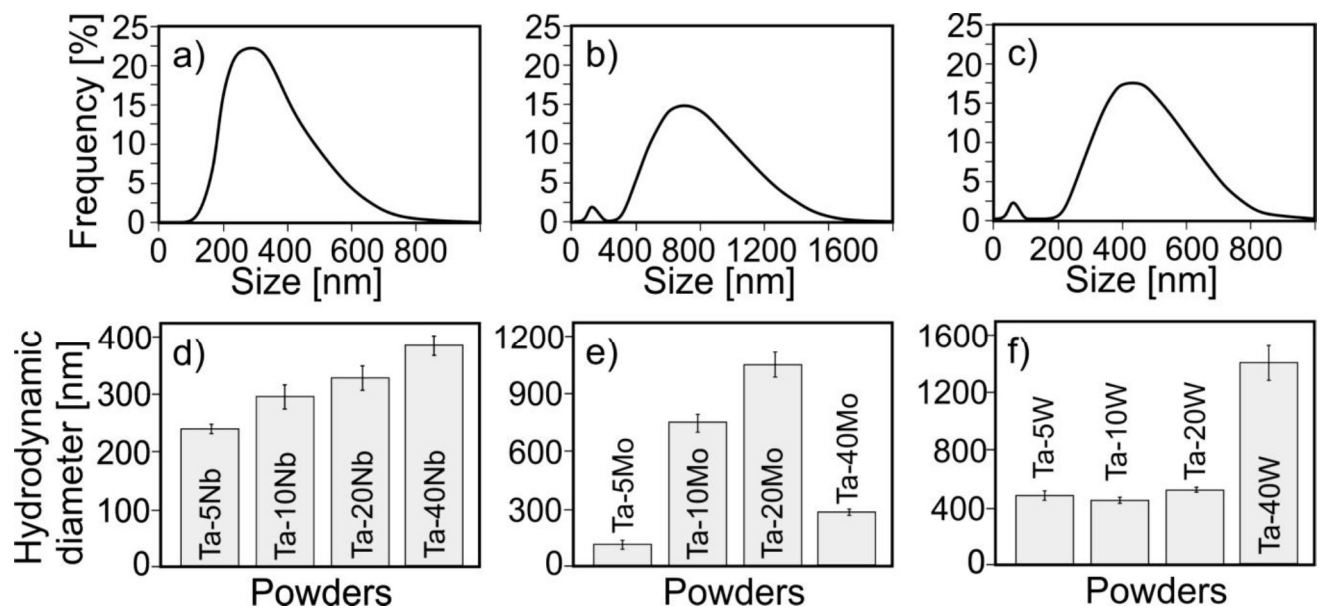
Figure 4. Example DLS particle size distribution of the Ta-10Nb (a), Ta-10Mo (b) and Ta-10W sample (c) and the average hydrodynamic size of particles (agglomerates) of the Ta-Nb (d), Ta-Mo (e) and Ta-W (f) powders

These agglomerates are stable even upon sonication. For pure nanocrystalline Ta, the agglomerate size was 269 nm (not shown in Fig. 4), whereas for the Ta-Nb alloys, the agglomerate size (hydrodynamic equivalent diameter) increased from 236 nm for the Ta-5Nb to 380 nm for the Ta-40Nb powders. Among the Ta-Mo powders, for Ta-5Mo, the agglomerates reached the lowest value of 130 nm, whereas for the Ta-W system, the agglomerates were significantly larger and for 5-20% of tungsten they were kept at the level of approx. 400 nm and significantly increased up to 1414 nm for the 40%W content.

The selected powders of the Ta and Ta-Nb alloys after the MA process were visualized using TEM (Fig. 5). TEM confirmed the nanostructure in the extensively milled materials (grain size <100 nm). TEM showed that the nanocrystalline Ta powder had a grain size of approx. 20 nm, Ta-5Nb, Ta-20Nb and Ta-40Nb had a grain size of 80 nm, 40 nm and 90 nm, respectively. The correlation of the TEM with the XRD results is quite good. The grain size estimated using TEM was slightly higher, but more tangible and reliable in comparison to those obtained using XRD.
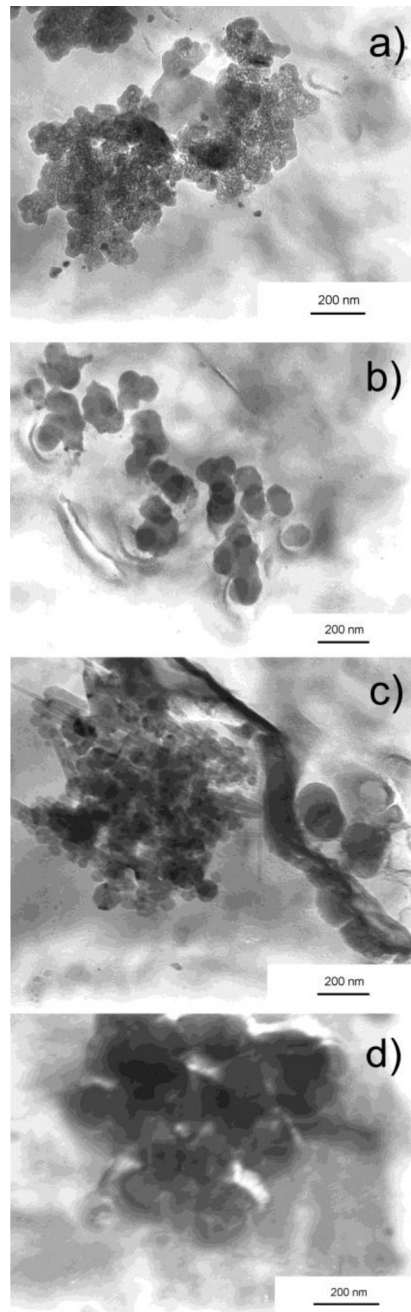
Figure 5. TEM images of the mechanically milled Ta (a) and mechanically alloyed Ta-5Nb (b), Ta-20Nb (c) and Ta-40Nb (d) nanocrystalline alloys

The hot-pressed alloys were investigated using AFM. The bulk samples were investigated approx. 1 mm under the original sample surface (samples were grinded and polished). The obtained AFM images (Fig. 6 and Fig. 7) have been shown using "deflection/error" signal, which enhances the visibility of the grain boundaries. Example AFM images with the grain size distributions for the Ta-W hot pressed alloys have been shown in Fig. 6. The smallest grains among all Ta-W alloys were formed in the Ta-10W alloy (c, d).
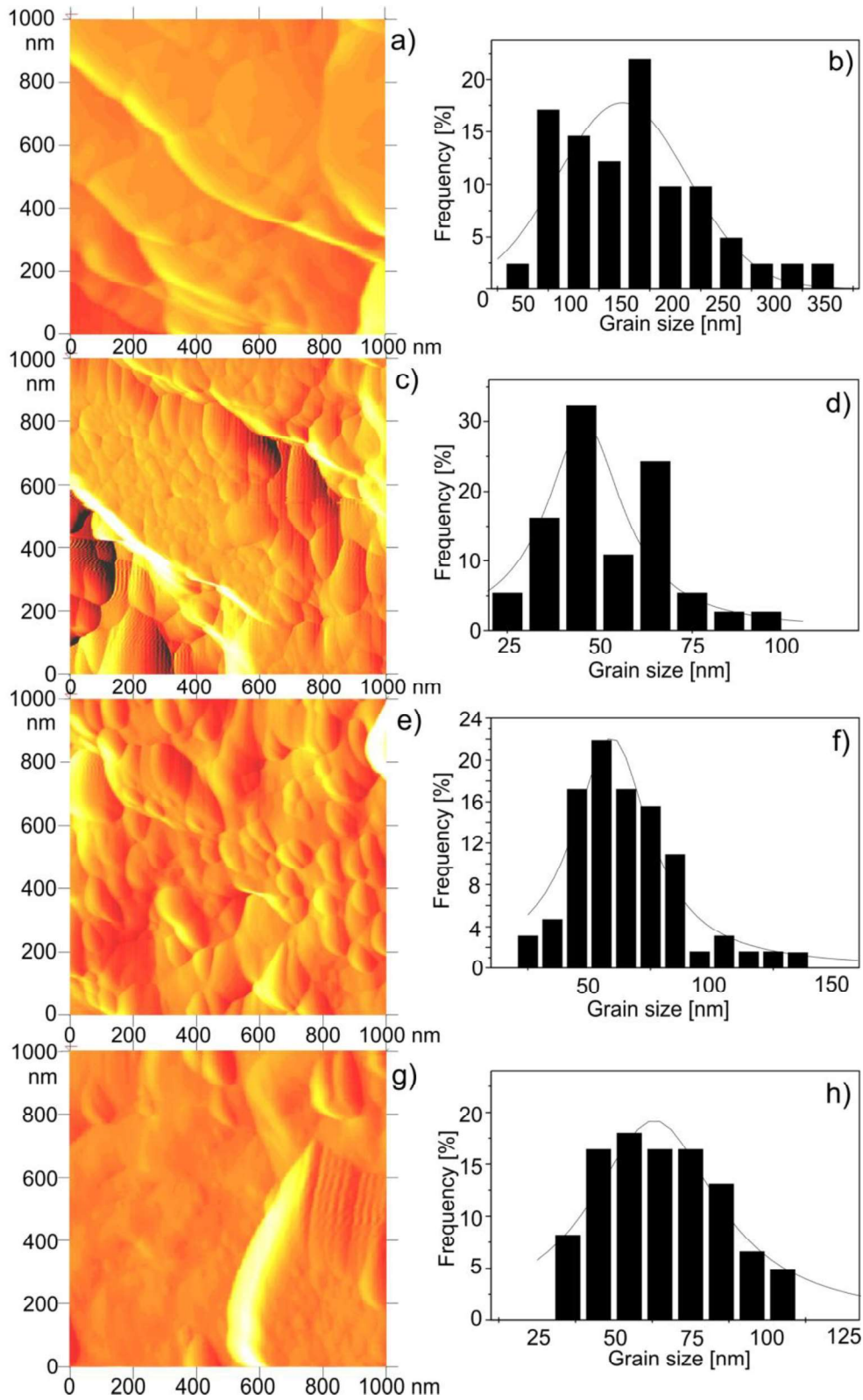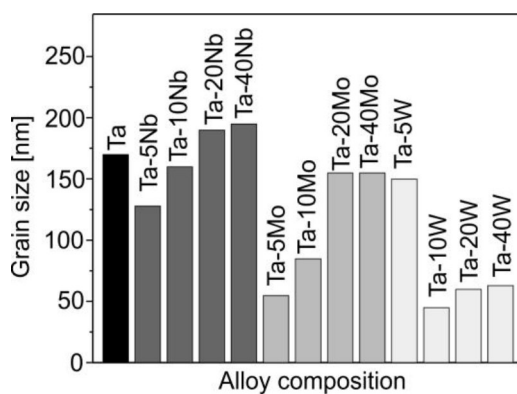
Figure 6. AFM images (a, c, e, g) and grain size distribution (b, d, f, h) of the hot-pressed Ta-xW alloys: Ta-5W (a, b), Ta-10W (c, d), Ta-20W (e, f) and Ta-40W (g, h)
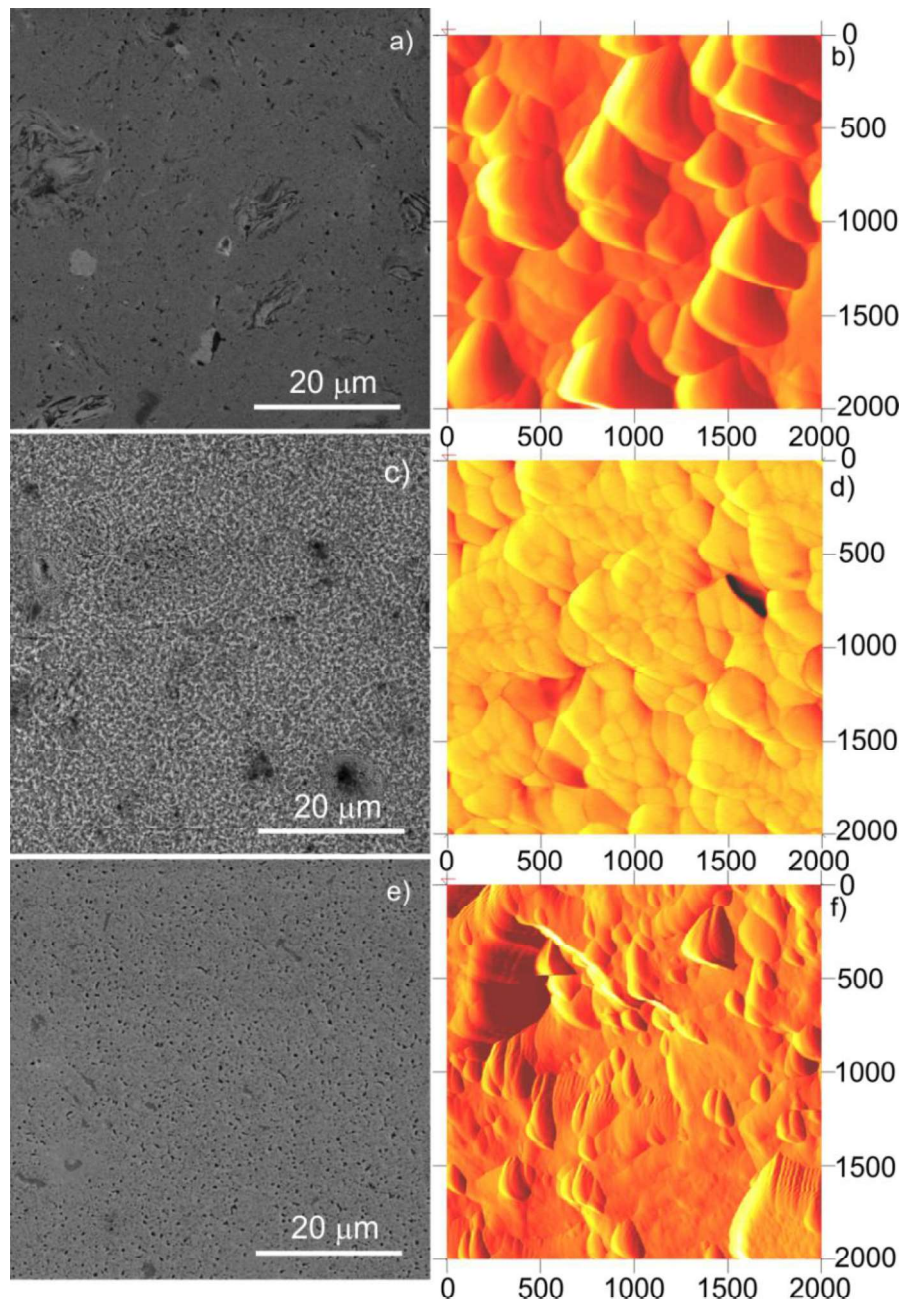
Figure 7. Example of SEM (a, c, e) and AFM (b, d, f) images of the Ta-40Nb (a, b), Ta-40 Mo (c, d) and Ta-40W (e, f) alloys after mechanical alloying and hot pressing

The comparison of the microstructure of the example Ta-40Nb (a, b), Ta-40Mo (c, d) and Ta-40W (e, f) alloys has been shown in Fig. 7. Both, SEM (a, c, e; lower magnification) and AFM (b, d, f; higher magnification) images have been shown, pointing to the difference in the grain size (at higher magnification) as well as the densification and residual porosity (at lower magnification) of the hot-pressed alloys. In the tantalum alloys, those that were modified by Nb, exhibit a larger grain size. The smallest grain size, measured by AFM, is representative of W doped alloys. The lowest and the smallest porosity and the pore size, respectively have alloys modified with tungsten. The Mo modified alloys have relatively the largest porosity. The density of the samples is approx. 93-95% of the theoretical value.

Based on the AFM images, the grain size distribution was determined for all alloy compositions and the results have been shown in Fig. 8. In the Ta-Nb alloys, the increased Nb content leads to a wider grain size distribution (not shown here). The alloy with 5% Nb has the narrowest grain size distribution with an average grain size of 128 nm. For 10% Nb, the average grain size is estimated to be 160 nm, whereas for 20% and 40% Nb, the average grain size is 190 and 195 nm, respectively. The Ta-Nb alloys have a relatively large and broad spectrum of the grain size (not shown here) from 30 to 350 nm. The largest grains were observed for a higher Nb content. In the Ta-Mo alloys, the grains are smaller in comparison to the Ta-Nb alloys. The smallest grains were observed for the 5%Mo content with an average value of 55 nm. The increased Mo content leads to an increased average grain size up to 155 nm. The increased Mo content also leads to a wider spectrum of the grain size distribution (not shown here) with the largest grains reaching 380 nm. In the Ta-W alloys, the 5%W does not lead to a grain size reduction as in the case of 5%Nb and 5%Mo, compared to pure Ta. For a higher W content, a significant reduction in the grain size was achieved and for Ta-10W a 45 nm average grain size was recorded. For 20%W and 40%W in the Ta alloy, the average grain size was 60 nm and 65 nm, respectively. For the Ta-W alloys, the grain size distribution was in the range from 20 to 350 nm. Generally, in all investigated alloys, the introduction of an alloying element results in a grain size reduction in a limited range. In alloys modified by Nb and Mo, the most significant reduction of the grain size was achieved for the 5-10% content, whereas for the W modified alloys, the most significant reduction of the grain size was achieved for 10÷40%W. Tungsten is the most effective in grain size reduction. The results of the grain size, obtained using the AFM measurements, are roughly consistent with those measured by XRD or TEM.

Figure 8. Average grain size for the Ta-xNb, Ta-xMo and Ta-xW alloys (x=0, 5, 10, 20, 40 wt.%); data obtained by AFM (not all AFM images and grain size distributions have been shown in this work)

The corrosion resistance was measured in chloride containing the Ringer's electrolyte and the results in the form of OCP-time dependence and polarization curves have been presented in Figs. 9-11 and in a qualitative form in Table 1. The measurement of stationary potential against time (OCP against time) determines the tendency of the material to corrode. Based on the OCP changes, the protective properties of the passive layer formed on the surface of the alloy can be estimated. Stationary potential measurement (OCP) is carried out in an open loop potentiostat. When the external

circuit is open, the current does not flow and the thermodynamic state is determined on the electrodes. The electrochemical cell is in the state of thermodynamic equilibrium.
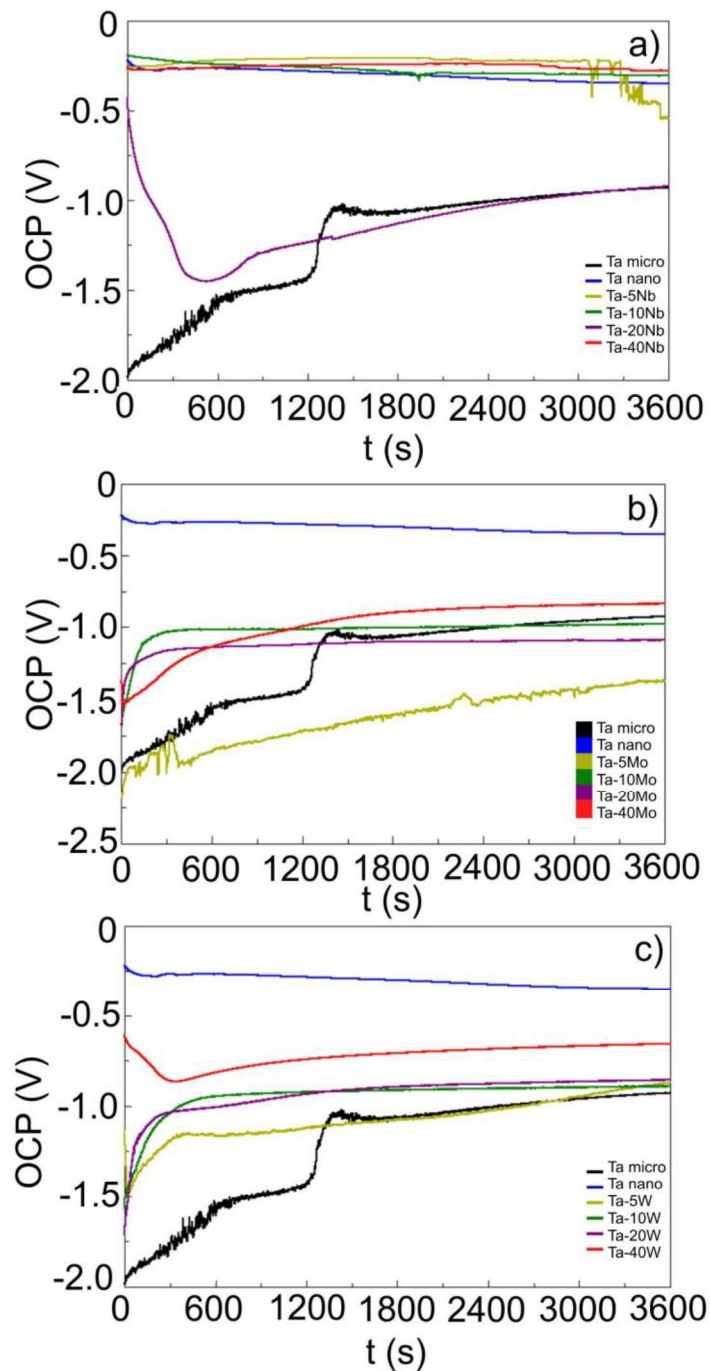
Figure 9. OCP as a function of time in the Ringer's electrolyte for the Ta-xNb (a), Ta-xMo (b) and Ta-xW (c) nanocrystalline alloys (x=5, 10, 20, 40 wt.%); for comparison, data for nano- and microcrystalline Ta have been included

The open-circuit-potential (OCP) indicates a stabilization of the passive oxide layer (Fig. 9). The lowest negative OCP value represents microcrystalline tantalum, and for the investigated alloys, greatly shifts to a more positive one. Generally, the increase in the OCP with time for the Ta-W and

Ta-Mo alloys indicates a trend for passivation and thickening of the native oxide, while for pure nanocrystalline tantalum and most Ta-Nb alloys, the heavily stable passive layer does not form (a drop of the OCP). The example of the polarization curves has been shown in Fig. 10 and Fig. 11.
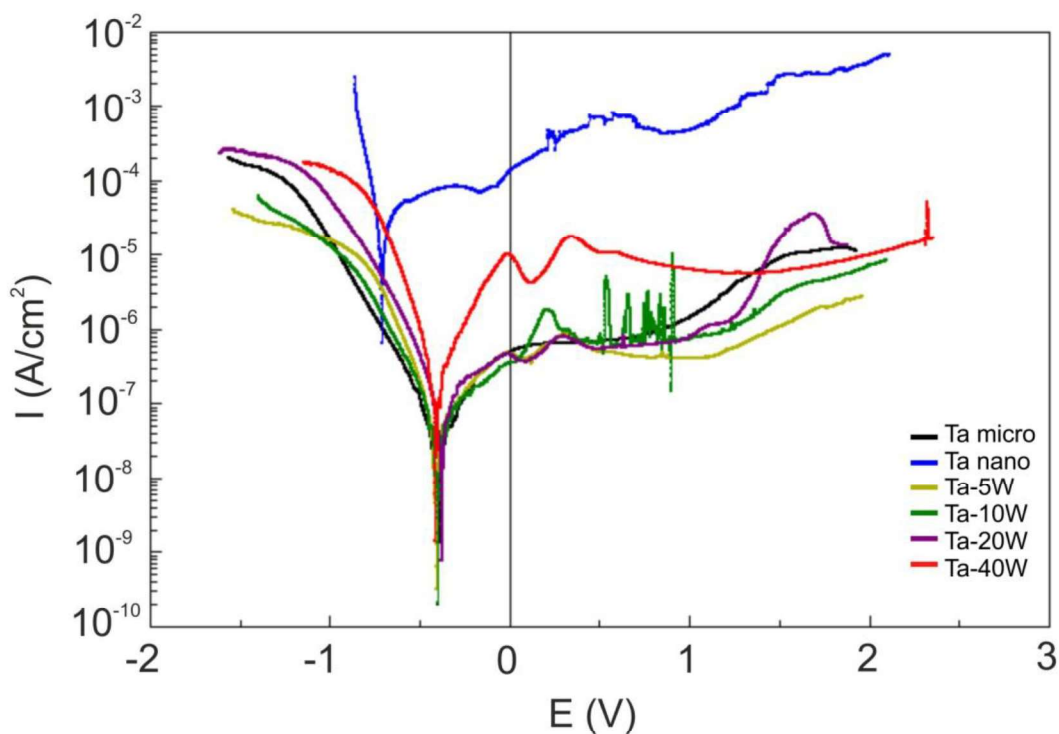
Figure 10. Polarization curves in the Ringer's electrolyte of the microcrystalline Ta, nanocrystalline Ta and nanocrystalline Ta-xW (x=5, 10, 20, 40 wt.%) alloys

Pure microcrystalline Ta (hot-pressed 325 mesh Ta powder) has a very good corrosion resistance. The corrosion current density (measured in the intersection of the Tafel tangent to the anodic and cathodic part of the polarization curve) was at the level of 10^{-8} A/cm^2 (Tab. 1). Hot-pressed pure nanocrystalline Ta has a significantly lower corrosion resistance and the corrosion current density was at the level of 10^{-5} A/cm^2. The deterioration of the corrosion resistance is the effect of a large volume of the grain boundaries and high internal energy of the nanocrystalline material. A modification of the chemical composition through an introduction of Nb, Mo and W affects the corrosion resistance. The Ta-10Nb nanocrystalline alloy has a better corrosion resistance by one order of magnitude in comparison to nanocrystalline pure Ta. For the other Nb containing alloys, no significant improvement or deterioration of the corrosion resistance was recorded. For the Ta-Mo alloys, the corrosion resistance was significantly better in comparison to the Ta-Nb alloys. For the Ta-5Mo nanocrystalline alloy the lowest corrosion current density of $1.173 \cdot 10^{-8}$ A/cm^2 was obtained (best corrosion resistance). The Ta-W alloys also exhibit a very high corrosion resistance. For the Ta-5W nanocrystalline alloy, the corrosion current density was $7.138 \cdot 10^{-8}$ A/cm^2. The Ta-Mo and Ta-W nanocrystalline alloys have the same level of corrosion current density I_{corr} as in the case of microcrystalline Ta and 3 orders of magnitude better than pure nanocrystalline Ta.
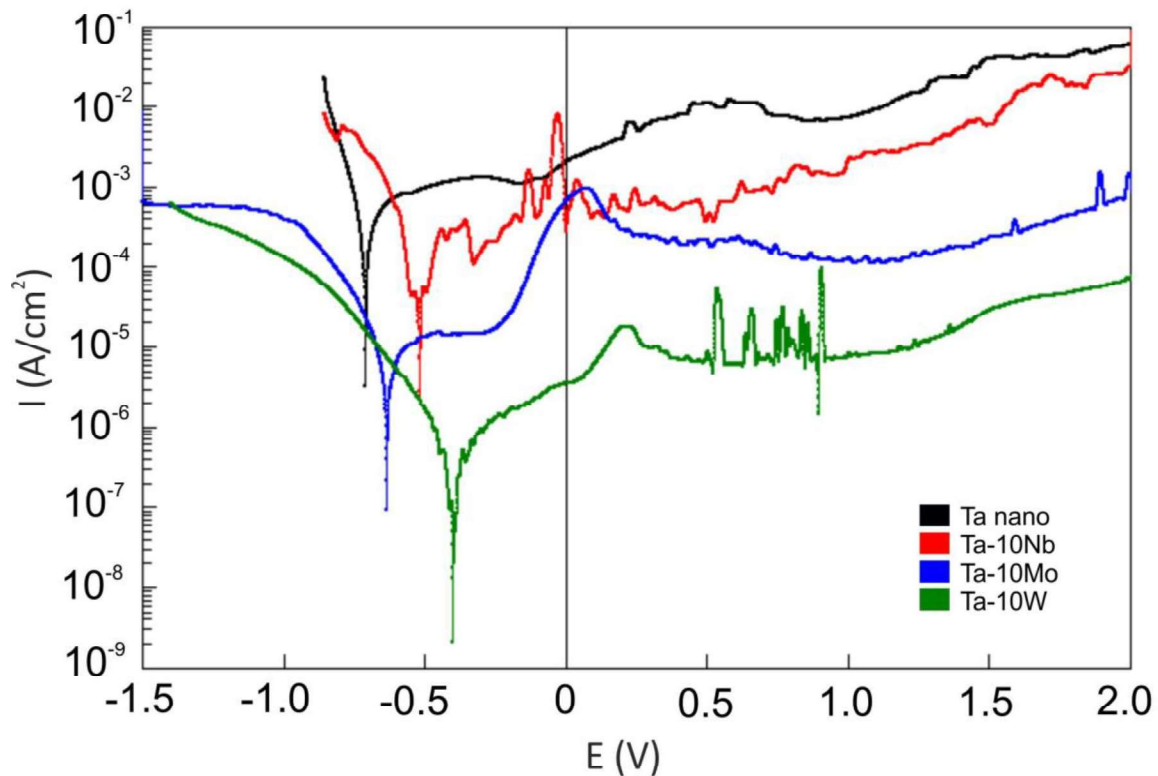
Figure 11. Polarization curves in the Ringer's electrolyte of the nanocrystalline Ta, nanocrystalline Ta-10Nb, nanocrystalline Ta-10Mo and nanocrystalline Ta-10W alloys

Table 1. Corrosion current density I_{corr}, corrosion potential E_{corr}, passivation potential E_p, current of passivation I_{kp}, Flade potential E_F, transpassivation potential E_{tp} and current in the passive range I_p of the investigated hot-pressed Ta alloys

| sample	I_{corr} [A/cm^2]	E_{corr} [V]	E_p [V]	I_{kp} [A/cm^2]	E_F [V]	E_{tp} [V]	I_p [A/cm^2]
Ta micro	$3.108 \cdot 10^{-8}$	-0.398	0.135	$6.166 \cdot 10^{-7}$	−	0.614	$7.134 \cdot 10^{-7}$
Ta nano	$1.198 \cdot 10^{-5}$	-0.711	-0.318	$1.298 \cdot 10^{-4}$	-0.160	−	−
Ta nano alloys:							
Ta-5Nb	$9.084 \cdot 10^{-5}$	-0.615	-0.364	$2.338 \cdot 10^{-4}$	0.081	−	−
Ta-10Nb	$5.852 \cdot 10^{-6}$	-0.519	−	−	−	−	−
Ta-20Nb	$9.182 \cdot 10^{-6}$	-1.023	-0.448	$5.717 \cdot 10^{-5}$	-0.187	-0.187	$5.268 \cdot 10^{-5}$
Ta-40Nb	$3.123 \cdot 10^{-5}$	-0.342	0.548	$4.205 \cdot 10^{-4}$	−	1.472	$5.57 \cdot 10^{-4}$
Ta-5Mo	$1.173 \cdot 10^{-8}$	-0.401	-0.351	$2.954 \cdot 10^{-7}$	−	−	−
Ta-10Mo	$4.201 \cdot 10^{-7}$	-0.635	-0.447	$1.626 \cdot 10^{-6}$	−	-0.278	$1.527 \cdot 10^{-6}$
Ta-20Mo	$1.778 \cdot 10^{-7}$	-0.587	−	−	−	-0.218	$9.673 \cdot 10^{-7}$
Ta-40Mo	$5.764 \cdot 10^{-8}$	-0.608	−	−	−	−	−
Ta-5W	$7.138 \cdot 10^{-8}$	-0.410	0.309	$8.601 \cdot 10^{-7}$	0.497	1.109	$4.222 \cdot 10^{-7}$
Ta-10W	$7.416 \cdot 10^{-8}$	-0.400	0.211	$1.812 \cdot 10^{-6}$	0.410	1.123	$8.383 \cdot 10^{-7}$
Ta-20W	$9.629 \cdot 10^{-8}$	-0.379	0.293	$7.948 \cdot 10^{-7}$	0.467	0.974	$7.276 \cdot 10^{-7}$
Ta-40W	$3.065 \cdot 10^{-7}$	-0.414	0.340	$1.742 \cdot 10^{-5}$	0.529	−	−

4. DISCUSSION

Refractory metals are classified as a group of metals of the melting temperature exceeding 2000°C. According to the melting temperature classification, pure refractory metals are: W, Re, Ta, Os, Mo, Ru, Ir, Nb, Hf, and Tc [28]. Only Mo, W, Ta, and Nb have important commercial applications in their pure form, whereas others have limited applications, due to limited availability and high cost, which is why, in this work, the alloy compositions based on the 4 above-mentioned elements were investigated.

The usual way for the alloy formation is conventional metallurgy, however significant differences in the melting temperatures constitute a problem in achieving high uniformity of the alloys. Alternatively, in this work an unconventional process of alloy synthesis was applied. In this process (mechanical alloying), the alloys were prepared from the elemental mixture of powders that were strongly deformed by the hitting balls in the milling reactor. The process of mechanical alloying eliminates the high temperature during alloy synthesis and the alloy formation takes place at room temperature, through mixing of powders, plastic deformation and cold welding. The heavy cold plastic deformation leads to a significant grain size reduction and uniform element distribution in the final powder mixture (Fig. 12). The final alloys are of high purity and the only impurity found was Fe (<2.1 wt.%), which originated in the milling vial (ball grinding). All alloying elements form a continuous solid solution. In the mechanical alloying, the final powders are in the form of agglomerates composed of nanograins. XRD, TEM and AFM provide comparable and complementary results of the grain size analysis. The microstructural analysis shows that mechanical synthesis is a good method to obtain nanocrystalline powders of designed composition.

Nanocrystalline powders are quite good candidates for consolidation and obtainment of bulk nanocrystalline metals. The nanocrystalline particles, owing to their very large surface area, should improve the densification process. The nanocrystalline particles, however, have a high cohesive force (large Van der Waals attraction force) resulting in the formation of agglomerates. Unfortunately, the agglomerates have significant voids between them, which may deteriorate densification [11]. The process of nanopowder consolidation requires the lowest possible temperature to avoid grain growth. Good choice is to use hot pressing, in which case the temperature, time and pressure are reduced in comparison to conventional powder metallurgy. Among different heating techniques, pulse plasma sintering (PPS) is one of the unconventional methods used for powder consolidation and grain growth reduction. The rising temperature during powder pressing improves densification and easier powder plastic deformation during compaction at a relatively low pressure, let alone reducing the voids between the consolidated powders. The high temperature contact of the reactive nanopowders with the graphite die and the punches leads to diffusion of carbon and formation of tantalum carbides during hot pressing. Instead of graphite, it is suggested to use a refractory metal [25]. The elevated temperature, however will limit the strength of the die. It is accepted that, for conventionally sintered microcrystalline powders, the temperature needed to achieve nearly full densification should be on the level of 0.8 of the melting temperature. Hence, for tantalum and its alloys, the sintering temperature should be over 2300°C [29].
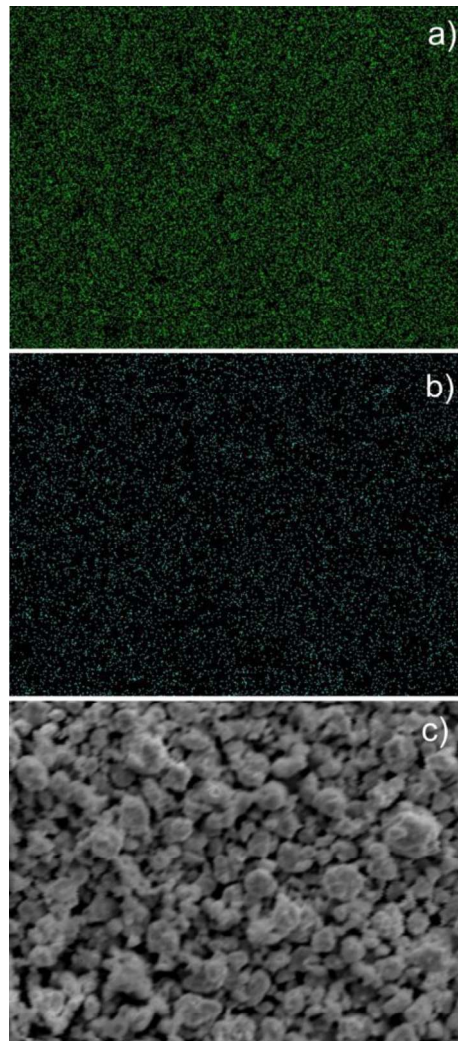
Figure 12. Example EDS map of the Ta (a) and W (b) distribution in the Ta-10W alloy powder after mechanical alloying (c)

For nanocrystalline or ultrafine-grained material densification, the consolidation temperature can be significantly lower [11, 24]. Additional reduction of the consolidation temperature can be achieved by the application of the hot pressing process [25]. The refractory alloying elements suppress grain growth during consolidation and, in this respect, out of the investigated alloys, tungsten exhibits the best behavior.

Tantalum has an extraordinary corrosion resistance. Tantalum is practically resistant in all concentrated and hot acidic environments [8]. Only 4% of the tantalum production, however, is used in the chemical industry for the production of corrosion resistant parts [8]. The limited use of tantalum in aggressive chemical environments is related to its high cost, which is approx. 10 and 5 times the cost of stainless steel and titanium for finished fabricated elements, respectively [30]. High corrosion resistance of tantalum is a consequence of the formation of a protective passive Ta_2O_5 oxide film. The stable oxides are formed during high temperature oxidation at temperatures in excess of 400°C. In other electrochemical surface treatment processes, the anodic oxidation would also lead to a formation of high quality oxide film. The anodic oxide has a significant thickness and cutoff of the aggressive

environments from pure metal background. The results of passivation are visible on the polarization curve. The oxidation of tantalum takes place in the reaction (eq.1) resulting in the most stable Ta_2O_5 oxide formation.

$$2Ta + 5H_2O \rightarrow Ta_2O_5 + 10H^+ + 10e \qquad\qquad\qquad\qquad\text{(eq. 1)}$$

The Ta_2O_5 is the most stable oxide and the formation of unstable sub-oxides such as TaO or TaO_2 is unfavorable.

The open-circuit-potential (OCP) measurements are useful in determining of the material stability in aggressive liquids. Decreasing the OCP with time suggests dissolution of the protective tantalum oxide and surface activation [31]. An increase in the OCP to more positive values indicates the trend towards passivation, whereas a constant value denotes stabilization of the passive layer. The OCP can change over time along with the changes of the conditions in the electrochemical cell. This potential can be considered as corrosion potential E_{corr} as they are very similar, yet, during the measurement of the polarization curve ,the obtained E_{corr} can deviate from the OCP because of various experimental parameters. The E_{corr} is therefore always taken from the polarization curve, not directly from the OCP and, hence the recorded different value of the OCP and E_{corr} (Figs. 9-11, Table 1).

In the conventional Ta-Nb alloys boiled in the H_2SO_4 solution, both α-Nb_2O_5 and β-Ta_2O_5 may form [8]. For a higher Ta content, only the Ta_2O_5 oxide forms and the material shows a higher corrosion resistance, whereas Nb deteriorates the corrosion resistance [8]. An increase in the alloying element (Nb, Mo or W) content in the Ta alloys leads to oxide composition changes, towards higher content of the oxide of the alloying element, for example Nb_2O_5 [8, 32]. The corrosion process carried out in the Ringer's electrolyte can lead to a reaction of the electrolyte components with the alloy elements and a formation of complex corrosion products (or oxide doped by Na^+, K^+, Ca^{2+}, Cl^-, which derive from the electrolyte) at higher anodic potentials. The nanostructure of high volume grain boundary can affect the corrosion products, due to a higher sensitivity to environments in comparison to the microcrystalline material of smaller volume grain boundary (this needs further investigations). The best corrosion resistance among the investigated alloys exhibit the Ta-W compositions. The Ta-Mo alloys also have very high corrosion resistance. The corrosion current density, which indicates the corrosion resistance, shows the lowest values (highest corrosion resistance) in the Ta-Mo and Ta-W system, comparable to those of microcrystalline pure Ta. Generally, the nanomaterials, due to a greater volume of the grain boundaries, have a lower corrosion resistance in comparison to their microcrystalline counterparts. In the case of the Ta-Mo and Ta-W alloys, the nanostructure shows a very good corrosion resistance and the problem of nanostructure was resolved in this matter.

5. CONCLUSIONS

This work discussed the formation and properties of the nanocrystalline Ta-xNb, Ta-xMo and Ta-xW alloys containing x = 5, 10, 20 and 40 wt.% of an additive element. The alloys were prepared using mechanical alloying, followed by hot pressing utilizing the pulse plasma sintering system. The structure, microstructure and corrosion resistance were investigated. The optimum properties for future applications in heavy working conditions exhibit the Ta-10W alloys, of the grain size of approx. 45 nm

and corrosion current density in the Ringer's electrolyte of $7.416 \cdot 10^{-8}$ A/cm^2. The nanocrystalline structure does not reduce the corrosion resistance in the Ta-Mo and Ta-W alloys, which is comparable to that of the microcrystalline pure Ta.

References

1. B. E. Schuster, J. P. Ligda, Z. L. Pan and Q. Wei, *JOM,* 63 (2011) 27.
2. R. W. Buckman, *JOM,* 52 (2000) 40.
3. R. A. Silva, M. Walls, B. Rondot, M. Da Cunha Belo and R. Guidoin, *J. Mater. Sci. Mater. Med.*, 13 (2002) 495.
4. F. F. Schmidt, D. J. Maykuth and H. R. Ogden, *JOM,*13 (1961) 487.
5. D. Gambale, *Adv. Mater. Processes.*, 168 (2010) 23.
6. S. M. Cordonnne, P. Kumar, C. A. Michaluk and H. D. Schwartz, *Int. J. Refract. Met. Hard. Mater.,* 13 (1995) 187.
7. K. A. De Souza and A. Robin, *Mater. Chem. Phys.*, 103 (2007) 351.
8. A. Robin and J. L. Rosa, *Int. J. Refract. Met. Hard. Mater.*, 18 (2000) 13.
9. Y. J. Lee, T. H. Lee, D. Y. Kim, H. H. Nersisyan, M. H. Han, K. S. Kang, K. K. Bae, Y. J. Shin and J. H. Lee, *Surf. Coat. Technol.,* 235 (2013) 819.
10. T.E. Mitchell and P. L. Raffo, *Can. J. Phys.,* 45 (1967) 1047.
11. S. H. Yoo, T. S. Sudarshan, K. Sethuram, G. Subhash and R. J. Sowding, *Nanostruct. Mater.*, 12 (1999) 23.
12. J. B. Clark, R. K. Garrett, T. L. Jungling, R. Vandermeer and C. L. Vold, *Metall. Mater. Trans. A,* 22 (1991) 2039.
13. C. A. Michaluk, in *Tantalum*, Warrendale, TMS (1996) 205.
14. J. B. Clark, R. K. Garrett, T. L. Jungling and R. I. Asfahani, *Metall. Trans. A*, 22 (1991) 2959.
15. C. L. Briant, E. MacDonald, R. W. Balliet and T. Luong, *Int. J. Refract. Met. Hard. Mater.*, 18 (2000) 1.
16. V. Kentheswaran, S. Dine, D. Vrel, J. P. Couzinie and G. Dirras, *J. Alloys. Comp.*, 679 (2016) 80.
17. C. Hertl, L. Koll, T. Schmitz, E. Werner and U. Gbureck, *Mater. Sci. Eng.* C, 41 (2014) 28.
18. H. H. Nersisyan, J. H. Lee and C.E. Won, *Int. J. Self-Propag. High-Temp. Synth.,* 2 (2003) 149.
19. J. R. Groza and A. K. Zavaliangos, *Mater. Sci.,* 28 (2000) 171.
20. W. M. Goldberger and R. R. Fessler, in. *Advances in Process Measurement for the Ceramic Industr*y, New York, Wiley (1999) 337.
21. L. A. Stanciu, V. Y. Kodash and J. R. Groza, *Met. Mat. Trans.*, 10 (2001) 2633.
22. P. Angerer, E. Neubauer, L. G. Yu and K. A. Khor, *Int. J. Refract. Met. Hard. Mater.,* 25 (2007) 280.
23. M. Dias, F. Guerreiro, J. B. Correia, A. Galatanu, M. Rosiński, M. A. Monge, A. Munoz, E. Alves and P. A. Carvalho, *Fusion. Eng. Des.,* 98-99 (2015) 1950.
24. Z. Fang, P. Maheshwari, X. Wang, H. Y. Sohn, A. Griffo and R. Riley, *Int. J. Refract. Met. Hard. Mater.,* 25 (2005) 249.
25. Y. Kim, E. P. Kim, J. W. Noh, S. H. Lee, Y. S. Kwon and I. S. Oh, *Int. J. Refract. Met. Hard. Mater.,* 48 (2015) 211.
26. J. Jakubowicz and M. Sopata, Structure and microstructure of high-energy ball-milled nanocrystalline tantalum, *Ann. Int. Conf. on Mater. Sci. Metal and Manufact.*, Singapore (2017) 1.

27. L. Smardz, K. Smardz, M. Jurczyk and J. Jakubowicz, *J. Alloys. Comp.,* 313 (2000) 192.
28. R. Morales, R. E. Aune, O. Grinder and S. Seetharaman, *JOM*, 55 (2003) 20.
29. R. M. German, *Sintering Theory and Practice*, John Wiley and Sons, (1996).
30. F. J. Hunkeler, in *Refractory Metals and Their Industrial Applications ASTM International*, Philadelphia, (1984) 28.
31. K. A. De Souza and A. Robin, *Mater. Lett.,* 57 (2003) 3010.
32. S. Komiyama, E. Tsuji, Y. Aoki, H. Habazaki, M. Santamaria, F. Di Quarto, P. Skeldon and G. E. Thompson, *J. Solid State Electrochem.,* 16 (2012) 1595.

6

Microstructure and Electrochemical Properties of Refractory Ta-Y$_2$O$_3$ and Ta-ZrO$_2$ Nanocomposites

M. Sopata, G. Adamek, J. Jakubowicz[*]

Poznan University of Technology, Institute of Materials Science and Engineering, Jana Pawla II, 24, 61-138 Poznan, Poland
[*]E-mail: jaroslaw.jakubowicz@put.poznan.pl

The refractory tantalum-ceramic oxide nanocomposites were made using mechanical alloying. The tantalum powder was synthesized together with Y$_2$O$_3$ or ZrO$_2$ powders in the concentration of 5, 10, 20 and 40 wt.%. The nanocomposite powders were hot-pressed using the pulse plasma sintering mode. To achieve good sample integrity, the hot pressing at the temperature of 1300-1500°C was done. The nanocomposites had a crystallite size below 100 nm. The corrosion resistance was measured using the potentiodynamic mode in the Ringer's electrolyte. The increase of oxide ceramic phase content leads to increased corrosion resistance. Best corrosion resistance is exhibited by the Ta-20Y$_2$O$_3$ and Ta-20ZrO$_2$ composites with the corrosion current density of up to 4 orders of magnitude lower than for pure nanocrystalline tantalum.

1. INTRODUCTION

Tantalum belongs to a group of elements of the highest corrosion resistance, higher than titanium or stainless steel [1]. Tantalum is corrosion resistant in concentrated and hot acidic environments, which results in the formation of a passive Ta$_2$O$_5$ oxide film. As the pure metallic element its mechanical strength is relatively low, however corrosion resistance is very high. Introduction of the alloying elements raises its strength, but the corrosion resistance may be lower [2]. Tantalum and its alloys as a refractory material have found specific applications in chemical, mechanical and aeronautical industry. The last decade saw an increased trend to use composite materials, mainly based on plastics such as carbon fiber reinforced epoxy resins. The very hard working conditions in many applications impose an application of new advanced metallic or ceramic-

based composites. Many alloys can be improved in terms of resistance to wear, corrosion and mechanical properties through the introduction of ceramic reinforced phases [3-6]. Similarly, the properties of ceramics can be improved through an introduction of other reinforced ceramic phases [7]. In the case of the refractory metals and alloys [8], their properties such as mechanical strength, hardness, wear resistance, creep or corrosion resistance can be improved through the introduction of reinforced refractory ceramic phases to their microstructure [9-11]. For high-temperature application the oxide ceramic is the most promising due to its resistance to decomposition in oxidative atmosphere at elevated temperatures. The behavior of carbides or nitrides may be different than that of oxides (for example they can decompose to oxides such as $SiC + 2O_2 \rightarrow SiO_2 + CO_2$, or $Si_3N_4 + 3O_2 \rightarrow 3SiO_2 + 2N_2$), however both (as oxides) will improve the mechanical properties at room and moderate temperatures [12].

New possibilities for the improvement of structural materials are the results of the advancement of nanomaterials. For nanomaterials the strength is improved according to the Hall–Petch equation, where the grain size reduction results in a mechanical strength improvement [13]. The main downside of nanomaterials having a high volume of the grain boundaries is lower corrosion resistance in comparison to their microcrystalline counterparts [14] as well as low-temperature stability that lead to grain growth. For that reason new solutions to this problem need to be found. Our proposal in the case of nanocrystalline tantalum is to make composites with reinforced refractory ceramics of higher corrosion resistance. In our previous work the authors showed the formation and mechanical properties of the Ta-ceramic nanocomposites [15]. In this work the authors show the corrosion properties of the Ta-ceramic oxides nanocomposites, where Y_2O_3 and ZrO_2 are the ceramic reinforcing phases. The nanocomposites were produced in the mechanical alloying process and the obtained powders were hot-pressed in the Pulse Plasma Sintering (PPS) mode. In this work the authors focus on the electrochemical properties of the nanocomposites while the structural results are shown only as examples for better understanding of the paper, because more detailed structural and mechanical properties of these composites have been shown in [15].

2. MATERIALS AND METHODS

In this work Ta-xY_2O_3 and Ta-xZrO_2 nanocomposites containing x = 5, 10, 20 and 40 wt.% of the ceramic phase were synthesized (marked as Ta-xY_2O_3 and Ta-xZrO_2, where x is 5, 10, 20 or 40 in wt.%). The tantalum-based nanocomposite powders were produced by mechanical alloying (MA). For the MA process the authors used a mixture of the tantalum powder (<44 µm; purity >99.97%; Alfa Aesar) with the ceramic powder: Y_2O_3 (<50nm; purity >99.9%; Sigma-Aldrich) and ZrO_2 (0.1-2µm; stabilized with 5.4% of Y_2O_3; Goodfellow). A mixture of 5.5g of the powders was blended and milled for 48h in the SPEX 8000M Mixer/Mill (Spex SamplePrep) according to the procedure described elsewhere [15]. At all the processing stages (powder handling, milling) argon atmosphere was applied.

The as-milled powders were axially hot-pressed at vacuum using graphite die and graphite movable punches. The pressure of the punches directed at the powder was 50 MPa. In the consolidation process, the Pulse Plasma Sintering mode (PPS) was applied. The experimental details

related to consolidation have been described elsewhere [15, 16]. The pressing temperature was fixed at 1300°C and 1500°C. Higher temperature was applied for higher ceramic phase content to achieve full sample integrity. Higher ceramic content in the composite needs a higher temperature for full consolidation, yet not too high, as it would result in excess grain growth. The time of sintering at a constant temperature was 5 s (the temperature rises up till it reaches the end value for 2-2.5min). The hot-pressed bulk samples were 8 mm in diameter and 4 mm in height.

The structure was analyzed using XRD (Empyrean; Panalytical) equipped with ICDD-JCPDS database. The crystallite size of the nanocomposites was estimated by the Williamson-Hall (W-H) method. The nanocomposite powders as well as the thin foil of the hot-pressed samples were analyzed using TEM (CM20 Super Twin; Philips).

The corrosion resistance was measured on hot-pressed samples using a Solartron 1285 Potentiostat (Solartron Analytical). The measurements started after OCP (open-circuit-potential) stabilization at a constant value and the polarization curves were recorded from −0.5V up to 2.5V vs. OCP. The scan rate was 0.5 mV/s. The graphite and Ag/AgCl were used as the counter and reference electrodes, respectively. A standard EG&G electrochemical cell (Princeton Applied Research) was used. The corrosion resistance was measured in the mixed and nitrogen purged Ringer's electrolyte containing chloride ions (147.2 mmol·l^{-1} Na^{+}, 4.0 mmol·l^{-1} K^{+}, 2.2 mmol·l^{-1} Ca^{2+}, 155.7 mmol·l^{-1} Cl^{-}). For the corrosion tests the bulk samples were grinded on sandpaper up to 1000 grit and polished in Al_2O_3 suspension to obtain a mirror-like surface of low roughness. As the reference materials, the authors used hot pressed micro- and nanocrystalline Ta.

3. RESULTS AND DISCUSSION

The tantalum-ceramic oxide nanocomposites were made using mechanical alloying and hot pressing. The examples of structural data for the considered nanocomposites have been presented in Fig. 1 showing the XRD spectra for pure Ta (a), Y_2O_3 (b) and ZrO_2 (c) powders as well as the spectra for example Ta-20Y_2O_3 (d) and Ta-20ZrO_2 (e) nanocomposites after mechanical alloying and further consolidation (f) and (g), respectively. The mechanical alloying results in the formation of nanocomposites with main broad peaks on the XRD spectra with their position corresponding to Tantalum. The peaks of Y_2O_3 and ZrO_2 in these nanocomposites are invisible because they are masked by the broad peaks of tantalum up to 20% of the oxide content [15]. The broad peaks also indicate the nanostructure formation. The hot pressing at an elevated temperature results in a reaction between the composite elements. The composite powders also react partially with the graphite matrix, which results in the formation of tantalum carbides (TaC, Ta_2C). Finally, the bulk composites obtain a complex structure with the main Ta, and Y_2O_3 or ZrO_2 phases as well as other minor phases (Y_3TaO_7, Ta_2O_5). The crystallite size was obtained based on the XRD spectra using the W-H plots (Fig. 2a,b). The mechanical alloying carried out at a room temperature leads to the formation of a metal-ceramic composite powder mixture [15]. The dynamic milling in the MA process leads to a significant Ta powders cold strengthening, increases their brittleness and finally the reduction of the Ta crystallite size. The high energy of impacts among the milling balls leads to a cracking through the brittle

ceramic particles and their refinement (Fig. 2c). The hot pressing increases the crystallite size (Fig. 2d).

The example TEM images (Fig. 3) show the Ta-20Y$_2$O$_3$ nanocomposite after mechanical alloying (a) and after hot pressing (b). The exemplary grains have been indicated. The mechanical alloying results in a uniform distribution of metal and ceramic particles. The Y$_2$O$_3$ nanoparticles after MA are smaller in comparison to the Ta nanoparticles in the powder mixture (a). The hot pressing increases the grain size and, for the presented Ta-20Y$_2$O$_3$ nanocomposite the average grain size is 75 nm, whereas the full grain size distribution is in the range of 25-150 nm (larger for the Ta grains). In all composites the average grain size is below 100 nm [15]. The data measured by TEM are roughly consistent with those calculated using the W-H method.
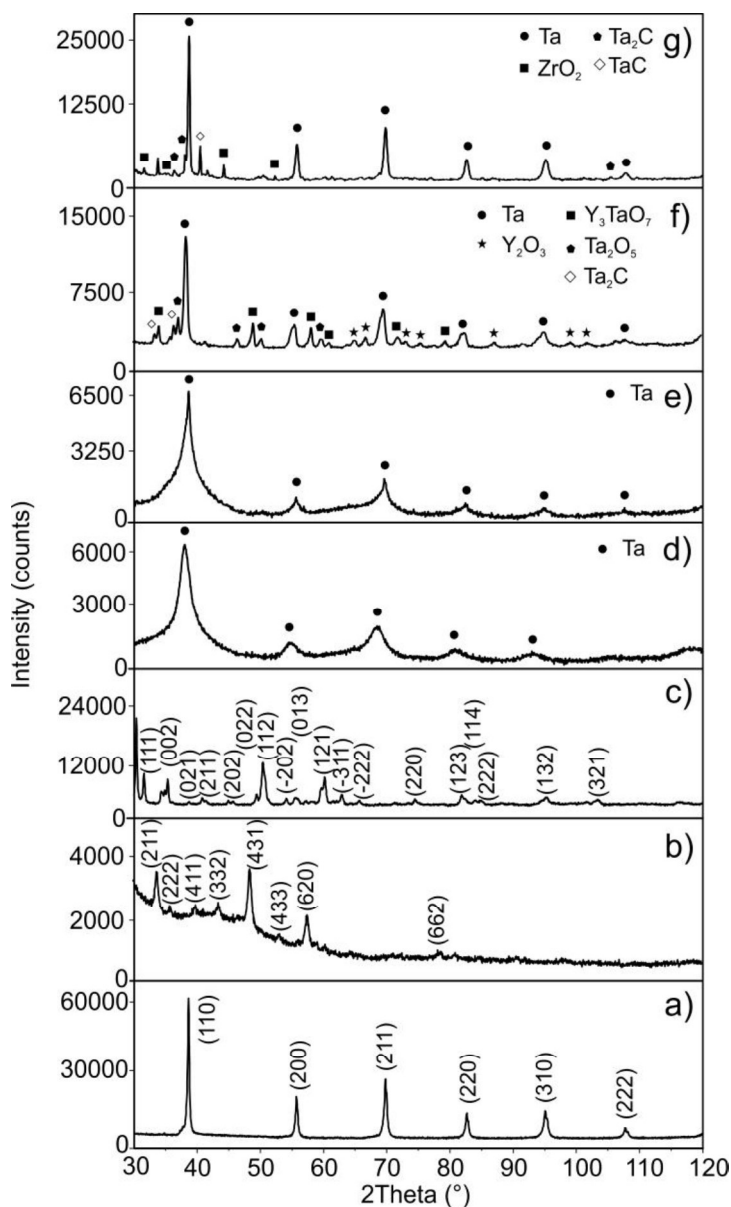
Figure 1. XRD of pure Ta (a), Y$_2$O$_3$ (b) and ZrO$_2$ (c) powders and example Ta-20Y$_2$O$_3$ (d) and Ta-20ZrO$_2$ (e) nanocomposites after mechanical alloying and after consolidation (f) and (g), respectively
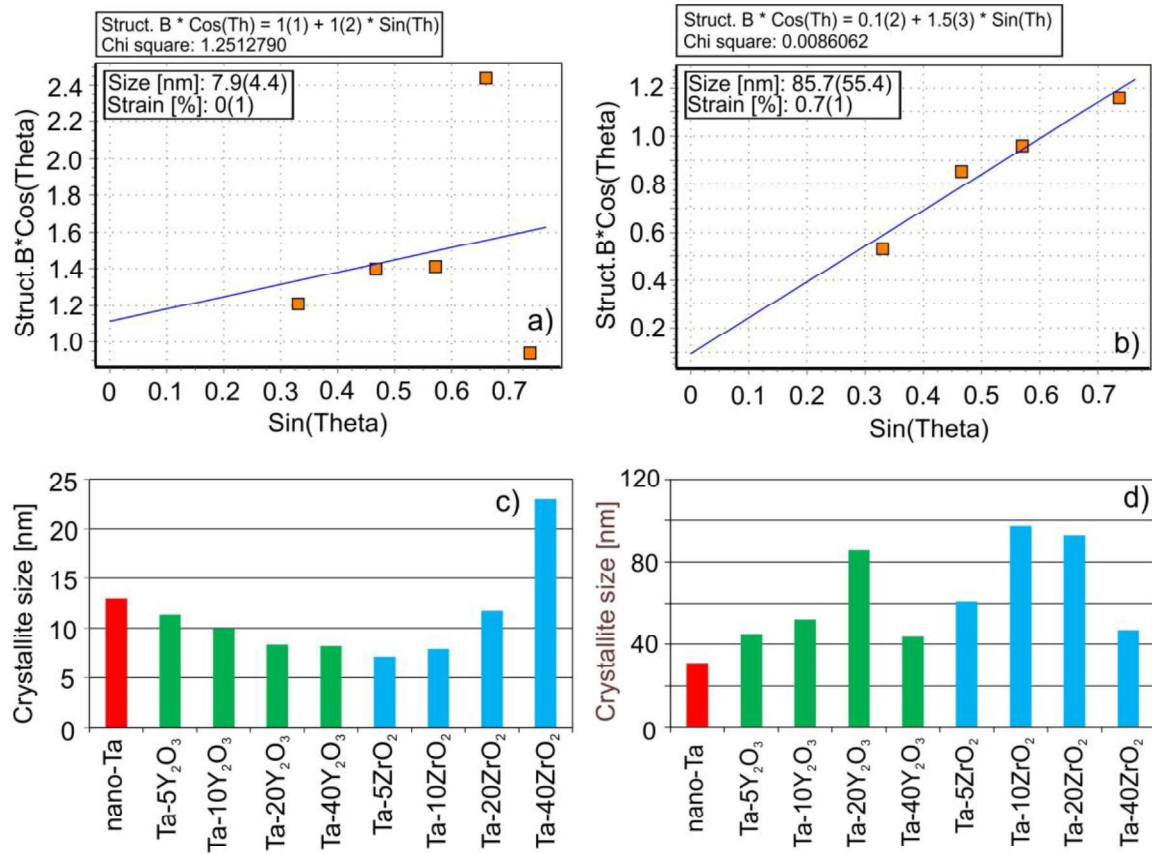
Figure 2. Example Williamson-Hall plot for the Ta-20Y$_2$O$_3$ nanocomposite after MA (a) and after hot pressing (b), and average crystallite size of the Ta-ceramic nanocomposites after MA (c) and after hot pressing (d)
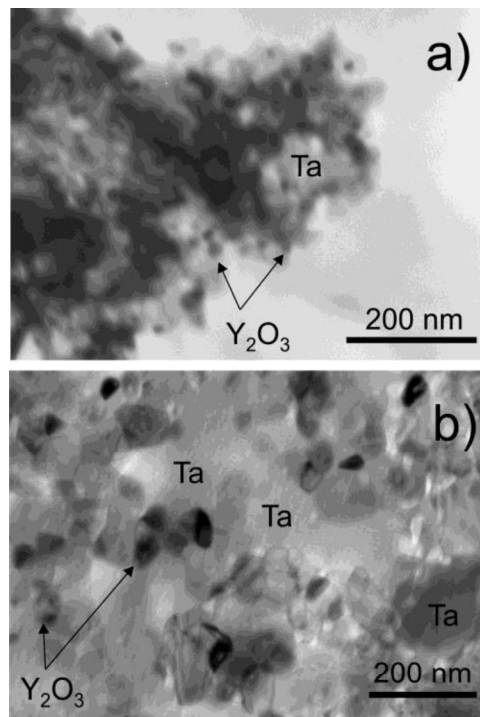
Figure 3. TEM images of the Ta-20Y$_2$O$_3$ nanocomposite after MA (a) and after hot pressing (b)

The corrosion resistance was measured in the Ringer's electrolyte. First, the samples were kept at OCP until they stabilized (Fig. 4). Later, the samples were polarized from the cathodic to the anodic potential range (Figs. 5, 6). The current density and values of potential read from the polarization curves have been summarized in Table 1.

The OCP is a stationary potential that changes in time and roughly shows the material tendency to corrode. The OCP changes during sample soaking in the electrolyte and provides information on how stable the passive oxide layer is (Fig. 4). The highest negative OCP value indicates the composites with the highest content of the ceramic oxide and a relatively high negative OCP also points to microcrystalline tantalum. The OCP shifts with time to a more positive value indicating a tendency for passivation and thickening of the native oxide layer. For pure nanocrystalline tantalum the OCP slightly shifts to a negative value and in this case a stable passive layer does not form.
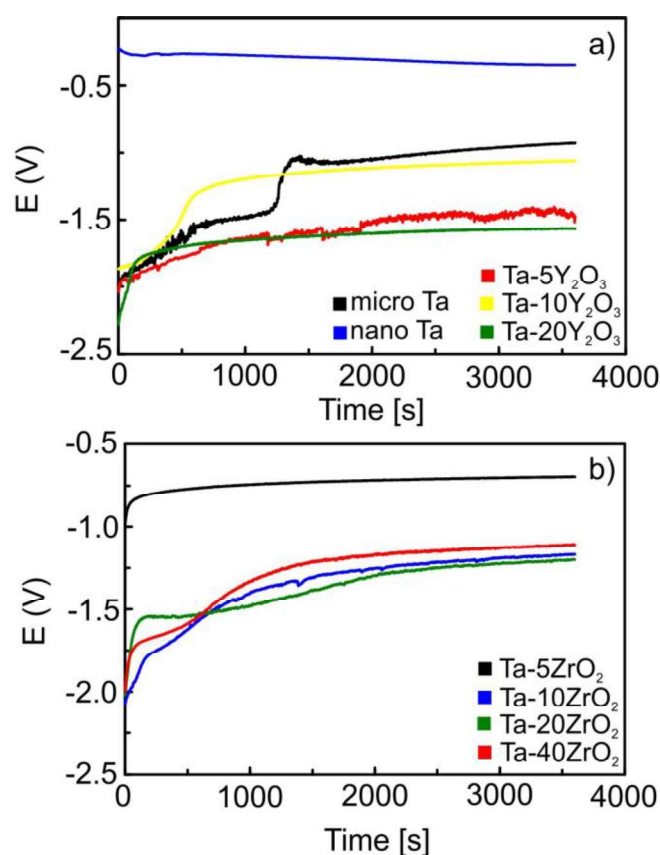

Figure 4. OCP as a function of time in the Ringer's electrolyte for the Ta-Y_2O_3 (a) and Ta-ZrO_2 (b) nanocomposites; for comparison data for nano- and microcrystalline Ta have been included in (a)

The polarization curves for the nanocomposites have been presented in Fig. 5 and Fig. 6. The results for reference micro- and nanocrystalline pure Ta have been shown in the authors' previous work [16]. For better clarity and comparison to the reference material the authors repeated the data for pure Ta only from their previous work [16]. Pure microcrystalline Ta as a reference material has very good corrosion resistance. The corrosion current density, which indicates the corrosion resistance is very low ($I_{corr} = 3.108 \cdot 10^{-8}$ A/cm^2). Nanocrystalline Ta has a significantly higher corrosion current

density (I_{corr} = 1.198·10^{-5} A/cm^2). Large volume of the grain boundaries results in deterioration of the corrosion resistance.
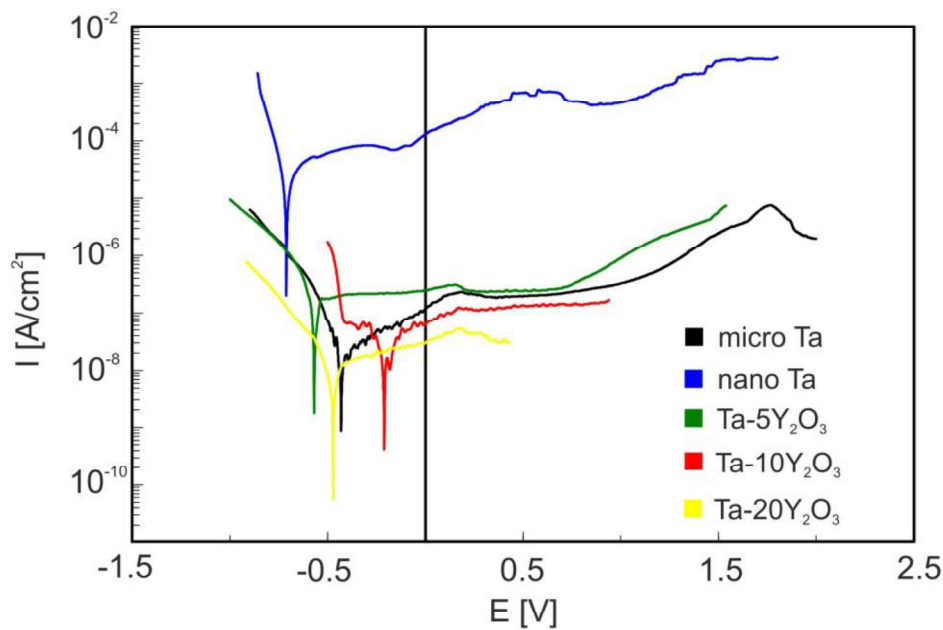
Figure 5. Polarization curves in the Ringer's electrolyte of the microcrystalline Ta, nanocrystalline Ta and Ta-xY$_2$O$_3$ nanocomposites (x=5, 10, 20 wt.%)
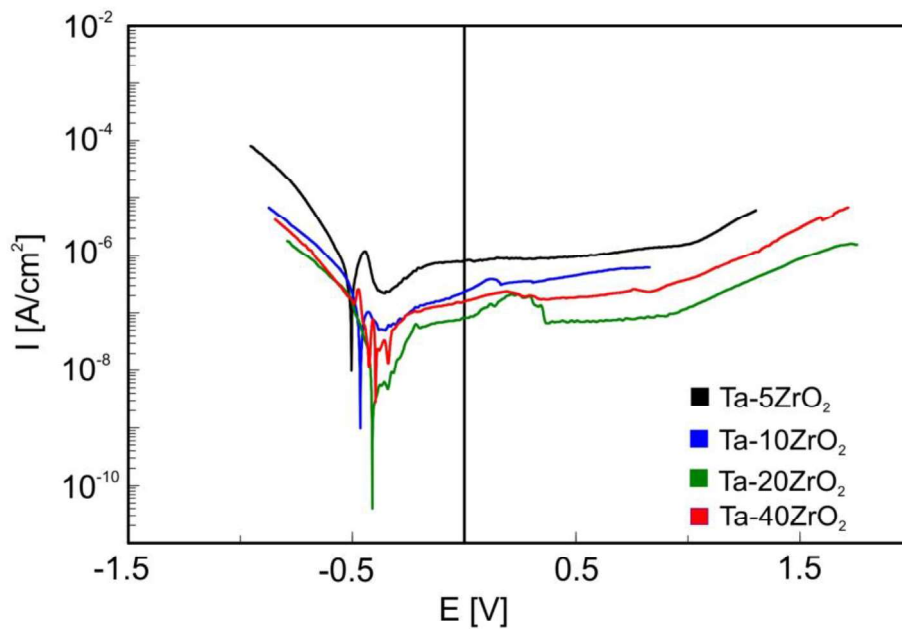
Figure 6. Polarization curves in the Ringer's electrolyte of the Ta-xZrO$_2$ (x=5, 10, 20, 40 wt.%) nanocomposites

As was presented in the authors' previous work [16], the modification of the chemical composition of Ta through an introduction of Nb, Mo, and W significantly improves the corrosion resistance of the nanocrystalline alloys in comparison to pure nanocrystalline Ta. In this work, the

authors focused on the Ta nanocomposites modified by ceramic oxide particles. It was expected that the oxides that have high energy of oxide formation improve the corrosion resistance of the composites in comparison to pure Ta whose energy is negative. The polarization curves were measured for all the investigated composites except of Ta-40%Y_2O_3. The very high content of the insulating oxide phase in the composite (here 40% of Y_2O_3) results in its poor electrical conductivity, which makes impossible to measure the polarization curve of this material. However it is expected that this material possesses a high corrosion resistance. The Ta-5Y_2O_3 shows a wide plateau in the passive range, however an increase in the Y_2O_3 content leads to a reduced corrosion current density and current density in the passive range. The comparable tendency was observed for the Ta-ZrO_2 composites. For Ta-5ZrO_2 the plateau was wide and the corrosion current density was the lowest for Ta-20ZrO_2. Based on the polarization curves the critical currents and potentials were measured and shown in Table 1.

The values of the Tafel slopes indicate the tendency to corrosion resistance of the materials. The Tafel slopes theoretical values of 120, 40 and 30 mV are observed for the Volmer, Heyrovsky and Tafel determining rate steps. For our experimental polarization curves the kinetics of reactions is complex and its hardly to fit to one theoretical model. The anodic values of Tafel slope b_a are higher in comparison to cathodic Tafel slope b_c, which means that materials have tendency toward passivation (Tab. 1). When the b_c would be higher than b_a, the materials will have tendency to corrode [17].

In the nanomaterials the large volume of the grain boundaries results in materials having a higher energy, which unfortunately deteriorates the corrosion resistance [14]. On the other hand, the grain boundaries provide a higher density of the nucleation sites for the formation of a passive film [18], which in some cases could lead to an improvement of the corrosion resistance.

Table 1. Corrosion current density I_{corr}, corrosion potential E_{corr}, passivation potential E_p, passivation current density I_{cp} as well as Tafel cathodic slope b_c and Tafel anodic slope b_a of the investigated hot-pressed Ta-ceramic nanocomposites; data for pure Ta for comparison [16]

sample	I_{corr} [A/cm^2]	E_{corr} [V]	E_p [V]	I_{cp} [A/cm^2]	b_c [mV]	b_a [mV]
micro-Ta	$3.108 \cdot 10^{-8}$	-0.398	0.135	$6.166 \cdot 10^{-7}$	-92.6	273.4
nano-Ta	$1.198 \cdot 10^{-5}$	-0.711	-0.318	$1.298 \cdot 10^{-4}$	-63.9	137.9
nanocomposites:						
Ta-5Y_2O_3	$1.433 \cdot 10^{-7}$	-0.573	0.160	$3.096 \cdot 10^{-7}$	-64.6	53.2
Ta-10Y_2O_3	$1.605 \cdot 10^{-8}$	-0.209	0.170	$1.235 \cdot 10^{-7}$	-95.6	135.5
Ta-20Y_2O_3	$4.064 \cdot 10^{-9}$	-0.470	0.175	$5.311 \cdot 10^{-8}$	-114.9	120.9
Ta-40Y_2O_3	–	–	–	–	–	–
Ta-5ZrO_2	$2.159 \cdot 10^{-7}$	-0.504	-0.439	$1.197 \cdot 10^{-6}$	-62.0	75.3
Ta-10ZrO_2	$4.185 \cdot 10^{-8}$	-0.464	-0.429	$1.045 \cdot 10^{-7}$	-52.9	54.7
Ta-20ZrO_2	$4.464 \cdot 10^{-9}$	-0.358	-0.214	–	-49.0	163.4
Ta-40ZrO_2	$3.720 \cdot 10^{-8}$	-0.414	0.190	$2.352 \cdot 10^{-7}$	-44.9	190.9

High mechanical properties of the investigated composites were presented in [15] while this work also shows that the nanocomposites have a very high corrosion resistance. The materials can find applications in heavy duty working conditions (friction wear and corrosion environments).

4. CONCLUSIONS

In this work the authors discussed the corrosion resistance of the Ta-xY_2O_3 and Ta-$xZrO_2$ nanocomposites containing x = 5, 10, 20 and 40 wt.% of the ceramic phase. The nanocomposites were prepared using mechanical alloying and subsequent hot pressing. The authors have observed that the introduction of oxides results in an extraordinarily improved corrosion resistance in all composites compared to pure nanocrystalline Ta. The introduction of oxides ensures comparable or even better properties than pure microcrystalline Ta. The best corrosion resistance was exhibited by composites having 20 and 40% content of oxide, yet for the Ta-$40Y_2O_3$ nanocomposite due to its insulating properties it was impossible to measure the polarization curve.

References

1. A. Robin, *Int. J. Refract. Met. Hard Mater*., 15 (1997) 317.
2. S.M. Cardonnne, P. Kumar, C.A. Michaluk and H.D. Schwartz, *Int. J. Refract. Met. Hard. Mater*., 13 (1995) 187.
3. P. Agrawal and C.T. Sun, *Compos. Sci. Techn*., 64 (2004) 1167.
4. F. Scherm, R. Völkl, A. Neubrand, F. Bosbach and U. Glatzel, *Mater. Sci. Eng. A,* 527 (2010) 1260.
5. K. Niespodziana, K. Jurczyk and M. Jurczyk, *Adv. Mater. Sci.* 14 (2007) 102.
6. P. Siwak and D. Garbiec, *Trans. Nonferrous Met. Soc. China,* 26 (2016) 2641.
7. T. Ohji, *Scripta Mater*., 44 (2001) 2083.
8. R. Morales, R.E. Aune, O. Grinder and S. Seetharaman, *JOM*, 55 (2003) 20.
9. X. Sun, W. Han, Q. Liu, P. Hu and Ch. Hong, *Mater. Design*, 31 (2010) 4427.
10. J.-H. Kim, M. Seo and S. Kang, *Int. J. Refract. Met. Hard Mater.*, 35 (2012) 49.
11. O. Gaballa, B.A. Cook and A.M. Russell, *Int. J. Refract. Met. Hard Mater.*, 41 (2013) 293.
12. K. Komeya and M. Matsui, High Temperature Engineering Ceramics, in *Materials Science and Technology*, (2006) 517.
13. N. Hansen, *Scripta Mater.*, 51 (2004) 801.
14. P. Herrasti, C. Ponce de León and F.C. Walsh, *Rev. Metal.*, 48 (2012) 377.
15. J. Jakubowicz, M. Sopata, G. Adamek, P. Siwak, and T. Kachlicki, *Adv. Mat. Sci. Eng*., 2018 (2018) 2085368.
16. J. Jakubowicz, G. Adamek, M. Sopata, J.K. Koper, T. Kachlicki and M. Jarzebski*, Int. J. Electrochem. Sci*., 13 (2018) 1956.
17. D. Mareci, G. Ungureanu, D.M. Aelenei and J.C. Mirza Rosca, *Mat. Corr*., 58 (2007) 848.
18. L. Jinlong, *J. Mat. Sci. Techn*., 34 (2018) 1685.

7

High temperature resistance of novel tantalum-based nanocrystalline refractory compounds

M. Sopata [a, *], M. Sadej [b], J. Jakubowicz [a]

[a] Poznan University of Technology, Institute of Materials Science and Engineering, Jana Pawla II 24, 61-138 Poznan, Poland
[b] Poznan University of Technology, Institute of Chemical Technology and Engineering, Berdychowo 4, 61-138 Poznan, Poland

ABSTRACT

In this work new tantalum-based nanocrystalline alloys and composites were made and tested under oxygen and nitrogen conditions using TGA. The materials were produced by mechanical alloying process. Niobium, molybdenum and tungsten were used as alloying elements, and TaC, ZrO_2, and Y_2O_3 were used as the ceramic reinforced phase in composites, all in 5, 10, 20, and 40 wt ratio (wt.%). The materials were studied using XRD, SEM, TEM and AFM. For the purpose of thermal gravimetric analysis, the weight gain was measured and turned out to be the lowest for the Ta-W alloys. All nanocrystalline Ta alloys and composites exhibit lower weight gain in comparison to pure microcrystalline Ta. The Ta-5W alloy exhibits the highest activation energy. For other Ta alloys and composites the activation energy is lower in comparison to pure microcrystalline Ta. Annealing of bulk hot-pressed Ta compounds in oxidative and nitrogen atmosphere leads to the formation of an external thick oxide coating which is loosely connected to the surface and of the diffusion nitride layer inside the material surface, respectively.

In this work the authors demonstrate that nanocrystalline Ta-based alloys and composites have a better thermal stability against oxidation in comparison to microcrystalline tantalum.

© 2019 Elsevier B.V. All rights reserved.

1. Introduction

Tantalum-based materials, such as alloys or composites reinforced with a ceramic phase are classified as refractory materials. Refractory metals are characterised by high melting temperature (exceeding 2000 °C). Taking into account melting temperature classification, pure refractory metals in the periodic table are: W (3422 °C), Re (3185 °C), Ta (3017 °C), Os (3033 °C), Mo (2623 °C), Ru (2334 °C), Ir (2466 °C), Nb (2477 °C), Hf (2233 °C), and Tc (2157 °C) [1]. It is commonly accepted that only Mo, W, Ta, and Nb have practical commercial applications in their pure form, while the remaining metals have limited application due to their low availability and high cost. Thus, alloy compositions based on the 4 above-mentioned elements were investigated.

The high melting point limits the maximum temperature of potential applications. Although refractory materials have high strength at very high temperatures, they are usually sensitive to oxidative atmosphere and dynamic load in low- or moderate-temperature applications. The main downside of these materials

is their high price, which restricts their potential application areas. In order to overcome these problems, it is recommended to use the above refractory elements in limited amounts or to combine them with other elements (in alloys) or compounds/phases (composites). Refractory metals such as Ta, Nb, W, Re or Mo can be melted together to form alloys [2,3] or can be combined with ceramics to form composites reinforced with ZrO_2, Y_2O_3, TaC, ZrC, WC, TiN or Si_3N_4 [4—6]. Due to significant differences in the properties of alloying elements which form refractory alloys or composites (such as: melting temperatures, limited mutual solubility, and densities), the conventional casting methods for the production of ingots have limited applications, particularly in the formation of composites. Given the above, powder metallurgy can be successfully applied and is very useful in the production of refractory metal-based components. Additionally, powder metallurgy offers additional benefits such as material savings and the possibility to use mechanical machining (the components have great dimensional accuracy as well as usually high hardness). Apart from their resistance to high temperatures, refractory compounds are also resistant to wear, which property is directly related to the high hardness of the materials and their phase composition [7].

Conventionally processed refractory materials (through casting

---

* Corresponding author.
E-mail address: mateusz.m.sopata@doctorate.put.poznan.pl (M. Sopata).

or conventional powder metallurgy) have a microstructure composed of microcrystalline grains. The application of unconventional processes (mechanical alloying followed by hot pressing or severe plastic deformation processes) can lead to the formation of a microstructure composed of nanocrystalline grains [8,9]. Nanocrystalline materials usually have higher mechanical properties in comparison to microcrystalline materials of the same composition. However, due to a large volume of grain boundaries of higher free energy, nanocrystalline materials are more unstable when the temperature rises and have a high driving force for rapid grain growth [10]. Grain growth occurs by the migration of grain boundaries. Boundary motion is the short-range diffusion of atoms from one side of the boundary to the other. Counteraction of grain boundary motion through the formation of precipitations, subgrains and dislocations is one of the methods of grain growth reduction. The grain boundary is pinned by the second-phase particles restricting grain growth [11]. Small precipitations of the other phases at grain boundaries in alloys or small grains of reinforced ceramic phase in composites can limit grain growth at elevated temperatures [11]. Hence, not only the melting point, but also the chemical, phase and microstructure composition determine the applications of the refractory materials. Grain growth of refractory nanomaterials deteriorates their mechanical properties and the process is irreversible, which limits their high-temperature applications.

Tantalum has an extremely high corrosion resistance in the most aggressive media, both concentrated and hot acidic [12]. High corrosion resistance of tantalum and its compounds is a consequence of the formation of a passive Ta_2O_5 oxide film. However, in alloys with higher alloying elements content, the corrosion resistance may decrease due to the formation of an alloying element oxide of lower corrosion resistance [12]. Stable oxides are formed during high temperature oxidation at temperatures in excess of 400 °C. Unfortunately, the oxygen diffusing through the grain boundaries also leads to the formation of oxides located at the grain boundaries. The oxides cause embrittlement and high temperature intensifies this effect. However, oxide precipitations prevent rapid grain growth at higher temperatures [13].

Literature reports usually include tantalum alloys with lower alloying elements weight ratio, mostly modified with tungsten [14]. The aim of our study was to create new types of tantalum-based compounds characterised by a relatively high content of alloying elements (in alloys) or by the second reinforced phase (in composites). For easier comparison of different compounds, both alloys and composites, we decided to make all our materials with the same weight ratio of alloying elements or the ceramic reinforced phase (5, 10, 20 and 40 wt%), respectively. Due to the differences in the chemical composition (weight ratio as well as type of alloying elements), microstructure (micro- and nanostructure) and lack of comparable studies in the literature, the comparison of our Ta-based compounds with those reported in the literature is rather difficult.

Although high-temperature oxidation of refractory alloys has recently been the subject of studies [15], to the best of our knowledge, the stability of nanocrystalline refractory alloys or composites has not. In this work the authors demonstrate the thermal stability of the novel refractory tantalum-based nanocrystalline alloys and composites.

2. Experimental details

Nanocrystalline alloys (Ta-xNb, Ta-xMo and Ta-xW) and composites (Ta-xY$_2$O$_3$, Ta-xZrO$_2$ and Ta-xTaC) where x = 5, 10, 20 and 40 wt% of the alloying element or the ceramic phase content were synthesized. The process included mechanical alloying (for the

production of the powder mixture of the designed composition) and hot pressing in the pulse plasma sintering mode (for the production of bulk materials using the powders made in the mechanical alloying process). All experimental steps were carried out under argon atmosphere. For mechanical alloying we used high energy ball mills (SPEX 8000 mill), with weight ratio of the balls to powder of 3:1. The milling time and frequency were 48 h and 875 cycles/minute, respectively. We used hardened steel vial and balls >62 HRC. The mechanical alloying was done at ambient temperature. The pulse plasma sintering was done in vacuum in a graphite die. The pressure of the punches directed at the powder was 50 MPa. The sintering temperature range was 1300–1500 °C, depending on the material composition, and the time of consolidation after 2–3 min during which the temperature rose to its end value was 5s. The hot-pressed bulk samples were 8 mm in diameter and 4 mm in height. All the experimental details related to the synthesis of the materials have been described elsewhere [16,17].

The structure analysis was performed using Panalytical Empyrean X-Ray diffractometer (CuKα radiation) and the ICDD-JCPDS database was used for phase identification. The investigations were carried out using CuKα radiation at 45 mV and anode current of 40 mA. The structure was investigated in 2θ range 30–120 deg., the step size was 0.0167 deg., and the time per step was 12.54 s/step. In this work, microscopic observations were conducted using Tescan Vega 5135 SEM, Quesant Q-Scope 250 AFM and Philips CM 20 Super Twin TEM. All the experimental details related to the materials microstructure characterization have been described elsewhere [16,17].

The main goal of this work was to present the results of thermogravimetric analysis (TGA). The TGA was performed using a Netzsch TG 209 F3 Tarsus thermo-microbalance. The analysis was conducted on the powders heated up to 880 °C. The measurements were performed for six samples of each compound. 13 mg of the material was placed in the Netzsch Al$_2$O$_3$ crucibles. The heating rate was 40 °C/min. The process was carried out under nitrogen atmosphere (20 mL/min). The degree of conversion or the share of the converted fraction α of the sample was calculated with the following equation (1) [18]:

$$\alpha = (W_0 - W_T)/(W_0 - W_\infty) \tag{1}$$

where:

- W_0 is the initial sample weight,
- W_T is the weight at temperature (T),
- W_∞ is the weight at the reaction end point.

Using a point of equivalent weight loss, which is beyond any initial weight loss due to the evolution of volatiles, a plot of ln [-{ln(1-α)}/T^2] vs 1/T was constructed (T— temperature of weight loss). The slope of this straight-line plot was then used to calculate the activation energy (E_a).

For the purpose of comparison, the effect of high temperature on the stability of the Ta compounds was studied by applying the annealing process performed on bulk hot-pressed samples under ambient pressure and nitrogen (0.15 MPa) atmosphere in a Nabertherm tube furnace at 1000 °C (2 h).

3. Results and discussion

The results related to the formation of nanocrystalline tantalum alloys and composites and their microstructure have already been presented in Refs. [16,17]. Fig. 1 shows example microscopic pictures of the selected alloy and composite after mechanical alloying as well as after hot pressing. After mechanical alloying the average
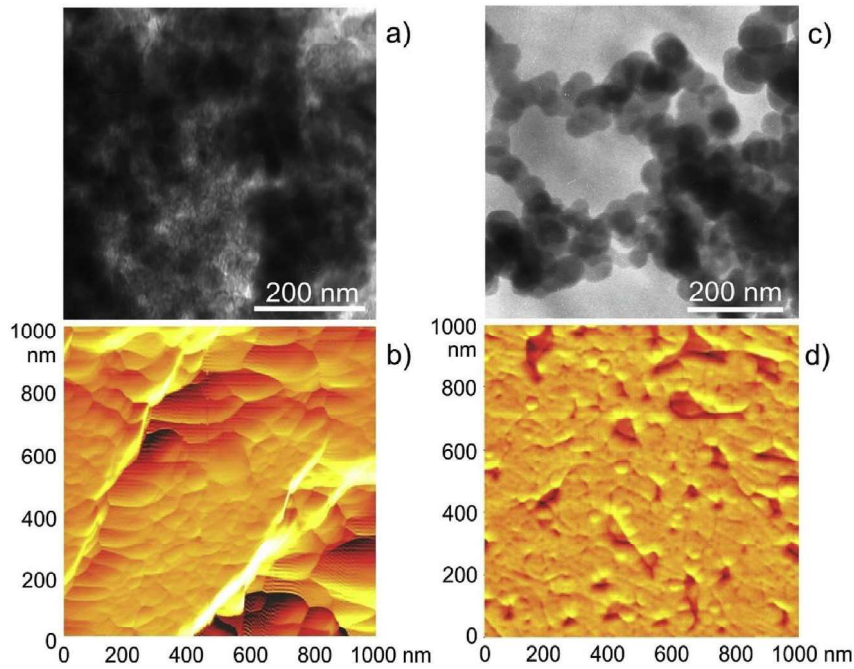
Fig. 1. TEM images of Ta-10W (a) and Ta-40Y$_2$O$_3$ powders (c), as well as AFM images of bulk hot-pressed Ta-10W (b) and Ta-40Y$_2$O$_3$ (d).

grain size is in the range 28—87 nm, and after hot pressing it increases to the value 43—195 nm (Table 1) [16,17]. The nanomaterials have high mechanical properties (high hardness and Young's modulus) and corrosion resistance at room temperature [16,17].

Before materials can be selected for use at high temperatures, their stability against oxidative atmosphere needs to be measured under such conditions. The thermogravimetric analysis (TGA)

Table 1
Grain size of tantalum-based alloys and composites after mechanical alloying (powder) and hot pressing (bulk).

Compound	Grain size [nm]	
	Powder	Bulk
Ta	54 ± 12	170 ± 24
Ta-5Nb	78 ± 14	128 ± 36
Ta-10Nb	86 ± 19	160 ± 29
Ta-20Nb	82 ± 15	190 ± 33
Ta-40Nb	87 ± 22	195 ± 41
Ta-5Mo	46 ± 16	55 ± 21
Ta-10Mo	53 ± 18	78 ± 26
Ta-20Mo	62 ± 9	155 ± 31
Ta-40Mo	58 ± 13	155 ± 42
Ta-5W	28 ± 8	47 ± 16
Ta-10W	32 ± 9	60 ± 14
Ta-20W	37 ± 12	65 ± 24
Ta-40W	36 ± 9	47 ± 23
Ta-5Y$_2$O$_3$	46 ± 7	76 ± 14
Ta-10Y$_2$O$_3$	38 ± 8	55 ± 12
Ta-20Y$_2$O$_3$	42 ± 19	75 ± 17
Ta-40Y$_2$O$_3$	31 ± 12	43 ± 26
Ta-5TaC	47 ± 8	76 ± 17
Ta-10TaC	48 ± 12	72 ± 21
Ta-20TaC	52 ± 17	105 ± 25
Ta-40TaC	58 ± 21	105 ± 34
Ta-5ZrO$_2$	38 ± 9	77 ± 28
Ta-10ZrO$_2$	36 ± 7	53 ± 19
Ta-20ZrO$_2$	41 ± 10	49 ± 18
Ta-40ZrO$_2$	43 ± 12	83 ± 26

results for the nanocrystalline Ta compounds are presented in Figs. 2 and 3 and in Table 2. The example thermogravimetric curves (weight gain vs temperature/time) for the selected Ta-based alloys are shown in Fig. 2A, and the curves for the selected Ta-ceramic composites are presented in Fig. 2B. The reference material (microcrystalline Ta) exhibits the highest weight gain. All the nanocrystalline Ta alloys and pure nanocrystalline Ta exhibit significantly better high-temperature stability against oxidation. The best stability was found in Ta-W alloys (Figs. 2A and 3, Table 2). In most cases, the nanocrystalline materials (except Ta-W alloys, see Ta-40W in Fig. 2A) start to oxidize at lower temperatures than microcrystalline Ta (Fig. 2). The example impact of weight ratio on high-temperature stability is presented in Fig. 2C. All Ta-W alloys show better stability than microcrystalline tantalum. Only the Ta-5W had an insignificantly higher weight gain than nanocrystalline tantalum.
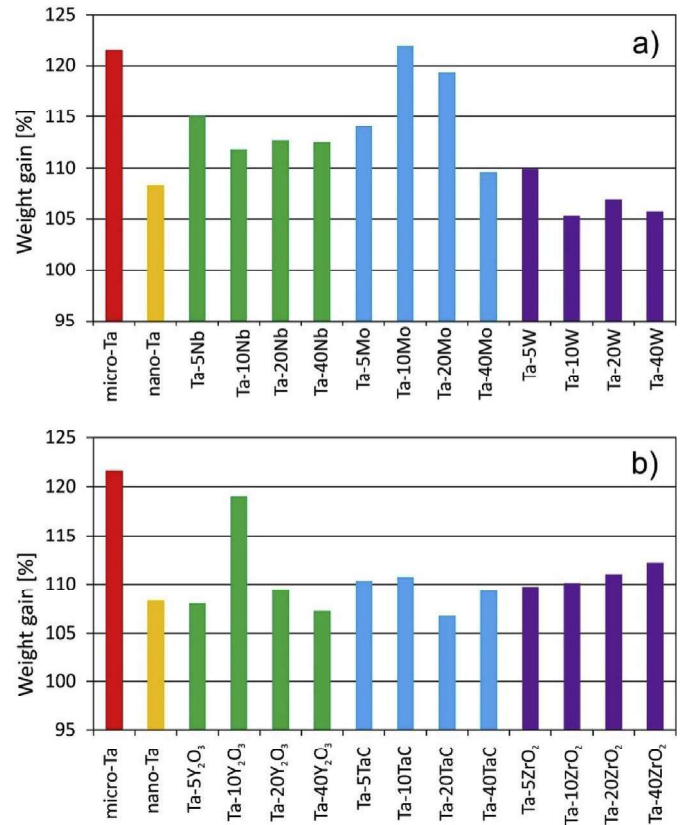
As for the Ta-ceramic composites (Figs. 2B and 3, Table 2), their stability is comparable to (except Ta-10Y$_2$O$_3$) or higher than that of microcrystalline Ta. Summarized data of the thermogravimetric analysis for all the investigated alloys and composites compared to pure micro- and nanocrystalline Ta are shown in Table 2 and Fig. 3. The microcrystalline Ta mass increases by 121.69% (where 100% is the starting mass) against the starting mass at RT. Similarly, tantalum in the nanocrystalline form has a significantly better temperature stability and the mass increases only by 108.34% when the temperature rises. All the nanocrystalline alloys and composites (except Ta-10Mo) exhibit a lower weight gain in comparison to pure microcrystalline Ta. With pure nanocrystalline Ta as the reference material, better stability is exhibited by the Ta-10W, Ta-20W, Ta-5Y$_2$O$_3$, Ta-40Y$_2$O$_3$ and Ta-20TaC compounds. We suppose that the weight gain is correlated with both microstructure and chemical composition. However, at this moment it is hard to say which factor dominates.

The sample XRD spectra of the Ta compounds are shown in Fig. 4. The spectrum (a) shows a cubic type structure of pure microcrystalline tantalum. High-temperature oxidation leads to the
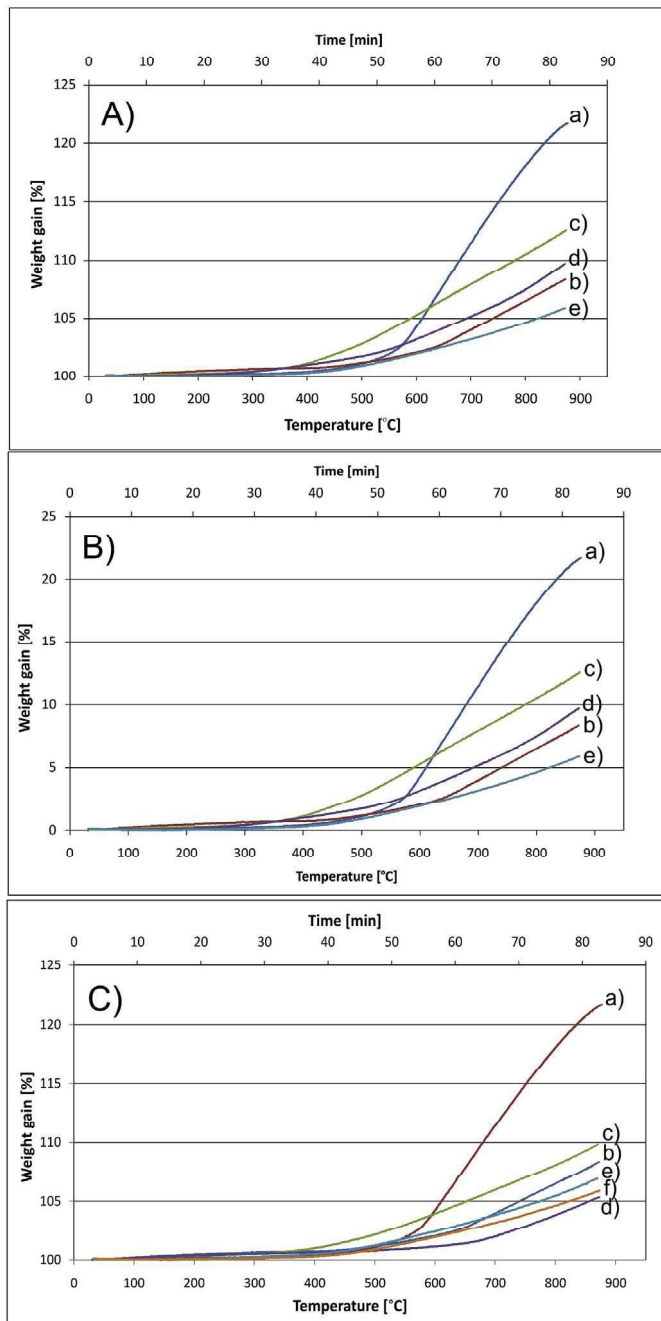
Fig. 2. Example TGA curves for nanocrystalline Ta-based alloys (A): micro-Ta (a), nano-Ta (b) and nanocrystalline alloys: Ta-40Nb (c), Ta-40Mo (d) and Ta-40W (e) as well as example TGA curves for Ta-ceramic composites (B): micro-Ta (a), nano-Ta (b) and nanocrystalline composites: Ta-40Y$_2$O$_3$ (c), Ta-40ZrO$_2$ (d) and Ta-40TaC (e). The TGA curves for Ta-xW alloys in comparison to pure Ta (C): micro-Ta (a), nano-Ta (b), Ta-5W (c), Ta-10W (d), Ta-20W (e), Ta-40W (f).


Fig. 3. Weight gain for nanocrystalline Ta-based alloys (a) and Ta-ceramic nano-composites (b); for comparison, data for micro-Ta and nano-Ta have been included.

formation of Ta$_2$O$_5$ in all of the investigated compounds (see examples in Fig. 4 b–d). Additionally, depending on their composition, other types of oxides are formed in the alloys and composites such as Nb$_2$O$_5$ in the Ta-Nb alloys (c), YTaO$_4$ in the Ta-Y$_2$O$_3$ composites (d). Additionally, for the Ta-Mo, Ta-W, Ta-ZrO$_2$ and Ta-TaC compounds, the following oxide phases were observed after oxidation: MoO$_2$, TaO$_2$, TaO, Ta$_{16}$W$_{18}$O$_{94}$, WO$_3$, ZrO$_2$, (not shown in Fig. 4, however found on the XRD spectra of the investigated compounds).

Examples of XRD spectra of tantalum based alloys and composites after annealing in nitrogen are shown in Fig. 5. The spectrum (a) represents microcrystalline tantalum. High-temperature annealing in nitrogen leads to the formation of TaN and Ta$_4$N. The presence of β-Ta was also observed. The nanocrystalline tantalum spectrum (b) shows four different types of nitrides: Ta$_5$N$_6$, Ta$_3$N$_5$, TaN, and Ta$_2$N. Additionally, a narrowing of the peaks occurred, which was caused by grain growth due to high temperature annealing. In the presented Ta-Nb type alloys, the formation of TaN, Ta$_4$N, NbN (c) and in the Ta-Mo type alloys, the formation of MoTaN, TaMo, TaN, Ta$_4$N were observed (d). The composites do not easily bond with nitrogen. The Ta-Y$_2$O$_3$ composites (e) showed no formation of nitrides. In the case of the Ta-TaC composites (f) only one nitride phase TaN was present. The nitrides TaN and TaZrN$_2$ were detected in the Ta-ZrO composites (g). In all three examples of the composites (e, f, g), the parent ceramic-reinforced phases Y$_2$O$_3$, TaC and ZrO$_2$ respectively are present after nitrogen annealing. The obtained phases for all annealed alloys and compound are summarized in Table 3.

The hot-pressed samples were oxidized under ambient and nitrogen atmosphere. All the samples annealed under ambient atmosphere underwent fast oxidation and were covered with a thick coating of oxide, which was non-uniform on the cylindrical sample edges (Fig. 6a). The oxide coating mainly grew outside of the sample towards the atmosphere. The thickness of the oxide coating on the smooth cylindrical sample surface reached 40 μm (b), while on the edges is enhanced and reached 500 μm (c). The oxide coating was non-uniform with many cracks (b, d) and exhibited a multi-layer morphology (d). The formed oxide coating was brittle and did not protect the material against further oxidation. The density

x

Table 2
Increase in the weight of the nanocrystalline Ta-based alloys and Ta-nanocomposites compared to micro-Ta and nano-Ta; TGA data after the 86-min continuous temperature increase from RT to 880 °C; reference starting weight is 100%.

Alloy composition													
micro-Ta	nano-Ta	Ta-5Nb	Ta-10Nb	Ta-20Nb	Ta-40Nb	Ta-5Mo	Ta-10Mo	Ta-20Mo	Ta-40Mo	Ta-5W	Ta-10W	Ta-20W	Ta-40W
Total weight gain [%]													
121.69 ± 1.83	108.34 ± 1.73	115.03 ± 1.67	111.87 ± 1.95	112.70 ± 1.87	112.53 ± 1.85	114.08 ± 2.09	122.05 ± 1.81	119.38 ± 1.74	109.60 ± 1.73	109.92 ± 1.67	105.34 ± 2.06	106.96 ± 1.98	105.78 ± 1.59

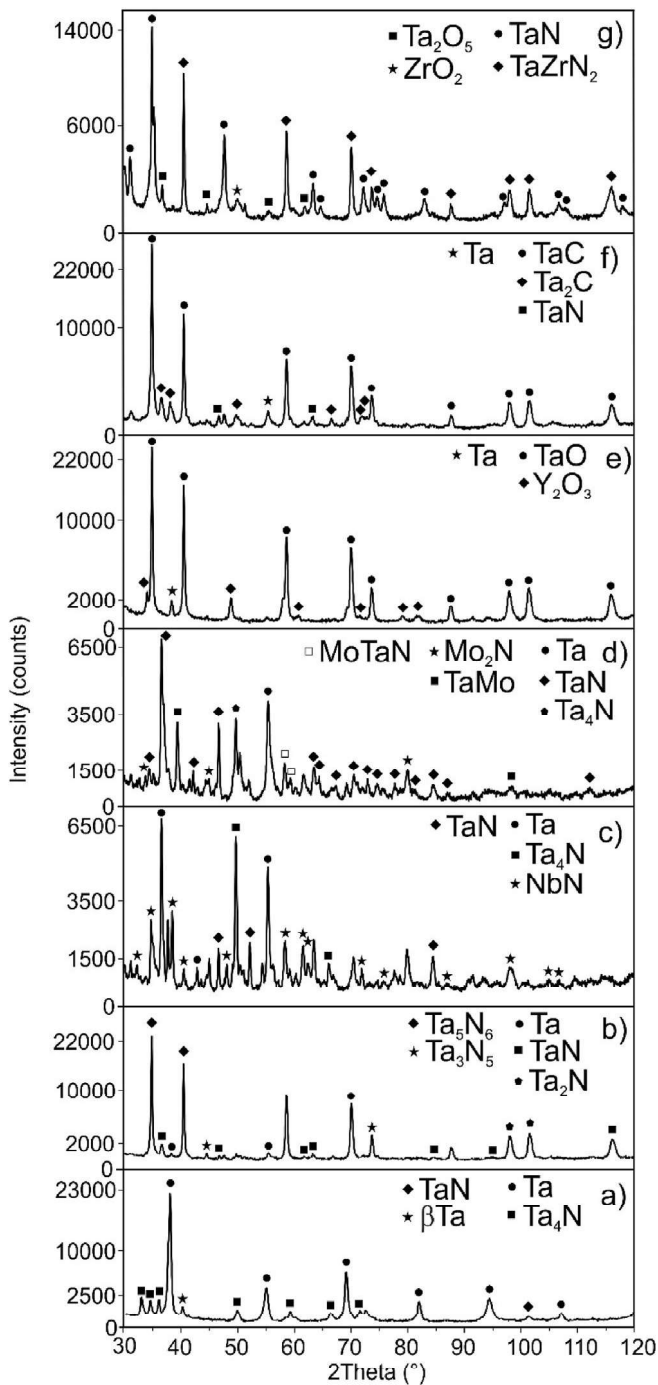| Composite composition													
micro-Ta	nano-Ta	Ta-5Y_2O_3	Ta-10Y_2O_3	Ta-20Y_2O_3	Ta-40Y_2O_3	Ta-5ZrO_2	Ta-10ZrO_2	Ta-20ZrO_2	Ta-40ZrO_2	Ta-5TaC	Ta-10TaC	Ta-20TaC	Ta-40TaC
Total weight gain [%]													
121.69 ± 1.83	108.34 ± 1.73	108.10 ± 1.72	119.04 ± 1.88	109.50 ± 1.91	107.28 ± 1.83	109.78 ± 1.72	110.17 ± 1.93	111.07 ± 1.84	112.27 ± 1.90	110.42 ± 1.75	110.76 ± 2.07	106.78 ± 1.70	109.36 ± 2.02
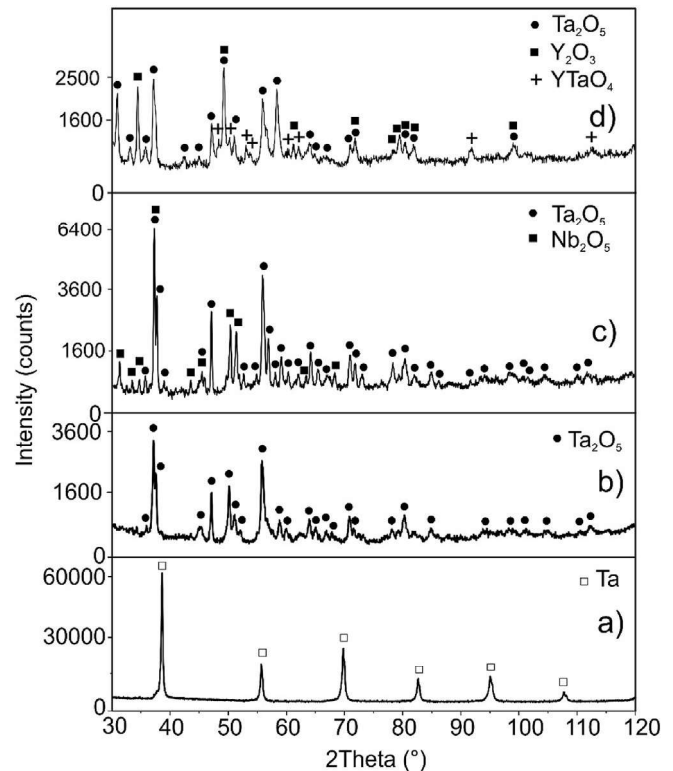
Fig. 4. Example XRD spectra of pure Ta (a) and Ta annealed in ambient atmosphere: pure Ta (b), Ta-40Nb nanocrystalline alloy (c) and Ta-40Y_2O_3 nanocomposite (d).

of Ta_2O_5 was twice smaller compared to Ta [19].

In the case of the hot-pressed samples, annealing under nitrogen atmosphere resulted in a smooth diffusion layer of various nitrides that grew into the sample (Fig. 7). The characteristic gold color of nitrides appeared (a, b). The thickness of the layer depended on sample composition and ranged between 50 and 140 μm (c, d). Hence, for the oxidation process, the oxide grows outside from the sample surface into the oxidizing atmosphere, while in the presence of nitrogen atmosphere, the nitrogen atoms diffuse towards the core of the material, forming a diffusion nitride layer rather than external coating.

When tantalum and its compounds were exposed to higher temperature and powerful oxidizing and/or nitriding atmosphere, the sample surface started to decompose. It is commonly accepted that annealing in both oxygen and nitrogen atmosphere is a high temperature oxidation process and can simply be referred to as 'high temperature oxidation' or 'gaseous corrosion'. Due to the oxidizing (and nitriding) atmosphere, various types of transition metal oxides or metal nitrides are formed. The nitrogen (and/or oxygen) atoms deposited in the crystal lattice of the metal lead to the formation of layers composed of interstitial nitrides, oxides and crystalline compounds of the host metal. The oxygen/nitrogen atoms occupy specific interstitial sites in the generally close-packed metal structure. It is general knowledge that the nitrogen and oxygen atoms can form multiple bonds (e.g. between the interstitial atoms). Therefore, when nanocrystalline alloys (Ta-xNb, Ta-xMo and Ta-xW) and nanocomposites (Ta-xY_2O_3, Ta-xZrO_2 and Ta-xTaC) react with nitrogen or oxygen, a number of nitrogenation and oxidation reactions take place. The formulas of these interstitial compounds may be different: MN, M_2N, M_4N, M_xN_y, MO, MO_2, M_xO_y, although their stoichiometries may vary (M is a metal). We suppose that these surface layer phases can be very hard and wear-resistant.

Fig. 5. Example XRD spectra after high-temperature annealing in nitrogen of micro-Ta (a), nano-Ta (b), and Ta-20Nb (c), Ta-20Mo (d) nanocrystalline alloys, as well as: Ta-20Y$_2$O$_3$ (e), Ta-20TaC (f) and Ta-20ZrO$_2$ (g) nanocomposites.

The high-temperature material stability tests (during TGA measurements in nitrogen flow of 20 mL/min) were supplemented by calculation of activation energy (E_a) of the oxidation kinetics of the materials. An isothermal and constant heating rate thermogravimetric analysis has been used to obtain the kinetic information through the constant heating rate method developed by Flynn and Wall [20]. The E_a is influenced by many factors such as the investigated substances or the oxidation temperature. The values of kinetic parameters can be successfully used to understand the high-temperature oxidation mechanism of a solid-state reaction. The differential thermal gravimetric (DTG) analysis showed different activation points of each material. DTG curves for the Ta-based alloys and composites are shown in Fig. 8. The higher the content of alloying elements or the ceramic reinforced phase, the sooner the process begins. Compounds with a weight ratio of 5% and 10% behave similarly to nanocrystalline tantalum (Fig. 8 A, B, D, E, F). This dependence was noticed for all compounds except Ta-W alloys (Fig. 8C). Ta-W alloys behave in the opposite way. The higher the weight ratio is, the more time is needed for the reaction to initiate.

The activation energies E_a of the oxidation in the nanocrystalline Ta-based alloys and the nanocrystalline Ta-composites referred to as micro-Ta and nano-Ta have been summarized in Table 4. These energies show that some chemical compositions have a strong effect (for example Ta-5W: 1626 kJ/mol), but most of them remain in the range of 760—999 kJ/mol for a wide variety of compounds. The modification of tantalum significantly changes the nature of the oxidation, leads to a decrease/increase in the temperature of the onset of oxidation and sometimes shifts the reaction towards higher temperatures. Such oxidation behaviors are mainly due to the diversity of the chemical bonding in the samples. Metal nitrides are characterised by differences in their chemical bonds, in which covalent and metallic bonding coexist. The calculated activation energy suggests that the rate-controlling process during oxidation results from a simultaneous inward and outward diffusion of tantalum through the formation of a protective layer that consists mainly of the nitride phase. The bond overlap population of the metal-metal bond plays an important role in the thermal stability of transition of the metal nitride [21]. For example, a higher Mo content in the Tantalum alloys decreases nitrogen diffusivity. Particularly promising is a new generation of composites containing TaC and Y$_2$O$_3$ as the ceramic phase having an outstanding oxidation resistance and satisfying the requirements of many diverse applications.

Having a high surface area, nanocrystalline powders are very sensitive to the oxidation process during material storage in air at room temperature (RT) as well as at elevated temperatures. The high reactivity of nanopowders results in surface oxidation of the particles and absorption of various gases from the atmosphere. The large and highly reactive surface area of tantalum exposed to oxygen or nitrogen leads to its fast diffusion, consequently leading to an increase in weight and high-temperature corrosion (both oxidation and nitrogenation). Oxygen absorption leads to a reduction of the dynamic ductility of tantalum [22], which is why high

Table 3
The obtained phases in Ta compounds after annealing in nitrogen and oxygen.

Compound	Phases after annealing in nitrogen	Phases after annealing in oxygen
micro-Ta	TaN, Ta$_4$N, β-Ta	Ta$_4$O, Ta$_2$O$_5$,
nano-Ta	TaN, Ta$_2$N, Ta$_3$N$_5$, Ta$_5$N$_6$	TaO, Ta$_2$O$_5$, Ta$_4$O, TaO$_2$
Ta-xNb	Ta, TaN, Ta$_4$N, NbN	Ta$_2$O$_5$, Nb$_2$O$_5$,
Ta-xMo	Ta, TaN, Ta$_4$N, TaMo, Mo$_2$N, TaMoN	TaO, Ta$_{12}$MoO$_{33}$, MoO, Ta$_2$O$_5$, MoO$_2$
Ta-xW	Ta, TaN, W$_2$N	Ta$_{16}$W$_{18}$O$_{94}$, Ta$_8$W$_9$O$_{47}$, TaO, Ta$_2$O$_5$, WO$_3$
Ta-xY$_2$O$_3$	Ta, TaO, Y$_2$O$_3$	YTaO$_4$, TaO, TaO$_4$, Y
Ta-xTaC	Ta, TaC, Ta$_2$C, TaN	TaO$_2$, Ta$_2$O$_5$, Ta$_2$C
Ta-xZrO$_2$	TaN, ZrO$_2$, TaZrN, Ta$_2$O$_5$	Ta$_2$O$_5$, TaO, ZrO$_2$, (Ta,Zr,O), Ta$_4$O
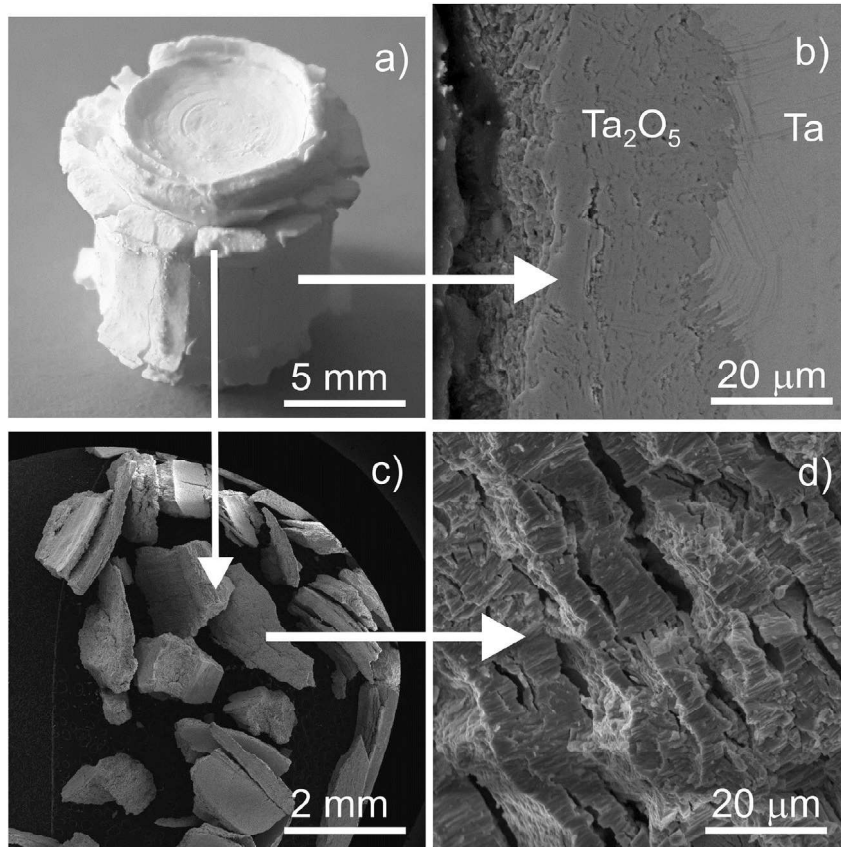
Fig. 6. Oxidized bulk hot-pressed pure Ta sample; general sample view (a), oxide coating on the cylindrical surface (b), crushed oxide coating acquired from the sample edges (c) and the enhanced view of the oxide coating cross section (d).
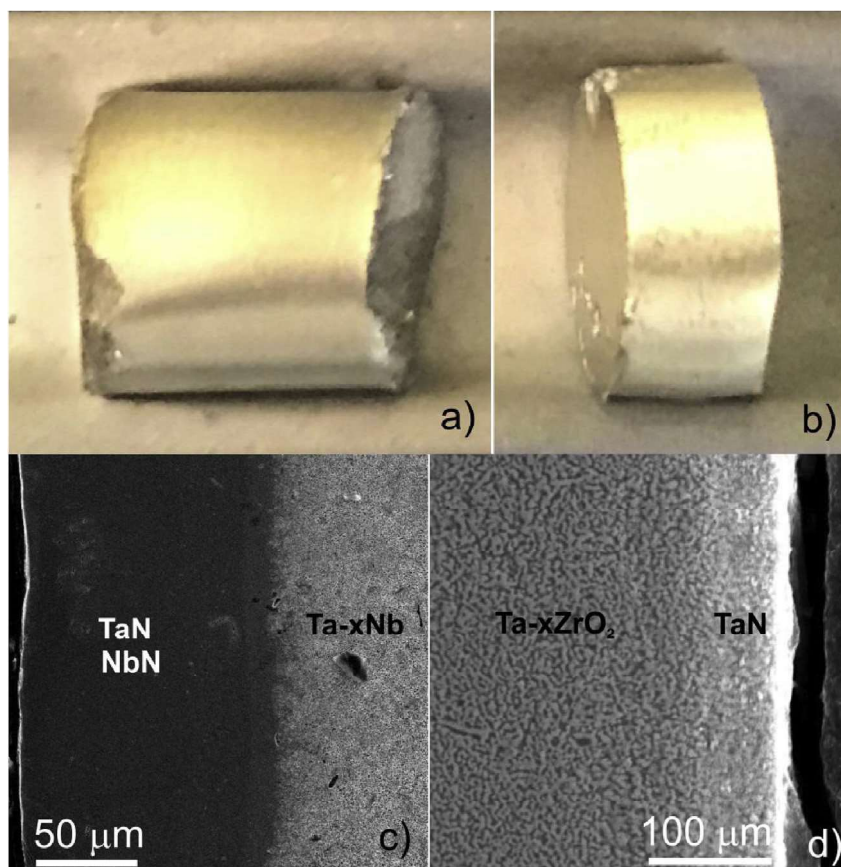
Fig. 7. General view of nitrided bulk hot-pressed microcrystalline Ta (a) and nanocrystalline Ta-20Nb alloy (b). SEM images of the samples with a visible nitride layer in Ta-20Nb alloy (c) and Ta-20ZrO$_2$ composite (d).
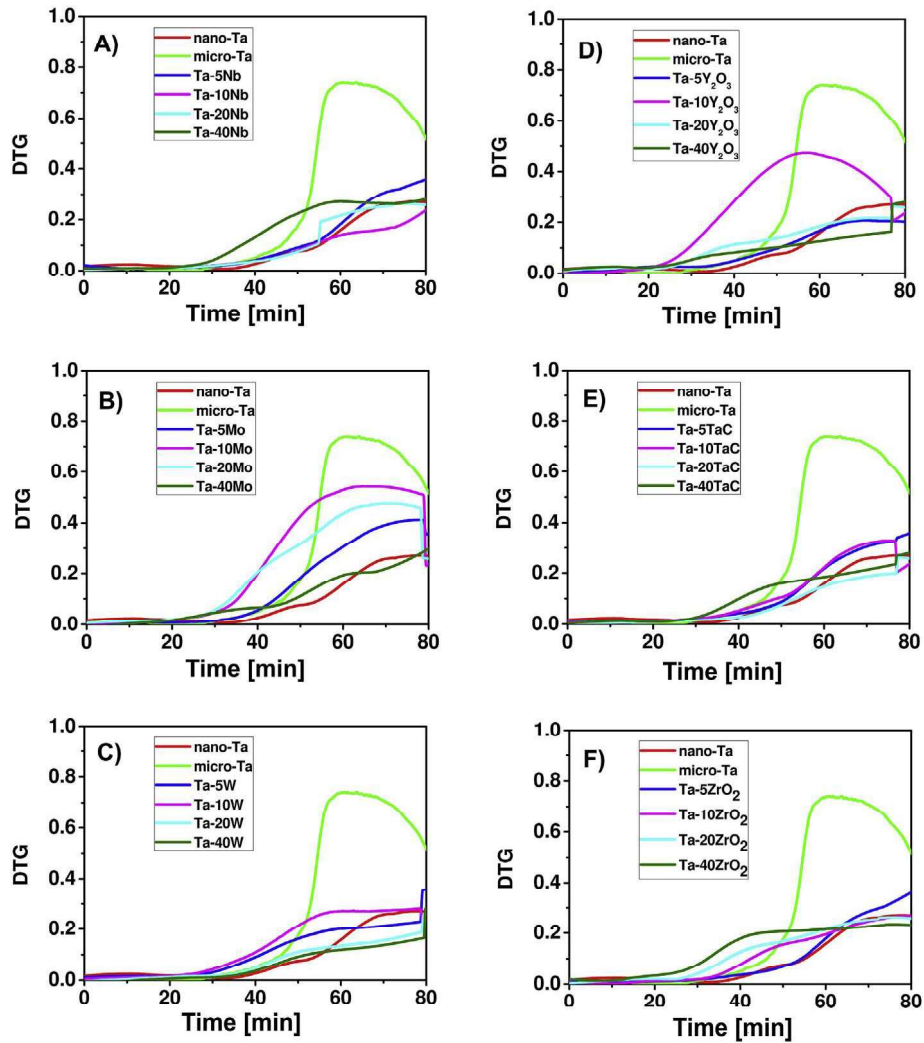
Fig. 8. DTG curves for Ta-based nanocrystalline alloys (A, B, C) and Ta-ceramic nanocomposite (D, E, F); for comparison, data for nano- and microcrystalline Ta have been included.

purity atmosphere is necessary throughout all the processing stages of tantalum at room as well as at elevated temperatures. High temperature diffusion of interstitial atoms, particularly oxygen, can limit potential application at elevated temperatures in oxidative environments.

At atmospheric air pressure conditions refractory metals have different oxidation rates (negligible below 200 °C, parabolic at 300—400 °C and linear above ~450—500 °C) [23]. The solubility of oxygen atoms is higher in tantalum and niobium than in tungsten and molybdenum lattice. The embrittlement of Ta-alloys can be boosted by elements of higher oxygen solubility such as Nb, in

which internal oxidation proceeds through the crystal lattice. Ta-based alloys with Mo and W, of lower oxygen solubility, may support the formation of the oxide film, reducing the penetration of crystal lattice by oxygen. The reinforced oxide ceramic phase (ZrO_2, Y_2O_3) in Ta-ceramic composites may become partially dissolved, resulting in internal oxidation of the Ta-matrix, although Zr lowers the solubility of oxygen in refractory materials [23].

Ta-compounds of various chemical composition may demonstrate differing oxidation behavior, which affects their thermal stability. In the case of nanomaterials, grain size may also have an impact on thermal stability. More research is needed to offer full

Table 4
Activation energy E_a of oxidation in the nanocrystalline Ta-based alloys and Ta-nanocomposites referred to as micro-Ta and nano-Ta.

	Alloy composition												
	micro-Ta	nano-Ta	Ta-5Nb	Ta-10Nb	Ta-20Nb	Ta-40Nb	Ta-5Mo	Ta-10Mo	Ta-20Mo	Ta-40Mo	Ta-5W	Ta-10W	Ta-20W	Ta-40W
Activation energy [kJ/mol]	803 ± 68	853 ± 72	849 ± 67	890 ± 72	854 ± 60	780 ± 58	810 ± 69	830 ± 71	928 ± 73	950 ± 76	1626 ± 131	985 ± 88	999 ± 81	990 ± 81
	Composite composition												
	micro-Ta	nano-Ta	Ta-5Y$_2$O$_3$	Ta-10Y$_2$O$_3$	Ta-20Y$_2$O$_3$	Ta-40Y$_2$O$_3$	Ta-5ZrO$_2$	Ta-10ZrO$_2$	Ta-20ZrO$_2$	Ta-40ZrO$_2$	Ta-5TaC	Ta-10TaC	Ta-20TaC	Ta-40TaC
Activation energy [kJ/mol]	803 ± 68	853 ± 72	444 ± 38	1005 ± 87	845 ± 74	908 ± 74	848 ± 68	795 ± 71	772 ± 73	760 ± 60	873 ± 72	840 ± 76	835 ± 64	983 ± 83

characterization of these materials.

4. Conclusions

Thermal stability of novel refractory nanocrystalline Ta-based alloys modified with the addition of Mo, Nb and W as well as composites reinforced by Y_2O_3, ZrO_2 and TaC was studied. Oxidation and nitridation lead to the formation of different types of oxides and nitrides in the nanocrystalline Ta-based compounds. Although all types of nanocrystalline alloys and composites exhibit a better resistance against high temperatures, they begin to oxidize more at lower temperatures compared to pure microcrystalline Ta.

The differences in the DTG analysis suggest that the amount of additives influences the oxidation process and its activation point in nanocrystalline Ta-based alloys and composites. The Ta–5W alloy has the highest activation energy value.

The tantalum nitrides formed at a high temperature result in the formation of a smooth, uniform and continuous diffusion protective layer, while oxides form an external coating during oxidation under ambient atmosphere. This coating is brittle, discontinuous and useless in improving the surface properties.

Acknowledgements

Appendix A. Supplementary data

Supplementary data to this article can be found online at https://doi.org/10.1016/j.jallcom.2019.02.230.

References

[1] R. Morales, R.E. Aune, O. Grinder, S. Seetharaman, The powder metallurgy processing of refractory metals and alloys, JOM 55 (2003) 20—23.
[2] S.M. Cordonne, P. Kumar, C.A. Michaluk, H.D. Schwartz, Tantalum and its alloys, Int. J. Refract. Metals Hard Mater. 13 (1995) 187—194.
[3] C.L. Briant, The properties and uses of refractory metals and their alloys, MRS Proc. 322 (1993) 305—314.
[4] H.O. Pierson, Handbook of Refractory Carbides and Nitrides. Properties, Characteristics, Processing and Applications, Noyes Publ, 1996.
[5] S.A. Ghaffari, M.A. Faghihi-Sani, F. Golestani-Fard, M. Nojabayy, Diffusion and solid solution formation between the binary carbides of TaC, HfC, ZrC, Int. J. Refract. Metals Hard Mater. 41 (2013) 180—184.
[6] E.P. Simonenko, N.P. Simonenko, S. Yu. Ezhov, V.G. Sevastyanov, N.T. Kuznetsov, Study of the synthesis of nanocrystalline mixed tantalum—zirconium carbide, Phys. Atom. Nucl. 78 (2015) 1357—1365.
[7] L. Xu, S. Wei, J. Li, G. Zhang, B. Dai, Preparation, microstructure and properties of molybdenum alloys reinforced by in-situ Al_2O_3 particles, Int. J. Refract. Metals Hard Mater. 30 (2012) 208—212.
[8] Y.S. Zhang, L.C. Zhang, H.Z. Niu, X.F. Bai, S. Yua, X.Q. Ma, Z.T. Yu, Deformation twinning and localized amorphization in nanocrystalline tantalum induced by sliding friction, Mater. Lett. 127 (2014) 4—7.
[9] O.N. Senkov, F.H. Froes, V.V. Stolyarov, R.Z. Valiev, J. Liu, Microstructure and microhardness of an AlFe alloy subjected to severe plastic deformation and aging, Nanostruct. Mater. 10 (1998) 691—698.
[10] T. Chookajorn, H.A. Murdoch, C.A. Schuh, Design of stable nanocrystalline alloys, Science 337 (2012) 951—955.
[11] H. Asgharzadeh, H.J. McQueen, Grain growth and stabilisation of nano-structured aluminium at high temperatures: review, Mater. Sci. Technol. 31 (2015) 1016—1034.
[12] A. Robin, J.L. Rosa, Corrosion behavior of niobium, tantalum and their alloys in hot hydrochloric and phosphoric acid solutions, Int. J. Refract. Metals Hard Mater. 18 (2000) 13—21.
[13] M. Bischof, S. Mayer, H. Leitner, H. Clemens, P. Straton, E. Geiger, A. Voiticek, W. Knabl, On the development of grain growth resistant tantalum alloys, Int. J. Refract. Metals Hard Mater. 24 (2006) 437—444.
[14] S. Nemat-Nasser, R. Kapoor, Deformation behavior of tantalum and tantalum tungsten alloy, Int. J. Plast. 17 (2001) 1351—1366.
[15] B. Gorr, F. Müller, M. Azim, H.-J. Christ, T. Müller, H. Chen, A. Kauffmann, M. Heilmaier, High-temperature oxidation behavior of refractory high-entropy alloys: effect of alloy composition, Oxid. Metals 88 (2017) 339—349.
[16] J. Jakubowicz, G. Adamek, M. Sopata, J.K. Koper, T. Kachlicki, M. Jarzębski, Microstructure and electrochemical properties of refractory nanocrystalline tantalum-based alloys, Int. J. Electrochem. Sci. 13 (2018) 1956—1975.
[17] J. Jakubowicz, M. Sopata, G. Adamek, P. Siwak, T. Kachlicki, Formation and properties of the Ta-Y_2O_3, Ta-ZrO_2, and Ta-TaC nanocomposites, Ann. Mater. Sci. Eng. (2018), 2085368.
[18] M. Carrier, L. Auret, A. Bridgwater, J.H. Knoetze, Using apparent activation energy as a reactivity criterion for biomass pyrolysis, Energy Fuels 30 (2016) 7834—7841.
[19] S. Ezhilvalavan, T.Y. Tseng, Preparation and properties of tantalum pentoxide (Ta_2O_5) thin films for ultra large scale integrated circuits (ULSIs) application – a review, J. Mater. Sci. Mater. Electron. 10 (1999) 9—31.
[20] J.H. Flynn, L.A. Wall, A quick, direct method for the determination of activation energy from thermogravimetric data, J. Polym. Sci. Part B: Polymer Lett. 4 (1966) 323—328.
[21] M. Takahashi, G.-C. Lai, K. Ohta, F. Kanamaru, Bond strength and thermal stability of transition metal nitrides, Adv. Quant. Chem. 29 (1998) 253—268.
[22] Y. Kim, E.P. Kim, J.W. Noh, S.H. Lee, Y.S. Kwon, I.S. Oh, Fabrication and mechanical properties of powder metallurgy tantalum prepared by hot isostatic pressing, Int. J. Refract. Metals Hard Mater. 48 (2015) 211—216.
[23] J.R. DiStefano, B.A. Pint, J.H. DeVan, Oxidation of refractory metals in air and low pressure oxygen gas, Int. J. Refract. Metals Hard Mater. 18 (2000) 237—243.

Oświadczenia o udziale w publikacjach

dr inż. Piotr Siwak

Oświadczenie o udziale mgr inż. Mateusza Sopaty we wspólnych publikacjach

J. Jakubowicz, G. Adamek, M. Sopata, J.K. Koper, P. Siwak, *Hot pressing of nanocrystalline tantalum using high frequency induction heating and pulse plasma sintering*, 6th Global Conference on Materials Science and Engineering, IOP Conf. Series: Materials Science and Engineering 283 (2017) 012001, DOI: 10.1088/1757-899X/283/1/012001

Udział mgr inż. Mateusza Sopaty polegał na wytworzeniu badanych materiałów wykorzystując proces mechanicznej syntezy oraz metodę prasowania na gorąco, wykonaniu badań strukturalnych, opracowaniu rysunków, udział w pisaniu publikacji - udział 30%.

J. Jakubowicz, M. Sopata, G. Adamek, P. Siwak, T. Kachlicki, *Formation and properties of the Ta-Y2O3, Ta-ZrO2 and Ta-TaC nanocomposites*, Advances in Materials Science and Engineering (2018) 2085368; DOI: 10.1155/2018/2085368

Udział mgr inż. Mateusza Sopaty polegał na wytworzeniu badanych materiałów wykorzystując proces mechanicznej syntezy, wykonaniu badań strukturalnych, analizie danych i opisaniu otrzymanych wyników badań, opracowaniu rysunków, udział w pisaniu publikacji - udział 35%.

25. 04. 2019

dr inż. Mariola Sądej

Oświadczenie o udziale mgr inż. Mateusza Sopaty we wspólnych publikacjach

M. Sopata, M. Sadej, J. Jakubowicz, *High temperature resistance of novel tantalum-based nanocrystalline refractory compounds*, Journal of Alloys and Compounds 788 (2019) 476-484.

Udział mgr inż. Mateusza Sopaty polegał na zainicjowaniu i zaproponowaniu programu badań, wykonaniu badań strukturalnych, przeprowadzeniu procesu wygrzewania, analizie danych i opisaniu otrzymanych wyników badań, opracowaniu rysunków, wiodący udział w pisaniu publikacji, nadzorowanie procesu wydawniczego - udział 75%.

24. 04. 2018

dr inż. Jeremiasz Koper

Oświadczenie o udziale mgr inż. Mateusza Sopaty we wspólnych publikacjach

J. Jakubowicz, G. Adamek, M. Sopata, J.K. Koper, T. Kachlicki, M. Jarzębski, *Microstructure and electrochemical properties of refractory nanocrystalline tatalum-based alloys*, International Journal of Electrochemical Science 13 (2018) 1956-1975; DOI: 10.20964/2018.02.67.

Udział mgr inż. Mateusza Sopaty polegał na wytworzeniu badanych materiałów wykorzystując proces mechanicznej syntezy, wykonaniu badań strukturalnych, analizie składu chemicznego metodą EDS, analizie danych i opisaniu otrzymanych wyników badań, opracowaniu rysunków, udział w pisaniu publikacji - udział 35%.

J. Jakubowicz, G. Adamek, M. Sopata, J.K. Koper, P. Siwak, *Hot pressing of nanocrystalline tantalum using high frequency induction heating and pulse plasma sintering*, 6th Global Conference on Materials Science and Engineering, IOP Conf. Series: Materials Science and Engineering 283 (2017) 012001, DOI: 10.1088/1757-899X/283/1/012001

Udział mgr inż. Mateusza Sopaty polegał na wytworzeniu badanych materiałów wykorzystując proces mechanicznej syntezy oraz metodę prasowania na gorąco, wykonaniu badań strukturalnych, opracowaniu rysunków, udział w pisaniu publikacji - udział 30%.

M. Sopata, J.K. Koper, J. Jakubowicz, *Odporność korozyjna prasowanych na gorąco nanokrystalicznych stopów tantalu*, Ochrona Przed Korozją 11 (2017) 365-367, DOI: 10.15199/40.2017.11.2

Udział mgr inż. Mateusza Sopaty polegał na zainicjowaniu i zaproponowaniu programu badań, wytworzeniu materiałów badanych wykorzystując proces mechanicznej syntezy oraz prasowanie na gorąco, przeprowadzenie badan odporności na korozję, opracowaniu rysunków, wiodący udział w pisaniu publikacji, nadzorowanie procesu wydawniczego- udział 80%.

29. 04. 2019.

1

dr inż. Tomasz Kachlicki

Oświadczenie o udziale mgr inż. Mateusza Sopaty we wspólnych publikacjach

J. Jakubowicz, M. Sopata, G. Adamek, P. Siwak, T. Kachlicki, *Formation and properties of the Ta-Y2O3, Ta-ZrO2 and Ta-TaC nanocomposites*, Advances in Materials Science and Engineering (2018) 2085368; DOI: 10.1155/2018/2085368

Udział mgr inż. Mateusza Sopaty polegał na wytworzeniu badanych materiałów wykorzystując proces mechanicznej syntezy, wykonaniu badań strukturalnych, analizie danych i opisaniu otrzymanych wyników badań, opracowaniu rysunków, udział w pisaniu publikacji - udział 35%.

J. Jakubowicz, G. Adamek, M. Sopata, J.K. Koper, T. Kachlicki, M. Jarzębski, *Microstructure and electrochemical properties of refractory nanocrystalline tatalum-based alloys*, International Journal of Electrochemical Science 13 (2018) 1956-1975; DOI: 10.20964/2018.02.67.

Udział mgr inż. Mateusza Sopaty polegał na wytworzeniu badanych materiałów wykorzystując proces mechanicznej syntezy, wykonaniu badań strukturalnych, analizie składu chemicznego metodą EDS, analizie danych i opisaniu otrzymanych wyników badań, opracowaniu rysunków, udział w pisaniu publikacji - udział 40%.
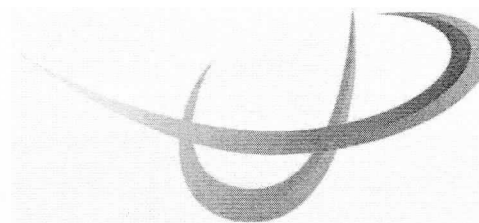
28.04.2019

Katedra Fizyki i Biofizyki
ul. Wojska Polskiego 38/42
60-637 Poznań
sekretariat: +48 61 848 7503

Uniwersytet Przyrodniczy w Poznaniu

dr n. techn. inż. dr n. fiz. Maciej JARZĘBSKI
tel. +48 535 255 775
email: maciej.jarzebski@up.poznan.pl

Vancouver, Poznań, 24.04.201'

Oświadczenie o udziale mgr inż. Mateusza Sopaty

we wspólnych publikacjach

J. Jakubowicz, G. Adamek, M. Sopata, J.K. Koper, T. Kachlicki, M. Jarzębski, Microstructure and electrochemical properties of refractory nanocrystalline tatalum-based alloys, International Journal of Electrochemical Science 13 (2018) 1956-1975; DOI:10.20964/2018.02.67.

Udział mgr inż. Mateusza Sopaty polegał na wytworzeniu badanych materiałów wykorzystując proces mechanicznej syntezy, wykonaniu badań strukturalnych, analizie składu chemicznego metodą EDS, analizie danych i opisaniu otrzymanych wyników badań, opracowaniu rysunków, udział w pisaniu publikacji - udział 35%.

Maciej Jarzębski

dr inż. Grzegorz Adamek

Oświadczenie o udziale mgr inż. Mateusza Sopaty we wspólnych publikacjach

J. Jakubowicz, G. Adamek, M. Sopata, J.K. Koper, P. Siwak, *Hot pressing of nanocrystalline tantalum using high frequency induction heating and pulse plasma sintering*, 6th Global Conference on Materials Science and Engineering, IOP Conf. Series: Materials Science and Engineering 283 (2017) 012001, DOI: 10.1088/1757-899X/283/1/012001

Udział mgr inż. Mateusza Sopaty polegał na wytworzeniu badanych materiałów wykorzystując proces mechanicznej syntezy oraz metodę prasowania na gorąco, wykonaniu badań strukturalnych, opracowaniu rysunków, udział w pisaniu publikacji - udział 30%.

J. Jakubowicz, M. Sopata, G. Adamek, P. Siwak, T. Kachlicki, *Formation and properties of the Ta-Y2O3, Ta-ZrO2 and Ta-TaC nanocomposites*, Advances in Materials Science and Engineering (2018) 2085368; DOI: 10.1155/2018/2085368

Udział mgr inż. Mateusza Sopaty polegał na wytworzeniu badanych materiałów wykorzystując proces mechanicznej syntezy, wykonaniu badań strukturalnych, analizie danych i opisaniu otrzymanych wyników badań, opracowaniu rysunków, udział w pisaniu publikacji - udział 35%.

J. Jakubowicz, G. Adamek, M. Sopata, J.K. Koper, T. Kachlicki, M. Jarzębski, *Microstructure and electrochemical properties of refractory nanocrystalline tatalum-based alloys*, International Journal of Electrochemical Science 13 (2018) 1956-1975; DOI: 10.20964/2018.02.67.

Udział mgr inż. Mateusza Sopaty polegał na wytworzeniu badanych materiałów wykorzystując proces mechanicznej syntezy, wykonaniu badań strukturalnych, analizie składu chemicznego metodą EDS, analizie danych i opisaniu otrzymanych wyników badań, opracowaniu rysunków, udział w pisaniu publikacji - udział 35%.

J. Jakubowicz, M. Sopata, G. Adamek, P. Siwak, T. Kachlicki, *Formation and properties of the Ta-Y2O3, Ta-ZrO2 and Ta-TaC nanocomposites*, Advances in Materials Science and Engineering (2018) 2085368; DOI: 10.1155/2018/2085368

Udział mgr inż. Mateusza Sopaty polegał na wytworzeniu badanych materiałów wykorzystując proces mechanicznej syntezy, wykonaniu badań strukturalnych, analizie

danych i opisaniu otrzymanych wyników badań, opracowaniu rysunków, udział w pisaniu publikacji - udział 35%.

J. Jakubowicz, G. Adamek, M. Sopata, *Characterization of high-energy ball-milled and hot-pressed nanocrystalline tantalum*, 2nd International Conference on Civil Engineering and Materials Science, IOP Conf. Series: Materials Science and Engineering 216 (2017) 012006, DOI: 10.1088/1757-899X/216/1/012006.

Udział mgr inż. Mateusza Sopaty polegał na wytworzeniu badanych materiałów wykorzystując proces wysokoenergetycznego rozdrabniania oraz wykonaniu badań strukturalnych, opracowaniu rysunków, udział w pisaniu publikacji - udział 30%.

25. 04. 2019

dr hab. inż. Jarosław Jakubowicz, prof. PP

Oświadczenie o udziale mgr inż. Mateusza Sopaty we wspólnych publikacjach

J. Jakubowicz, G. Adamek, M. Sopata, J.K. Koper, P. Siwak, *Hot pressing of nanocrystalline tantalum using high frequency induction heating and pulse plasma sintering*, 6th Global Conference on Materials Science and Engineering, IOP Conf. Series: Materials Science and Engineering 283 (2017) 012001, DOI: 10.1088/1757-899X/283/1/012001

Udział mgr inż. Mateusza Sopaty polegał na wytworzeniu badanych materiałów wykorzystując proces mechanicznej syntezy oraz metodę prasowania na gorąco, wykonaniu badań strukturalnych, opracowaniu rysunków, udział w pisaniu publikacji - udział 30%.

J. Jakubowicz, M. Sopata, G. Adamek, P. Siwak, T. Kachlicki, *Formation and properties of the Ta-Y2O3, Ta-ZrO2 and Ta-TaC nanocomposites*, Advances in Materials Science and Engineering (2018) 2085368; DOI: 10.1155/2018/2085368

Udział mgr inż. Mateusza Sopaty polegał na wytworzeniu badanych materiałów wykorzystując proces mechanicznej syntezy, wykonaniu badań strukturalnych, analizie danych i opisaniu otrzymanych wyników badań, opracowaniu rysunków, udział w pisaniu publikacji - udział 35%.

J. Jakubowicz, G. Adamek, M. Sopata, J.K. Koper, T. Kachlicki, M. Jarzębski, *Microstructure and electrochemical properties of refractory nanocrystalline tatalum-based alloys*, International Journal of Electrochemical Science 13 (2018) 1956-1975; DOI: 10.20964/2018.02.67.

Udział mgr inż. Mateusza Sopaty polegał na wytworzeniu badanych materiałów wykorzystując proces mechanicznej syntezy, wykonaniu badań strukturalnych, analizie składu chemicznego metodą EDS, analizie danych i opisaniu otrzymanych wyników badań, opracowaniu rysunków, udział w pisaniu publikacji - udział 35%.

J. Jakubowicz, M. Sopata, G. Adamek, P. Siwak, T. Kachlicki, *Formation and properties of the Ta-Y2O3, Ta-ZrO2 and Ta-TaC nanocomposites*, Advances in Materials Science and Engineering (2018) 2085368; DOI: 10.1155/2018/2085368

Udział mgr inż. Mateusza Sopaty polegał na wytworzeniu badanych materiałów wykorzystując proces mechanicznej syntezy, wykonaniu badań strukturalnych, analizie

danych i opisaniu otrzymanych wyników badań, opracowaniu rysunków, udział w pisaniu publikacji - udział 35%.

M. Sopata, J.K. Koper, J. Jakubowicz, *Odporność korozyjna prasowanych na gorąco nanokrystalicznych stopów tantalu*, Ochrona Przed Korozją 11 (2017) 365-367, DOI: 10.15199/40.2017.11.2

Udział mgr inż. Mateusza Sopaty polegał na zainicjowaniu i zaproponowaniu programu badań, wytworzeniu materiałów badanych wykorzystując proces mechanicznej syntezy oraz prasowanie na gorąco, przeprowadzenie badan odporności na korozję, opracowaniu rysunków, wiodący udział w pisaniu publikacji, nadzorowanie procesu wydawniczego - udział 80%.

M. Sopata, M. Sadej, J. Jakubowicz, *High temperature resistance of novel tantalum-based nanocrystalline refractory compounds*, Journal of Alloys and Compounds 788 (2019) 476-484.

Udział mgr inż. Mateusza Sopaty polegał na zainicjowaniu i zaproponowaniu programu badań, wykonaniu badań strukturalnych, przeprowadzeniu procesu wygrzewania, analizie danych i opisaniu otrzymanych wyników badań, opracowaniu rysunków, wiodący udział w pisaniu publikacji, nadzorowanie procesu wydawniczego - udział 75%.

J. Jakubowicz, G. Adamek, M. Sopata, *Characterization of high-energy ball-milled and hot-pressed nanocrystalline tantalum*, 2nd International Conference on Civil Engineering and Materials Science, IOP Conf. Series: Materials Science and Engineering 216 (2017) 012006, DOI: 10.1088/1757-899X/216/1/012006.

Udział mgr inż. Mateusza Sopaty polegał na wytworzeniu badanych materiałów wykorzystując proces wysokoenergetycznego rozdrabniania oraz wykonaniu badań strukturalnych, opracowaniu rysunków, udział w pisaniu publikacji - udział 30%.

25.04.2019